NTNU – Trondheim
Norwegian University of
Science and Technology

Signatures of the Transition between Topologically and Magnetically Ordered Ground States in the Schwinger-Boson Mean Field Theory of Frustrated Quantum Antiferromagnets

An analysis of the triangular lattice
Heisenberg model with nearest and next
nearest neighbour interactions

Christian Øyn Naversen

Master of Science in Physics and Mathematics
Submission date: June 2015
Supervisor: John Ove Fjærestad, IFY

Norwegian University of Science and Technology
Department of Physics

Abstract

We present three different methods of finding the critical spin value S_c of the quantum phase transition between the spin liquid and the Néel order phase on the mean field triangular Heisenberg antiferromagnet at $T = 0$K. These methods are: using the sublattice magnetization as an order parameter, looking at the scaling of the energy difference of topologically degenerate states in different phases, and the quantum fidelity approach. All of these methods are able to pick up the signal of the phase transition, and their estimated numerical values of S_c agree for systems where the relative strength of next nearest neighbour interaction compared to the nearest neighbour interaction is small. For the relative interaction strength $j = 0$ and $j = 0.1$, all three methods predict $S_c \approx 0.21$ and $S_c \approx 0.25$ respectively, while $j = 0.2$ gives deviating results. This deviation might be caused by the influence of other magnetically ordered states that we have not accounted for in our calculations, and so we restrict the validity of our results to $j < 0.125$.

Sammendrag

Vi presenterer i denne rapporten tre ulike metoder for å finne den kritiske spinnverdien S_c i faseovergangen mellom spinnvæskefasen og den Néel-ordede fasen i en middelfelts-Heisenberg-antiferromagnet på det triangulære gitteret ved $T = 0$K. De tre metodene er: bruk av magnetiseringen som en ordensparameter, sammenligning av skaleringen av energidifferansen mellom degenererte topologisk ordnete tilstander i de forskjellige fasene, og beregning av det "kvantemekaniske overlappet" (quantum fidelity). Alle disse metodene klarer å fange opp faseovergangen, og deres estimat av S_c stemmer overens med hverandre i systemer der den relative styrken mellom nest-nærmeste-nabo-vekselvirkninger og nærmeste-nabo-vekselvirkninger er liten. Med en relativ vekselvirkningsstyrke på $j = 0$ og $j = 0.1$, så estimerer alle metodene henholdsvis $S_c \approx 0.21$ og $S_c \approx 0.25$, mens resultatene for $j = 0.2$ er sprikende. Dette kan komme av forstyrrelser fra andre magnetisk ordnede faser som vi ikke har tatt hensyn til i utregningene, så våre resultater er gyldige for $j < 0.125$.

Contents

Preface and Acknowledgements

This master thesis is the culmination of my 5 year siv.ing./M.Sc. degree in Applied Physics and Mathematics at NTNU. It is also a continuation of a specialization project I did last semester as part of my degree, which focused on the sublattice magnetization.

I would like to take this opportunity to thank my supervisor John Ove Fjærestad for his patience and excellent tutoring for the past two semesters. All the friends I have made and all the strange people I have met during my stay at NTNU also deserve a big thanks for making the years seem to fly by. I offer a warm digital hand shake to all the excellent and eccentric professors who have made an effort to actually teach me something useful.

CØN

1 Introduction

What is the fundamental and defining difference between different states of matter? What is it that really separates a material in the liquid phase from a solid crystal? Precisely classifying different phases and understanding how they transition into one another is truly the heart of condensed matter physics. The classical theory to describe phases and phase transitions, is known as Landau symmetry breaking theory [1, 2]. The elegant idea behind this very successful theory, is that the order of the system can be characterized by its symmetry. For instance, a solid is a phase where all particles have formed in a grid structure with regular spacing between one another. This system can be labelled by its discrete translational symmetry in addition to other symmetry actions leaving the grid unchanged, such as rotations and reflections. Compared to the liquid phase, where all particles have a random distribution, there is a continuous rather than discrete translational symmetry. This is really the essence of the difference between these phases, a difference in symmetry.

What physically happens in a phase transition, is that a new system configuration suddenly becomes energetically preferable compared to the old structure. This translates into a spontaneous breaking of one of the Hamiltonian's symmetries in the context of Landau symmetry breaking theory, like the change from a continuous to a discrete translational symmetry in the case of a liquid freezing. A discontinuous change in the particle density of the system is also considered as a phase transition, and the symmetry does not necessarily have to change in this case. This allows us to have some different phases with the same symmetry, such as the liquid and gas states [1]. This framework allows us to classify more than just the everyday phases of matter, like the phenomenon of magnetism. Take the phase transition of the ferromagnet as an example: The spins of each atom or molecule in a ferromagnetic material are fluctuating with no long range correlation due to thermal excitations at high temperature. In terms of symmetries, this means that the system does not break the spin rotational symmetry of the Hamiltonian. Yet, when we lower the temperature beyond a certain critical point, the spins will align in the same direction and spontaneously break the rotational symmetry. Phase transitions are always accompanied by an order parameter, a quantity which changes abruptly when the system undergoes the transition [1]. The order parameter in the case of the ferromagnet would be the sublattice magnetization as this quantity is related to the long range spin correlation. Its value will therefore change from zero to non-zero when the symmetry is broken. The order parameter offer a useful tool to probe and precisely locate where the phase transition occurs, but a knowledge of the symmetry being broken is needed in order to define the appropriate order parameter.

Not all phase transitions are driven by the change of temperature. Quantum phase transitions are transitions at $T = 0$K, where quantum mechanical effects take over the role of thermal fluctuations. These transitions are created by changing a physical parameter of the system, such as the particle interaction strength or the strength of an external magnetic field. This is the type

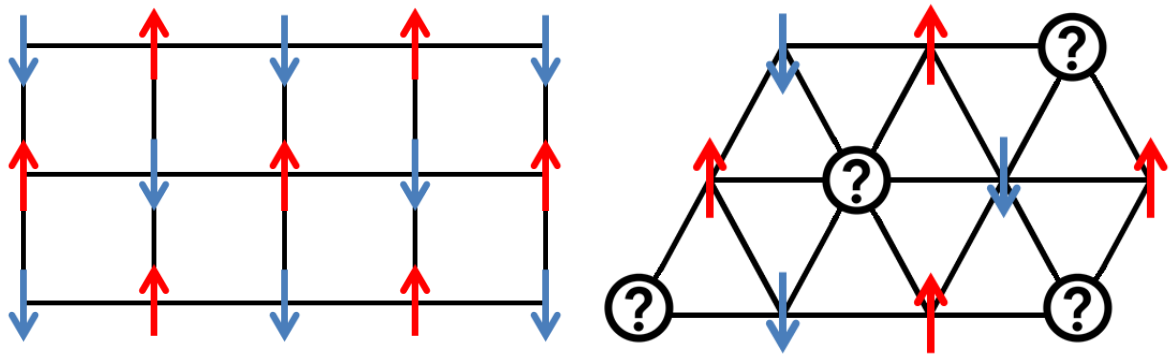

(a) The Ising antiferromagnet on the square lattice. (b) The Ising antiferromagnet on the triangular lattice.

Figure 1.1: Illustration of the Ising antiferromagnet on two different lattices. One Ising spin is placed in each vertex (lattice point), and lines indicate interaction between the spins. The Ising spins can either point up or down, i.e. out of or in to the paper plane.

of phase transition we will encounter in this report.

There are a multitude of different states of matter that can be described by the theory of spontaneous symmetry breaking, ranging from classical liquids and solids to inherently quantum mechanical materials like magnets. However, it turns out that some phases of matter can not be described in this way. Such states were discovered in the 1980s, and so a new type of order was needed to describe them in addition to their symmetries [2]. This new order is known as topological order, which is observed in systems with long range quantum entanglement. It is not easy to get a good grasp of what the essence of topological order really is, as opposed to the simple notion of "different phases have different symmetry" in regular symmetry breaking theory, but one of its characteristics is a topological degeneracy of ground states [2]. This degeneracy is closely related to the topology of the surface on which the system is embedded, which we will later demonstrate in section 4.1.

In this report, we will focus on a topologically ordered phase known as the spin liquid. This is a phase which breaks no symmetries of the grid and also retains spin rotation symmetry [3, 4]. The telltale long range quantum entanglement of a topologically ordered phase is in our case the result of a mechanic known as frustration. The system we will use to produce this phase is an antiferromagnet situated on a geometrically frustrating lattice. The idea of a frustrated magnet is a simple one, yet the results are far from trivial. It is best illustrated by considering a 2D lattice of Ising spins. An Ising spin is a very simplified version of a real spin: it may only point in two directions, up or down, and it is not treated as a quantum mechanical object. In addition, assume that the Ising spins only interact with their nearest neighbours. Now, in the ground state of an antiferromagnet, all spins would prefer to align in an antiparallel fashion with respect to their neighbours, as opposed to a ferromagnet where all spins would point in the same direction. As shown in fig. 1.1a, there is no trouble achieving antiparallel order on a

square lattice, the frustration first comes into play when we consider a grid such as the triangular lattice in fig. 1.1b. Since the neighbours of one Ising spin are also neighbours with each other, there is no way for all of the Ising spins to point in their preferred direction. This is the heart of frustration, competing interactions making it impossible to minimize the energy for all participants. There are many other ways to frustrate a system, for instance by introducing next nearest neighbour interactions or having a mixture of ferromagnetic and antiferromagnetic interactions. In the case of the Ising spin antiferromagnet on the triangular lattice, the frustration leads to a large degeneracy in ground states, shown in 1950 by Wannier [5], destroying the magnetic order.

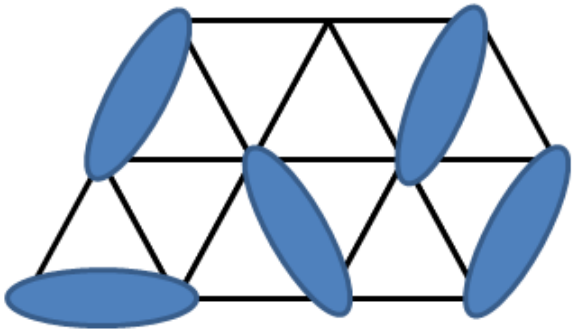

Figure 1.2: Illustration of a disordered valence bond state. The ovals represent a superposition of two spins, called a valence bond. In a spin liquid, longer ranged valence bonds are also present.

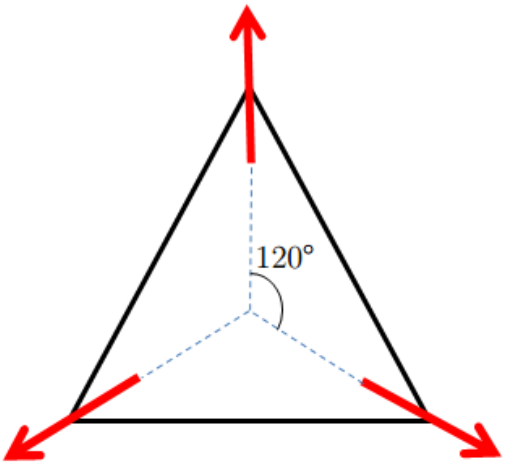

Figure 1.3: Illustration of the Néel order on the triangular lattice.

As one would imagine, a system of real physical spins has other possible ways to deal with

frustration than the Ising spin system. First of all, a spin is free to point in more than two directions, making it possible to achieve types of long range magnetic order different from the strictly antiparallel one. The solution for classical spins on the triangular lattice is a so called Néel order, where all of the spins are rotated 120° in relation to their nearest neighbours [6], see fig. 1.3. A spin is also exposed to Heisenberg's uncertainty principle, and behaves classically only if its magnitude $S \gg \frac{1}{2}$. However, when S is comparable to its smallest possible non-zero value, $S = \frac{1}{2}$, the quantum nature of the spins become important. In 1973, Anderson [7] suggested that the spins of a $S = \frac{1}{2}$ antiferromagnet could form entangled spin states, where two and two spins enter a quantum mechanical superposition called valence bonds. There are different types of such entangled states, one example is sown in fig. 1.2. A superposition of different disordered valence bond states where long range entanglement is included does preserve all spatial symmetries, making it a spin liquid [3, 4]. The first solid evidence that spin liquids exist came as late as 2011 [8], and so it remains a very hot topic in solid state physics today.

Anderson proposed that the Heisenberg antiferromagnet model, described by the Hamiltonian in eq. (2.1), could lead to a spin liquid state for $S = \frac{1}{2}$ on the triangular lattice. Since 1973, it has been concluded that the Heisenberg antiferromagnet does not result in a spin liquid for $S = \frac{1}{2}$, but shows the more classical Néel order in the ground state [6, 9, 10]. Nonetheless, if we treat the spin value as a continuous parameter, as is natural to do in a mean field theory, we do indeed find a spin liquid state for smaller S, $S < 0.21$ with only nearest neighbour interactions [9]. This means that there is a quantum phase transition from the magnetically unordered spin liquid phase to a magnetically ordered Néel state as we increase S for this model. This transition is what we will explore further, with the main objective of comparing different methods of finding the critical spin value resulting in a phase transition. We will describe the problem using Schwinger-boson mean field theory, which is a method for simplifying the Hamiltonian to the point where it can be diagonalized analytically. Compared to methods of numerical exact diagonalization, the mean field approximation makes it viable to study relatively large systems by sacrificing some numerical accuracy. We will focus on three different methods of detecting the phase transition:

We will first apply a standard method of investigating a magnetic phase transition, which is to use the sublattice magnetization as an order parameter. Our results are shown in chapter 3.

The second method we will use to detect the phase transition takes advantage of the ground state degeneracy of the topologically ordered spin liquid. The energy difference between the energetically degenerate states should be zero in the spin liquid phase, so we expect that $\Delta E \to 0$ as the system size $N \to \infty$. The difference in the scaling of ΔE as a function of N in the spin liquid phase and the Néel state will be looked into in chapter 4. As far as we know, a method like this has not been used before in this context.

The final tool we consider in chapter 5 is known as the quantum fidelity, or simply just fidelity, which is a measure of the difference between two quantum mechanical states [11]. The similarity of two states on different sides of a phase transition should be less than that of two states in the

same phase, and therefore the fidelity should be able to pick up on this change. The fidelity has been used to determine critical points in phase transitions in other similar system [11, 12].

2 The Mean Field Approximation

2.1 Initial Form

The model we will use to describe our system of N interacting spins on the triangular lattice, is the simple Heisenberg model. This model considers the particles located at each lattice point to be stationary, and only looks at interactions where two spins are involved. The Hamiltonian is given as

$$\mathcal{H} = \frac{1}{2}\sum_{\langle ij\rangle} J_{\langle ij\rangle}\hat{\mathbf{S}}_i \cdot \hat{\mathbf{S}}_j, \tag{2.1}$$

where $\hat{\mathbf{S}}_i$ is the spin vector on lattice site i and the strength and interaction type is described by the function $J_{\langle ij\rangle}$. A ferromagnetic interaction between the spins occur when $J_{\langle ij\rangle} < 0$, while $J_{\langle ij\rangle} > 0$ results in an antiferromagnet, which will be our focus. In the simplest case the sum runs over all closest neighbouring lattice sites i and j, but we will also include interactions between next nearest neighbouring spins. We will use the Schwinger-boson representation of the spin operators in our calculations, where the spin vector components are defined as [10]

$$\begin{aligned}
\hat{S}^x_j &= \frac{1}{2}\left(\hat{b}^\dagger_{j\uparrow}\hat{b}_{j\downarrow} + \hat{b}^\dagger_{j\downarrow}\hat{b}_{j\uparrow}\right)\\
\hat{S}^y_j &= \frac{1}{2i}\left(\hat{b}^\dagger_{j\uparrow}\hat{b}_{j\downarrow} - \hat{b}^\dagger_{j\downarrow}\hat{b}_{j\uparrow}\right)\\
\hat{S}^z_j &= \frac{1}{2}\left(\hat{b}^\dagger_{j\uparrow}\hat{b}_{j\uparrow} - \hat{b}^\dagger_{j\downarrow}\hat{b}_{j\downarrow}\right).
\end{aligned} \tag{2.2}$$

Here, $\hat{b}_{i\sigma}$ and $\hat{b}^\dagger_{i\sigma}$ are the bosonic annihilation and creation operators for bosons on lattice site i with spin index $\sigma \in \{+1, -1\} \equiv \{\uparrow, \downarrow\}$ respectively. They follow the commutator relations

$$\begin{aligned}
\left[\hat{b}_\mu, \hat{b}_\nu\right] &= 0\\
\left[\hat{b}^\dagger_\mu, \hat{b}^\dagger_\nu\right] &= 0\\
\left[\hat{b}_\mu, \hat{b}^\dagger_\nu\right] &= \delta_{\mu,\nu},
\end{aligned} \tag{2.3}$$

shown in eq. (A.5) in appendix A. The dot product of the spin operators can be expressed in a simpler way by introducing the $\hat{A}$ and $\hat{B}$ operators, also called the A and B fields,

$$\begin{aligned}\hat{A}^\dagger_{ij} &= \frac{1}{2}\sum_\sigma \sigma \hat{b}^\dagger_{i\sigma}\hat{b}^\dagger_{j\bar{\sigma}} = \frac{1}{2}\left(\hat{b}^\dagger_{i\uparrow}\hat{b}^\dagger_{j\downarrow} - \hat{b}^\dagger_{i\downarrow}\hat{b}^\dagger_{j\uparrow}\right) \\ \hat{B}^\dagger_{ij} &= \frac{1}{2}\sum_\sigma \hat{b}^\dagger_{i\sigma}\hat{b}_{j\sigma} \;\; = \frac{1}{2}\left(\hat{b}^\dagger_{i\uparrow}\hat{b}_{j\uparrow} + \hat{b}^\dagger_{i\downarrow}\hat{b}_{j\downarrow}\right),\end{aligned} \tag{2.4}$$

where $\bar{\sigma}$ is the compliment of σ. As shown in eq. (A.11), we have the relation

$$\hat{\mathbf{S}}_i \cdot \hat{\mathbf{S}}_j = :\hat{B}^\dagger_{ij}\hat{B}_{ij}: - \hat{A}^\dagger_{ij}\hat{A}_{ij} = \hat{B}^\dagger_{ij}\hat{B}_{ij} - \hat{A}^\dagger_{ij}\hat{A}_{ij} - \frac{1}{4}\left(\hat{b}^\dagger_{i\uparrow}\hat{b}_{i\uparrow} + \hat{b}^\dagger_{i\downarrow}\hat{b}_{i\downarrow}\right). \tag{2.5}$$

The :: indicates normal ordering of the boson operators, meaning that the creation operators should be on the left of their corresponding annihilation operator. To achieve a quadratic Hamiltonian, we must simplify eq. (2.5). To do this, we perform a so called mean field approximation of the A and B fields. First, we rewrite the fields as a deviation from their expectation value,

$$\hat{A}_{ij} \equiv \left\langle \hat{A}_{ij} \right\rangle + \delta\hat{A}_{ij}, \tag{2.6}$$

where the expectation value in our case can be taken as a real number

$$\left\langle \hat{A}_{ij} \right\rangle \equiv \mathcal{A}_{ij}. \tag{2.7}$$

Inserting this back into eq. (2.5), as shown in eq. (A.12), gives the decoupled equation

$$\hat{\mathbf{S}}_i \cdot \hat{\mathbf{S}}_j = \mathcal{A}^2_{ij} - \mathcal{B}^2_{ij} + \mathcal{B}_{ij}\hat{B}_{ij} + \mathcal{B}_{ij}\hat{B}^\dagger_{ij} - \mathcal{A}_{ij}\hat{A}_{ij} - \mathcal{A}_{ij}\hat{A}^\dagger_{ij} - \frac{1}{4}\left(\hat{b}^\dagger_{i\uparrow}\hat{b}_{i\uparrow} + \hat{b}^\dagger_{i\downarrow}\hat{b}_{i\downarrow}\right) + \mathcal{O}(\delta^2). \tag{2.8}$$

Making the approximation that the deviations in the fields are small, i.e. neglecting terms of $\mathcal{O}(\delta^2)$, we get the mean field Hamiltonian

$$\mathcal{H}_{MF} = \frac{1}{2}\sum_{\langle ij\rangle} J_{\langle ij\rangle}\left(\mathcal{A}^2_{ij} - \mathcal{B}^2_{ij} + \mathcal{B}_{ij}\hat{B}_{ij} + \mathcal{B}_{ij}\hat{B}^\dagger_{ij} - \mathcal{A}_{ij}\hat{A}_{ij} - \mathcal{A}_{ij}\hat{A}^\dagger_{ij} - \frac{1}{4}\left(\hat{b}^\dagger_{i\uparrow}\hat{b}_{i\uparrow} + \hat{b}^\dagger_{i\downarrow}\hat{b}_{i\downarrow}\right)\right), \tag{2.9}$$

which is quadratic instead of quartic in the boson operators. Instead of summing over the index $\langle ij\rangle$, we can eliminate j by defining the vector spatially separating the two neighbouring lattice sites i and j,

$$\boldsymbol{d} \equiv \boldsymbol{r}_j - \boldsymbol{r}_i. \tag{2.10}$$

This set of vectors will consist of two subsets of vectors in our analysis, the vectors $\boldsymbol{\delta}$ connecting two nearest neighbours, and the vectors $\boldsymbol{\Delta}$ connecting two next nearest neighbours. There are 6 vectors in each subset on the triangular lattice, but their exact form is not important in this chapter[1]. The sum $\sum_{\langle ij\rangle}$ can now be written as $\sum_i \sum_{\boldsymbol{d}}$ if we let $j \to i + \boldsymbol{d}$ in the indices of our

[1] See eq. (B.3) and eq. (B.4) for a description of the different vectors.

equations[2]. We now let the interaction strength J be independent of position in the lattice, that is $J_{\langle ij\rangle} \to J_{\boldsymbol{d}}$. This forces the mean values of the A and B fields to also be independent of their lattice positions due to the symmetry restrictions of the triangular lattice and spin liquid state. See section 2.3 for a more detailed explanation. In other words, $\mathcal{A}_{ij} \to \mathcal{A}_{\boldsymbol{d}}$ and $\mathcal{B}_{ij} \to \mathcal{B}_{\boldsymbol{d}}$.

As it turns out, completing the spin algebra

$$\hat{S}_i^2 |\Psi\rangle = S(S+1)|\Psi\rangle \tag{2.11}$$

in the Schwinger-boson representation of our problem imposes a restriction on the number of bosons on each site. Equation (A.14) shows that we must require

$$\hat{n}_i |\Psi\rangle = 2S|\Psi\rangle\,. \tag{2.12}$$

Here, the operator

$$\hat{n}_i \equiv \hat{n}_{i\uparrow} + \hat{n}_{i\downarrow} \equiv \hat{b}_{i\uparrow}^\dagger \hat{b}_{i\uparrow} + \hat{b}_{i\downarrow}^\dagger \hat{b}_{i\downarrow} \tag{2.13}$$

is known as the number operator, as its eigen value counts the number of bosons on lattice site i [13]. Instead of imposing this as an eigen value constraint, we will approximate it as a constraint on the expectation value:

$$\langle \hat{n}_i \rangle = 2S. \tag{2.14}$$

The method of Lagrange multipliers is a natural way to incorporate the constraint into our Hamiltonian. To strictly satisfy the constraint, we would need N Lagrange multipliers, one for each lattice site:

$$\lambda_i (\hat{n}_i - 2S) = 0. \tag{2.15}$$

However, we will also relax this constraint, and only try to satisfy it on average

$$\lambda \sum_i (\hat{n}_i - 2S) = 0. \tag{2.16}$$

The resulting Hamiltonian reads

$$\begin{aligned}
\overline{\mathcal{H}}_{MF} =& \mathcal{H}_{MF} + \lambda \sum_i \left(\hat{b}_{i\uparrow}^\dagger \hat{b}_{i\uparrow} + \hat{b}_{i\downarrow}^\dagger \hat{b}_{i\downarrow} \right) - 2NS\lambda \\
=& \frac{1}{2} \sum_{i,\boldsymbol{d}} J_{\boldsymbol{d}} \Big(\mathcal{A}_{\boldsymbol{d}}^2 - \mathcal{B}_{\boldsymbol{d}}^2 + \mathcal{B}_{\boldsymbol{d}} (\hat{B}_{i,i+\boldsymbol{d}} + \hat{B}_{i,i+\boldsymbol{d}}^\dagger) - \mathcal{A}_{\boldsymbol{d}} (\hat{A}_{i,i+\boldsymbol{d}} + \hat{A}_{i,i+\boldsymbol{d}}^\dagger) - \frac{1}{4} \left(\hat{b}_{i\uparrow}^\dagger \hat{b}_{i\uparrow} + \hat{b}_{i\downarrow}^\dagger \hat{b}_{i\downarrow} \right) \Big) \\
&+ \lambda \sum_i \left(\hat{b}_{i\uparrow}^\dagger \hat{b}_{i\uparrow} + \hat{b}_{i\downarrow}^\dagger \hat{b}_{i\downarrow} \right) - 2NS\lambda.
\end{aligned} \tag{2.17}$$

[2] The somewhat confusing notation $i + \boldsymbol{d}$ is equivalent to $\boldsymbol{r}_i + \boldsymbol{d}$.

2.2 Diagonalizing the Hamiltonian

We would like to express eq. (2.17) as a simple diagonal Hamiltonian, reminiscent of the Hamiltonian describing decoupled harmonic oscillators. In our case, a diagonal Hamiltonian would only consist of pairs of annihilation and creation operators, where all pairs would be non-interacting/decoupled [14]. This is the point of the mean field approximation, but eq. (2.17) is clearly not yet diagonal, as the A field contains anomalous terms[3] and both fields mix bosons on different lattice sites. The process of diagonalizing the Hamiltonian will involve two different transformations: the Fourier transform and the Bogoliubov transform.

2.2.1 Fourier Transform

The first step in diagonalizing the Hamiltonian (2.17) is to perform a Fourier transformation. The Fourier transformation of the Schwinger-boson operators is defined as

$$\hat{b}_{i\sigma} = \frac{1}{\sqrt{N}} \sum_{\boldsymbol{k}} e^{i\boldsymbol{k}\cdot\boldsymbol{r}_i} \hat{b}_{\boldsymbol{k}\sigma}, \tag{2.18}$$

with the inverse transformation

$$\hat{b}_{\boldsymbol{k}\sigma} = \frac{1}{\sqrt{N}} \sum_{i} e^{-i\boldsymbol{k}\cdot\boldsymbol{r}_i} \hat{b}_{i\sigma}. \tag{2.19}$$

Here, the sum in eq. (2.18) runs over all wave vectors $\boldsymbol{k}$ in the first Brillouin zone, see fig. B.3 and appendix B for a more detailed look at the transformation. The Fourier transformed operators leaves the commutator relation eq. (2.3) unchanged, this is shown in eq. (A.6). Inserting the Fourier transformed operators into the Hamiltonian (2.17) and performing the sum over i, we get

$$\begin{aligned}
\overline{\mathcal{H}}_{MF} = & \frac{1}{2} N \sum_{\boldsymbol{d}} J_{\boldsymbol{d}} \left(\mathcal{A}_{\boldsymbol{d}}^2 - \mathcal{B}_{\boldsymbol{d}}^2 \right) + \frac{1}{2} \sum_{\boldsymbol{k},\boldsymbol{d}} J_{\boldsymbol{d}} \mathcal{B}_{\boldsymbol{d}} \cos(\boldsymbol{k}\cdot\boldsymbol{d}) \left(\hat{b}_{\boldsymbol{k}\uparrow}^\dagger \hat{b}_{\boldsymbol{k}\uparrow} + \hat{b}_{\boldsymbol{k}\downarrow}^\dagger \hat{b}_{\boldsymbol{k}\downarrow} \right) \\
& - \frac{1}{4} \sum_{\boldsymbol{k},\boldsymbol{d}} J_{\boldsymbol{d}} \mathcal{A}_{\boldsymbol{d}} \left(\cos(\boldsymbol{k}\cdot\boldsymbol{d}) - i \sin(\boldsymbol{k}\cdot\boldsymbol{d}) \right) \left(\hat{b}_{-\boldsymbol{k}\downarrow} \hat{b}_{\boldsymbol{k}\uparrow} - \hat{b}_{-\boldsymbol{k}\uparrow} \hat{b}_{\boldsymbol{k}\downarrow} \right) \\
& - \frac{1}{4} \sum_{\boldsymbol{k},\boldsymbol{d}} J_{\boldsymbol{d}} \mathcal{A}_{\boldsymbol{d}} \left(\cos(\boldsymbol{k}\cdot\boldsymbol{d}) + i \sin(\boldsymbol{k}\cdot\boldsymbol{d}) \right) \left(\hat{b}_{-\boldsymbol{k}\downarrow}^\dagger \hat{b}_{\boldsymbol{k}\uparrow}^\dagger - \hat{b}_{-\boldsymbol{k}\uparrow}^\dagger \hat{b}_{\boldsymbol{k}\downarrow}^\dagger \right) \\
& - \frac{1}{8} \sum_{\boldsymbol{k},\boldsymbol{d}} J_{\boldsymbol{d}} \left(\hat{b}_{\boldsymbol{k}\uparrow}^\dagger \hat{b}_{\boldsymbol{k}\uparrow} + \hat{b}_{\boldsymbol{k}\downarrow}^\dagger \hat{b}_{\boldsymbol{k}\downarrow} \right) + \lambda \sum_{\boldsymbol{k}} \left(\hat{b}_{\boldsymbol{k}\uparrow}^\dagger \hat{b}_{\boldsymbol{k}\uparrow} + \hat{b}_{\boldsymbol{k}\downarrow}^\dagger \hat{b}_{\boldsymbol{k}\downarrow} \right) - 2NS\lambda,
\end{aligned} \tag{2.20}$$

where we have used eq. (A.15) and eq. (A.16). The first Brillouin zone is symmetric in $\boldsymbol{k}$, so we may relabel and sum over $-\boldsymbol{k}$ instead, to simplify the anomalous terms in the expression above. Due to the symmetries of $\cos(\boldsymbol{k}\cdot\boldsymbol{d})$ and $\sin(\boldsymbol{k}\cdot\boldsymbol{d})$, this leads to

[3] Anomalous in the sense that the terms do not consist of one creation and one annihilation operator.

$$\sum_{\boldsymbol{k}} \cos(\boldsymbol{k}\cdot\boldsymbol{d})\left(\hat{b}_{-\boldsymbol{k}\downarrow}\hat{b}_{\boldsymbol{k}\uparrow} - \hat{b}_{-\boldsymbol{k}\uparrow}\hat{b}_{\boldsymbol{k}\downarrow} + \hat{b}^{\dagger}_{-\boldsymbol{k}\downarrow}\hat{b}^{\dagger}_{\boldsymbol{k}\uparrow} - \hat{b}^{\dagger}_{-\boldsymbol{k}\uparrow}\hat{b}^{\dagger}_{\boldsymbol{k}\downarrow}\right) = 0, \tag{2.21}$$

and

$$\sum_{\boldsymbol{k}} \sin(\boldsymbol{k}\cdot\boldsymbol{d})\left(\hat{b}_{-\boldsymbol{k}\downarrow}\hat{b}_{\boldsymbol{k}\uparrow} - \hat{b}_{-\boldsymbol{k}\uparrow}\hat{b}_{\boldsymbol{k}\downarrow} - \hat{b}^{\dagger}_{-\boldsymbol{k}\downarrow}\hat{b}^{\dagger}_{\boldsymbol{k}\uparrow} + \hat{b}^{\dagger}_{-\boldsymbol{k}\uparrow}\hat{b}^{\dagger}_{\boldsymbol{k}\downarrow}\right) = 2\sum_{\boldsymbol{k}} \sin(\boldsymbol{k}\cdot\boldsymbol{d})\left(\hat{b}_{-\boldsymbol{k}\downarrow}\hat{b}_{\boldsymbol{k}\uparrow} - \hat{b}^{\dagger}_{-\boldsymbol{k}\downarrow}\hat{b}^{\dagger}_{\boldsymbol{k}\uparrow}\right). \tag{2.22}$$

With the definitions

$$\gamma^{B}_{\boldsymbol{k}} \equiv \frac{1}{2}\sum_{\boldsymbol{d}} J_{\boldsymbol{d}}\mathcal{B}_{\boldsymbol{d}}\cos(\boldsymbol{k}\cdot\boldsymbol{d}) \tag{2.23}$$

$$\gamma^{A}_{\boldsymbol{k}} \equiv \frac{1}{2}\sum_{\boldsymbol{d}} J_{\boldsymbol{d}}\mathcal{A}_{\boldsymbol{d}}\sin(\boldsymbol{k}\cdot\boldsymbol{d}), \tag{2.24}$$

eq. (2.20) becomes

$$\begin{aligned}\overline{\mathcal{H}}_{MF} = &\frac{1}{2}N\sum_{\boldsymbol{d}} J_{\boldsymbol{d}}\left(\mathcal{A}^2_{\boldsymbol{d}} - \mathcal{B}^2_{\boldsymbol{d}}\right) - 2SN\lambda + \sum_{\boldsymbol{k}}\left(\gamma^{B}_{\boldsymbol{k}} + \lambda - \frac{1}{8}\sum_{\boldsymbol{d}} J_{\boldsymbol{d}}\right)\left(\hat{b}^{\dagger}_{\boldsymbol{k}\uparrow}\hat{b}_{\boldsymbol{k}\uparrow} + \hat{b}^{\dagger}_{\boldsymbol{k}\downarrow}\hat{b}_{\boldsymbol{k}\downarrow}\right)\\ &+ i\sum_{\boldsymbol{k}}\gamma^{A}_{\boldsymbol{k}}\left(\hat{b}_{-\boldsymbol{k}\downarrow}\hat{b}_{\boldsymbol{k}\uparrow} - \hat{b}^{\dagger}_{-\boldsymbol{k}\downarrow}\hat{b}^{\dagger}_{\boldsymbol{k}\uparrow}\right).\end{aligned} \tag{2.25}$$

This expression can be simplified further by defining

$$\tilde{\lambda} \equiv \lambda - \frac{1}{8}\sum_{\boldsymbol{d}} J_{\boldsymbol{d}} \tag{2.26}$$

and

$$\tau \equiv \frac{1}{2}\sum_{\boldsymbol{d}} J_{\boldsymbol{d}}\left(\mathcal{A}^2_{\boldsymbol{d}} - \mathcal{B}^2_{\boldsymbol{d}} - \frac{S}{2}\right), \tag{2.27}$$

resulting in the slightly more compact form of the Hamiltonian:

$$\overline{\mathcal{H}}_{MF} = N\tau - 2SN\tilde{\lambda} + \sum_{\boldsymbol{k}}(\gamma^{B}_{\boldsymbol{k}} + \tilde{\lambda})\left(\hat{b}^{\dagger}_{\boldsymbol{k}\uparrow}\hat{b}_{\boldsymbol{k}\uparrow} + \hat{b}^{\dagger}_{\boldsymbol{k}\downarrow}\hat{b}_{\boldsymbol{k}\downarrow}\right) + i\gamma^{A}_{\boldsymbol{k}}\left(\hat{b}_{-\boldsymbol{k}\downarrow}\hat{b}_{\boldsymbol{k}\uparrow} - \hat{b}^{\dagger}_{-\boldsymbol{k}\downarrow}\hat{b}^{\dagger}_{\boldsymbol{k}\uparrow}\right). \tag{2.28}$$

By defining

$$\hat{\phi}_{\boldsymbol{k}} \equiv \begin{pmatrix} \hat{b}_{\boldsymbol{k}\uparrow} \\ i\hat{b}^{\dagger}_{-\boldsymbol{k}\downarrow} \end{pmatrix} \tag{2.29}$$

and

$$M_{\boldsymbol{k}} \equiv \begin{pmatrix} \gamma^{B}_{\boldsymbol{k}} + \tilde{\lambda} & -\gamma^{A}_{\boldsymbol{k}} \\ -\gamma^{A}_{\boldsymbol{k}} & \gamma^{B}_{\boldsymbol{k}} + \tilde{\lambda} \end{pmatrix}, \tag{2.30}$$

the Hamiltonian can be written in matrix form:

$$\begin{aligned}\overline{\mathcal{H}}_{MF}&=N\tau-2NS\tilde{\lambda}+\sum_k \hat{\phi}_k^\dagger M_k \hat{\phi}_k-\sum_k(\gamma_k^B+\tilde{\lambda})\\&=N\tau-2N(S+\frac{1}{2})\tilde{\lambda}+\sum_k \hat{\phi}_k^\dagger M_k \hat{\phi}_k,\end{aligned} \tag{2.31}$$

where we have used eq. (A.17).

2.2.2 Bogoliubov Transform

We are getting close to a diagonalized Hamiltonian, but it is necessary to perform one last transformation. This is known as a Bogoliubov transformation, where the aim is to find a set of new operators $\{\hat{\eta}_{k\sigma}\}$, to diagonalize M_k. We define

$$\hat{\psi}_k \equiv \begin{pmatrix}\hat{\eta}_{k\uparrow}\\ \hat{\eta}_{k\downarrow}^\dagger\end{pmatrix}, \tag{2.32}$$

and transform the operators in the following way:

$$\hat{\psi}_k = \begin{pmatrix}u_k & v_k\\ x_k & y_k\end{pmatrix}\hat{\phi}_k \equiv C_k\hat{\phi}_k. \tag{2.33}$$

All the elements of matrix C_k are chosen to be real functions of $\boldsymbol{k}$ in this transformation. We require that the new operators follow the same commutator relations, see eq. (2.3), as the old operators. That is:

$$\begin{aligned}[\hat{\eta}_{k\uparrow},\hat{\eta}_{k'\uparrow}^\dagger]&=\delta_{k,k'}\\ [\hat{\eta}_{k\downarrow},\hat{\eta}_{k'\downarrow}^\dagger]&=\delta_{k,k'}\\ [\hat{\eta}_{k\uparrow},\hat{\eta}_{k'\downarrow}]&=0\end{aligned} \tag{2.34}$$

These relations reduce to three constraints on the functions of C_k,

$$\begin{aligned}u_k^2-v_k^2&=1,\\ y_k^2-x_k^2&=1,\\ u_k x_k&=v_k y_k,\end{aligned} \tag{2.35}$$

shown in eq. (A.7). Inspired by the hyperbolic relation $\cosh^2(a)-\sinh^2(a)=1$, we parameterize these functions in a similar way. The two first constraints give

$$u_k = \cosh(\theta_k),\, v_k = \sinh(\theta_k)$$
$$x_k = \sinh(\chi_k)\,,\, y_k = \cosh(\chi_k), \tag{2.36}$$

and the third can then be written as

$$\tanh(\theta_k) = \tanh(\chi_k), \tag{2.37}$$

which holds if $\theta_k = \chi_k$ for all $\boldsymbol{k}$. Inserting this back into eq. (2.33) gives us

$$\hat{\psi}_k = \begin{pmatrix} \cosh(\theta_k) & \sinh(\theta_k) \\ \sinh(\theta_k) & \cosh(\theta_k) \end{pmatrix} \hat{\phi}_k \Longrightarrow \hat{\phi}_k = \begin{pmatrix} \cosh(\theta_k) & -\sinh(\theta_k) \\ -\sinh(\theta_k) & \cosh(\theta_k) \end{pmatrix} \hat{\psi}_k. \tag{2.38}$$

Now, the Hamiltonian (2.31) reads

$$\overline{\mathcal{H}}_{MF} = N\tau - 2N(S + \frac{1}{2})\tilde{\lambda} + \sum_{\boldsymbol{k}} \hat{\psi}^\dagger_{\boldsymbol{k}} \Big((C^{-1}_{\boldsymbol{k}})^\dagger M_{\boldsymbol{k}} C^{-1}_{\boldsymbol{k}} \Big) \hat{\psi}_{\boldsymbol{k}}, \tag{2.39}$$

where the matrix we want to diagonalize is

$$(C^{-1}_{\boldsymbol{k}})^\dagger M_{\boldsymbol{k}} C^{-1}_{\boldsymbol{k}} = \begin{pmatrix} (\gamma^B_{\boldsymbol{k}} + \tilde{\lambda})\cosh(2\theta_{\boldsymbol{k}}) + \gamma^A_{\boldsymbol{k}} \sinh(2\theta_{\boldsymbol{k}}) & -\gamma^A_{\boldsymbol{k}} \cosh(2\theta_{\boldsymbol{k}}) - (\gamma^B_{\boldsymbol{k}} + \tilde{\lambda})\sinh(2\theta_{\boldsymbol{k}}) \\ -\gamma^A_{\boldsymbol{k}} \cosh(2\theta_{\boldsymbol{k}}) - (\gamma^B_{\boldsymbol{k}} + \tilde{\lambda})\sinh(2\theta_{\boldsymbol{k}}) & (\gamma^B_{\boldsymbol{k}} + \tilde{\lambda})\cosh(2\theta_{\boldsymbol{k}}) + \gamma^A_{\boldsymbol{k}} \sinh(2\theta_{\boldsymbol{k}}) \end{pmatrix}.$$

A diagonal Hamiltonian is achieved when the diagonal components of this matrix are zero, which happens when

$$-\gamma^A_{\boldsymbol{k}} \cosh(2\theta_{\boldsymbol{k}}) - (\gamma^B_{\boldsymbol{k}} + \tilde{\lambda})\sinh(2\theta_{\boldsymbol{k}}) = 0. \tag{2.40}$$

This equation can more conveniently be written as two equations,

$$\cosh(2\theta_{\boldsymbol{k}}) = \frac{|\gamma^B_{\boldsymbol{k}} + \tilde{\lambda}|}{\sqrt{(\gamma^B_{\boldsymbol{k}} + \tilde{\lambda})^2 - (\gamma^A_{\boldsymbol{k}})^2}} = \mathrm{sgn}(\gamma^B_{\boldsymbol{k}} + \tilde{\lambda}) \frac{\gamma^B_{\boldsymbol{k}} + \tilde{\lambda}}{\sqrt{(\gamma^B_{\boldsymbol{k}} + \tilde{\lambda})^2 - (\gamma^A_{\boldsymbol{k}})^2}}, \tag{2.41}$$

$$\sinh(2\theta_{\boldsymbol{k}}) = \mathrm{sgn}(\gamma^B_{\boldsymbol{k}} + \tilde{\lambda}) \frac{-\gamma^A_{\boldsymbol{k}}}{\sqrt{(\gamma^B_{\boldsymbol{k}} + \tilde{\lambda})^2 - (\gamma^A_{\boldsymbol{k}})^2}}, \tag{2.42}$$

and we see that

$$\theta_{-\boldsymbol{k}} = -\theta_{\boldsymbol{k}}. \tag{2.43}$$

We have finally arrived at a diagonal Hamiltonian,

$$\begin{aligned}\overline{\mathcal{H}}_{MF} &= N\tau - 2N(S+\frac{1}{2})\tilde{\lambda} + \sum_{\boldsymbol{k}} \hat{\psi}^{\dagger}_{\boldsymbol{k}} \begin{pmatrix} \omega_{\boldsymbol{k}} & 0 \\ 0 & \omega_{\boldsymbol{k}} \end{pmatrix} \hat{\psi}_{\boldsymbol{k}} \\ &= N\tau - 2N(S+\frac{1}{2})\tilde{\lambda} + \sum_{\boldsymbol{k}} \omega_{k} + \sum_{\boldsymbol{k}} \omega_{\boldsymbol{k}} \left(\hat{\eta}^{\dagger}_{\boldsymbol{k}\uparrow} \hat{\eta}_{\boldsymbol{k}\uparrow} + \hat{\eta}^{\dagger}_{\boldsymbol{k}\downarrow} \hat{\eta}_{\boldsymbol{k}\downarrow} \right), \end{aligned} \tag{2.44}$$

with the dispersion relation

$$\omega_{\boldsymbol{k}} = \sqrt{(\gamma^{B}_{\boldsymbol{k}} + \tilde{\lambda})^2 - (\gamma^{A}_{\boldsymbol{k}})^2}, \tag{2.45}$$

where we have used eq. (2.41) and eq. (2.42). Note that the factor $\mathrm{sgn}(\gamma^{B}_{\boldsymbol{k}} + \tilde{\lambda})$ must be equal to +1 for all $\boldsymbol{k}$ for the diagonalization to work, as a negative sign here would result in a negative dispersion relation. A negative $\omega_{\boldsymbol{k}}$ would mean that we could lower the energy of the system by inserting more bosons into the negative energy states, and since there is no limit to how many bosons we can squeeze into one state, the system would no longer have a ground state. So, the plus sign is assumed to hold from this point on, and will be handled in the numerical analysis.

2.2.3 The Mean Field Equations

Equation (2.44) is the final form of our Hamiltonian, which is very similar to a Hamiltonian of 2N decoupled simple harmonic oscillators. The ground state $|G\rangle$ is characterized by

$$\begin{aligned} \hat{\eta}_{\boldsymbol{k}\sigma} |G\rangle &= 0 \\ \langle G| \hat{\eta}^{\dagger}_{\boldsymbol{k}\sigma} &= 0, \end{aligned} \tag{2.46}$$

since it minimizes the variable term in the Hamiltonian, and the ground state energy of the system at $T = 0$K is given as

$$E_0 \equiv \left\langle \overline{\mathcal{H}}_{MF} \right\rangle = N\tau - 2N(S+\frac{1}{2})\tilde{\lambda} + \sum_{\boldsymbol{k}} \omega_{k}. \tag{2.47}$$

We now impose the original constraint (2.16) as well as minimizing E_0 with respect to the parameters $\mathcal{A}_{\boldsymbol{d}}$ and $\mathcal{B}_{\boldsymbol{d}}$ by differentiating, as is usual when dealing with a minimization problem:

$$\begin{aligned} \frac{\partial E_0}{\partial \mathcal{A}_{\boldsymbol{d}}} &= 0 \\ \frac{\partial E_0}{\partial \mathcal{B}_{\boldsymbol{d}}} &= 0 \\ \frac{\partial E_0}{\partial \lambda} &= 0. \end{aligned} \tag{2.48}$$

This gives us the so-called mean field equations,

$$\begin{aligned}\mathcal{A}_{\boldsymbol{d}} &= \frac{1}{2N}\sum_{\boldsymbol{k}} \frac{\gamma_{\boldsymbol{k}}^{A}}{\omega_{\boldsymbol{k}}} \sin(\boldsymbol{k}\cdot\boldsymbol{d}) \\ \mathcal{B}_{\boldsymbol{d}} &= \frac{1}{2N}\sum_{\boldsymbol{k}} \frac{\gamma_{\boldsymbol{k}}^{B}+\tilde{\lambda}}{\omega_{\boldsymbol{k}}} \cos(\boldsymbol{k}\cdot\boldsymbol{d}) \\ S+\frac{1}{2} &= \frac{1}{2N}\sum_{\boldsymbol{k}} \frac{\gamma_{\boldsymbol{k}}^{B}+\tilde{\lambda}}{\omega_{\boldsymbol{k}}},\end{aligned} \tag{2.49}$$

derived in eq. (A.18).

2.3 Symmetries of the System

We now have the core equations needed to perform any numerical analysis of our spin system. However, some simplifications can be made by utilizing the underlying symmetries of the spin liquid state, the triangular grid and the A and B fields. We have already, and without much explanation, used the translational symmetry of the triangular grid to reduce the number of mean field parameters drastically. We will now take a closer look at the symmetry arguments and simplify the mean field equations further.

In contrast to a magnetically ordered system, the spin liquid state breaks no spatial symmetries. Therefore, we are able to translate, reflect and rotate our system without changing the physical state of it as long as we obey the geometry of the lattice. The triangular grid has four distinct symmetry actions that leave it unchanged, translation by a lattice constant in two directions T_1 and T_2 [4], a reflection σ through[5] a nearest neighbour bond and a rotation R of $\pi/3$ about the axis through a lattice point perpendicular to the lattice plane. We need not require the states before and after a symmetry operation to be precisely identical, as long as the physical picture is unchanged. This means that we can allow such states to be different up to a gauge transformation. It is clear that we do have a gauge freedom in our system, as the transformation

$$\hat{b}_{j\sigma} \Rightarrow e^{i\phi_j}\hat{b}_{j\sigma}. \tag{2.50}$$

leaves all our physical observables, notably the spin vector, unchanged [9]. This transforms the A and B fields in the following way:

$$\hat{A}_{ij} \Rightarrow e^{-i(\phi_i+\phi_j)}\hat{A}_{ij} \tag{2.51}$$

$$\hat{B}_{ij} \Rightarrow e^{i(\phi_i-\phi_j)}\hat{B}_{ij}. \tag{2.52}$$

[4] See fig. B.1 and eq. (B.1).

[5] Not to be confused by the spin index σ.

So if we translate the system in direction T_1, we should only have to perform a gauge transformation as shown above to connect the original to the translated system. However, as Wang and Vishwanath show in their paper [9], only certain values of the phases ϕ_j can be chosen for the system to still describe a spin liquid state. Each of the four symmetry operations have their own respective gauge phase, and they are as follows:

$$\begin{aligned} \phi_{T_1} &= \phi_{T_2} = \phi_\sigma = 0 \\ \phi_R &= \pi/2. \end{aligned} \tag{2.53}$$

Notice that the phases are all independent of the lattice position, so all of the Schwinger-bosons are transformed in the same way. This set of gauge phases describe what is call the zero-flux phase in paper [9], but there are other sets describing more complicated phases. The π-flux phase has a unit cell which is double that of the zero-flux phase, and becomes energetically preferable for high next nearest neighbour interactions [9]. The phase diagram in figure 8 in paper [9] shows the boundary between the zero-flux phase and the π-flux phase, and we will not enter the π-flux part of the phase diagram in our calculations.

We may now use these phases to greatly reduce the number of parameters needed to describe our system. We only need to know the mean field parameters associated with the bonds connecting a lattice point to its neighbours, as the other parameters are found by simply translating the system and performing a gauge transformation with $\phi = 0$. This can be written as

$$\mathcal{A}_{ij} \Rightarrow \mathcal{A}_{\boldsymbol{d}} \tag{2.54}$$

$$\mathcal{B}_{ij} \Rightarrow \mathcal{B}_{\boldsymbol{d}}, \tag{2.55}$$

as we have already done in our previous calculations. By also using the antisymmetric and symmetric properties of the A and B field respectively,

$$\hat{A}_{ij} = -\hat{A}_{ji} \Rightarrow \mathcal{A}_{\boldsymbol{d}} = -\mathcal{A}_{-\boldsymbol{d}} \tag{2.56}$$

$$\hat{B}_{ij} = \hat{B}^\dagger_{ji} \quad \Rightarrow \mathcal{B}_{\boldsymbol{d}} = \mathcal{B}_{-\boldsymbol{d}}, \tag{2.57}$$

we have reduced the number of mean field parameters from $24N + 1$ to $12 + 1$[6]. We have yet to use the reflection and rotational symmetry of the lattice, doing so requires a bit more thought. Consider fig. 2.1 which shows a close up picture of the triangular lattice with only nearest neighbour interactions. Each bond has an arrow attached to it to signify the "direction" of the A field, the A field is positive in the direction of the arrow. There is no arrow needed to keep track of the B field, as it is symmetric and has no direction in this sense. The configuration of the arrow directions is one of 8 equivalent possibilities that respect the antisymmetry of the A

[6] 3 A field and 3 B field parameters for the nearest neighbour A and B fields, $3 + 3$ parameters for the next nearest neighbour A and B fields, and $\tilde{\lambda}$ for the boson number constraint.

field, and is simply chosen for convenience. The bonds are labelled 1-3, with their respective mean field parameters $\mathcal{A}_1$-$\mathcal{A}_3$ and $\mathcal{B}_1$-$\mathcal{B}_3$. Now, consider a rotation of the system of $\pi/3$ about the lattice pint located at the origin, transforming the state of the system:

$$\Big(\mathcal{A}_1,\mathcal{A}_2,\mathcal{A}_3\Big)\overset{R}{\Rightarrow}\Big(-\mathcal{A}_3,-\mathcal{A}_1,-\mathcal{A}_2\Big) \tag{2.58}$$

$$\Big(\mathcal{B}_1,\mathcal{B}_2,\mathcal{B}_3\Big)\overset{R}{\Rightarrow}\Big(\mathcal{B}_3,\mathcal{B}_1,\mathcal{B}_2\Big). \tag{2.59}$$

Note that the sign changes for the A field is due to the directions of the arrows. We may now perform a gauge transformation of $e^{-i\cdot 2\phi_R} = -1$ for the A field and $e^{i(\phi_R-\phi_R)} = +1$ for the B field:

$$\Big(-\mathcal{A}_3,-\mathcal{A}_1,-\mathcal{A}_2\Big)\overset{\phi_R}{\Longrightarrow}\Big(\mathcal{A}_3,\mathcal{A}_1,\mathcal{A}_2\Big) \tag{2.60}$$

$$\Big(\mathcal{B}_3,\mathcal{B}_1,\mathcal{B}_2\Big) \quad \overset{\phi_R}{\Longrightarrow}\Big(\mathcal{B}_3,\mathcal{B}_1,\mathcal{B}_2\Big). \tag{2.61}$$

As the system should now be in the same state as before the rotation, we may equate the parameters:

$$\mathcal{A}_1{=}\mathcal{A}_3\ ,\ \mathcal{A}_2{=}\mathcal{A}_1\ ,\ \mathcal{A}_3{=}\mathcal{A}_2 \tag{2.62}$$

$$\mathcal{B}_1{=}\mathcal{B}_3\ ,\ \mathcal{B}_2{=}\mathcal{B}_1\ ,\ \mathcal{B}_3{=}\mathcal{B}_2, \tag{2.63}$$

which gives us $\mathcal{A}_i \equiv \mathcal{A}$ and $\mathcal{B}_i \equiv \mathcal{B}$. If we follow the same procedure for a reflection through bond number 3 in fig. 2.1, we end up with the same conclusion. To incorporate the sign change of the A field into our equations, we write

$$\mathcal{A}_{\boldsymbol{\delta}}{\equiv}\,\mathrm{sgn}(\mathcal{A}_{\boldsymbol{\delta}})\mathcal{A} \tag{2.64}$$

$$\mathcal{B}_{\boldsymbol{\delta}}{\equiv}\mathcal{B}, \tag{2.65}$$

where $\mathrm{sgn}(\mathcal{A}_{\boldsymbol{\delta}})$ is positive when the arrow on the corresponding bond is pointing out from the lattice point.

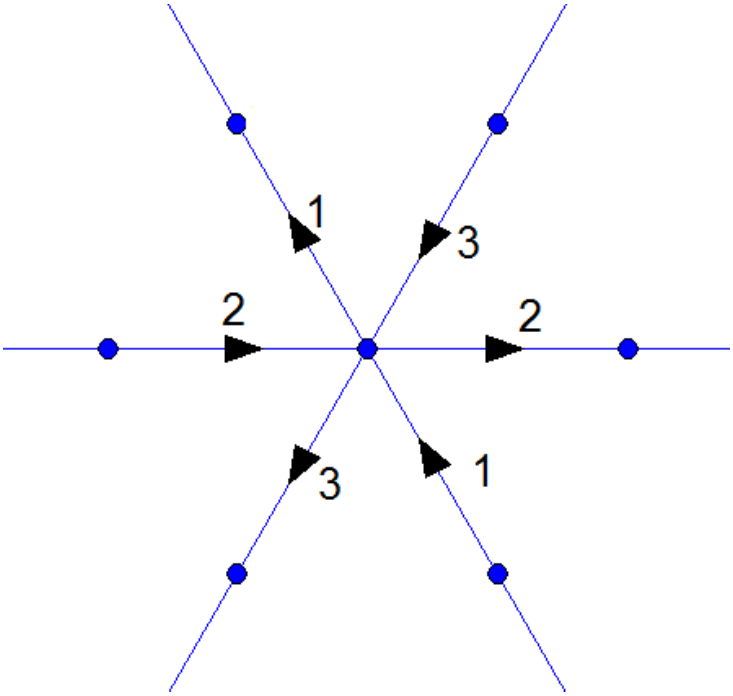

Figure 2.1: A close up illustration of the triangular lattice with the 6 nearest neighbour bonds of the central lattice point drawn as lines. The bonds are marked 1-3, and the arrows indicate in which direction the A field is positive.

We will now perform the same procedure for next nearest neighbour interactions, see fig. 2.2. We will draw these parameters with an overline to separate the from the nearest neighbour parameters. Rotating the system gives the same results as for nearest neighbour interactions, that is $\overline{\mathcal{A}}_i \equiv \overline{\mathcal{A}}$ and $\overline{\mathcal{B}}_i \equiv \overline{\mathcal{B}}$. However, when reflecting the system through the same bond as before, we find that:

$$\left(\overline{\mathcal{A}}_1, \overline{\mathcal{A}}_2, \overline{\mathcal{A}}_3\right) \overset{\sigma}{\Rightarrow} \left(-\overline{\mathcal{A}}_1, -\overline{\mathcal{A}}_3, -\overline{\mathcal{A}}_2\right) \overset{\phi_\sigma}{\Longrightarrow} \left(-\overline{\mathcal{A}}_1, -\overline{\mathcal{A}}_3, -\overline{\mathcal{A}}_2\right) \tag{2.66}$$

$$\left(\overline{\mathcal{B}}_1, \overline{\mathcal{B}}_2, \overline{\mathcal{B}}_3\right) \overset{\sigma}{\Rightarrow} \left(\overline{\mathcal{B}}_1, \overline{\mathcal{B}}_3, \overline{\mathcal{B}}_2\right) \overset{\phi_\sigma}{\Longrightarrow} \left(\overline{\mathcal{B}}_1, \overline{\mathcal{B}}_3, \overline{\mathcal{B}}_2\right). \tag{2.67}$$

It follows that $\overline{\mathcal{A}}_i \equiv \overline{\mathcal{A}} = 0$, while $\overline{\mathcal{B}}_i \equiv \overline{\mathcal{B}} \neq 0$ in general.

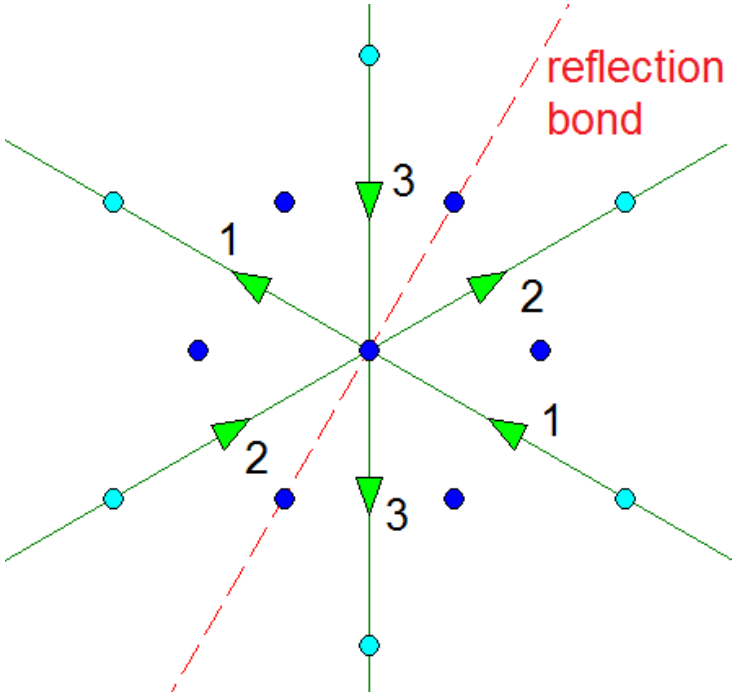

Figure 2.2: The next nearest neighbour bonds are shown and labelled, and the reflection bond is marked as a red striped line.

Now we have all the results needed to further simplify eq. (2.49). We define the geometric factors

$$\begin{aligned}\Gamma_k^A &\equiv \frac{1}{2}\sum_{\delta}\mathrm{sgn}(\mathcal{A}_\delta)\sin(\boldsymbol{k}\cdot\boldsymbol{\delta})\\ \Gamma_k^B &= \frac{1}{2}\sum_{\delta}\cos(\boldsymbol{k}\cdot\boldsymbol{\delta})\\ \overline{\Gamma_k^B} &= \frac{1}{2}\sum_{\Delta}\cos(\boldsymbol{k}\cdot\boldsymbol{\Delta}),\end{aligned} \tag{2.68}$$

and as shown in eq. (A.19), we then end up with the four equations

$$\mathcal{A} = \frac{1}{6N}\sum_{\boldsymbol{k}} \frac{\gamma_{\boldsymbol{k}}^{A}}{\omega_{\boldsymbol{k}}}\Gamma_{\boldsymbol{k}}^{A} \tag{2.69}$$

$$\mathcal{B} = \frac{1}{6N}\sum_{\boldsymbol{k}} \frac{\gamma_{\boldsymbol{k}}^{B}+\tilde{\lambda}}{\omega_{\boldsymbol{k}}}\Gamma_{\boldsymbol{k}}^{B} \tag{2.70}$$

$$\overline{\mathcal{B}} = \frac{1}{6N}\sum_{\boldsymbol{k}} \frac{\gamma_{\boldsymbol{k}}^{B}+\tilde{\lambda}}{\omega_{\boldsymbol{k}}}\overline{\Gamma_{\boldsymbol{k}}^{B}} \tag{2.71}$$

$$S+\frac{1}{2} = \frac{1}{2N}\sum_{\boldsymbol{k}} \frac{\gamma_{\boldsymbol{k}}^{B}+\tilde{\lambda}}{\omega_{\boldsymbol{k}}}. \tag{2.72}$$

2.4 Numerical Solution of The Mean Field Equations

We will now go through how the mean field equations can be solved numerically. The code used to solve them is written in C++, and can be found in a separate .zip file handed in together with this report. Any post processing of the data, such as curve fitting and plotting, was done in python.

2.4.1 Assumptions and scaling

The very first assumption we make is that the interactions between neighbouring spins are the same for all $\boldsymbol{d} \in \boldsymbol{\delta}$:

$$J_{\boldsymbol{\delta}} \equiv J_1 \tag{2.73}$$

and for all $\boldsymbol{d} \in \boldsymbol{\Delta}$:

$$J_{\boldsymbol{\Delta}} \equiv J_2. \tag{2.74}$$

Now we can scale the mean field equations given in eqs. (2.69) to (2.72), by letting $\tilde{\lambda} \to J_1\tilde{\lambda}$ and introducing the ratio between the interaction strengths

$$J_2/J_1 \equiv j. \tag{2.75}$$

The mean field parameters $\mathcal{A}$, $\mathcal{B}$ and $\overline{\mathcal{B}}$ are already unitless, so we do not need to scale these. We can eliminate the factor of J_1 in all equations, as we can write

$$\gamma_{\boldsymbol{k}}^{A} = J_1\mathcal{A}\cdot\Gamma_{\boldsymbol{k}}^{A} \tag{2.76}$$

$$\gamma_{\boldsymbol{k}}^{B} = J_1\left(\mathcal{B}\Gamma_{\boldsymbol{k}}^{B} + j\cdot\overline{\mathcal{B}}\cdot\overline{\Gamma_{\boldsymbol{k}}^{B}}\right) \tag{2.77}$$

$$\omega_{\boldsymbol{k}} = J_1\sqrt{(\gamma_{\boldsymbol{k}}^{B}+\tilde{\lambda})^2 - (\gamma_{\boldsymbol{k}}^{A})^2}, \tag{2.78}$$

where we have used the geometric factors from eq. (2.68). All factors of J_1 will now cancel in eqs. (2.69) to (2.72), and we are left with properly scaled and unitless equations. Note that this choice of scaling also makes us calculate the energy of the system in units of J_1.

The size of the system we simulate, i.e. the number of lattice points/wave vectors, is $N_1 \cdot N_2 = N$, where N_i is the number of lattice points in direction[7] $\boldsymbol{a}_i$. It is convenient to choose both N_1 and N_2 to be even numbers, but they should also be divisible by 3. This has to do with the location of the important wave vector $\boldsymbol{Q}$, see section chapter 3 and eq. (3.12), which is not in the set of $\boldsymbol{k}$ if N_1 and N_2 are not multiples of 3. All in all, this means that N must be divisible by 36 in our numerical analysis. We will also always choose $N_1 = N_2 = \sqrt{N}$. This choice is mainly out of convenience, as it eliminates a variable and simplifies some calculations in chapter 4.

2.4.2 Numerical Method and Convergence

An iterative method was used to solve the mean field equations for $\mathcal{A}$, $\mathcal{B}$ and $\overline{\mathcal{B}}$, while $\tilde{\lambda}$ is implicitly defined for a set of parameters $\{\mathcal{A}, \mathcal{B}, \overline{\mathcal{B}}\}$ through eq. (2.72). The method used to solve the equations is summarized below:

1. Choose initial values $\mathcal{A}_0 = S$, $\mathcal{B}_0 = -0.4S$ and $\overline{\mathcal{B}_0} = 0.4S$. These values were found to be suitable initial conditions through trial and error.
2. Calculate the initial value $\tilde{\lambda}_0$ from eq. (2.72) using the initial values $\mathcal{A}_0$, $\mathcal{B}_0$ and $\overline{\mathcal{B}}_0$.
3. Calculate $\mathcal{A}_n$, $\mathcal{B}_n$ and $\overline{\mathcal{B}}_n$ from the right hand side of eqs. (2.69) to (2.71) using the values $\mathcal{A}_{n-1}$, $\mathcal{B}_{n-1}$, $\overline{\mathcal{B}}_{n-1}$ and $\tilde{\lambda}_{n-1}$.
4. Calculate $\tilde{\lambda}_n$ implicitly from eq. (2.72) using the values $\mathcal{A}_n$, $\mathcal{B}_n$ and $\overline{\mathcal{B}}_n$.
5. Stop the process when the change in values from generation n to $n+1$ is sufficiently small.

The right hand side of eqs. (2.69) to (2.71) are straight forward to solve, simply plug in the values of the parameters from generation $n-1$ and perform the sum over $\boldsymbol{k}$ according to eq. (B.11) to find the values for generation n. However, solving eq. (2.72) for $\tilde{\lambda}$ requires more work as $\omega_{\boldsymbol{k}}$ is a function of $\tilde{\lambda}$. First we rewrite the equation[8]

$$
\begin{aligned}
S + \frac{1}{2} &= \frac{1}{2N} \sum_{\boldsymbol{k}} \frac{\gamma_{\boldsymbol{k}}^B + \tilde{\lambda}}{\omega_{\boldsymbol{k}}} \\
\Rightarrow \qquad 2N(S + \frac{1}{2}) &= \tilde{\lambda} \sum_{\boldsymbol{k}} \omega_{\boldsymbol{k}}^{-1} + \sum_{\boldsymbol{k}} \frac{\gamma_{\boldsymbol{k}}^B}{\omega_{\boldsymbol{k}}} \\
\Rightarrow \tilde{\lambda} &= \frac{1}{\sum_{\boldsymbol{k}} \omega_{\boldsymbol{k}}^{-1}} \left(2N(S + \frac{1}{2}) - \sum_{\boldsymbol{k}} \frac{\gamma_{\boldsymbol{k}}^B}{\omega_{\boldsymbol{k}}} \right) \equiv T(\tilde{\lambda}),
\end{aligned}
\tag{2.79}
$$

[7] See fig. B.1 and eq. (B.1).

[8] This is not necessary, but the solution can be found with higher precision by rewriting the equation in this way.

and try to find the root of $\tilde{\lambda} - T(\tilde{\lambda})$. We have implemented this in a simple way in our code, where we increase $\tilde{\lambda}$ until the sign of $\tilde{\lambda} - T(\tilde{\lambda})$ changes, then decrease $\tilde{\lambda}$ until it changes again, and repeat until the precision of the solution is sufficient. At the end of section 2.2.2, it was mentioned that $\gamma^B_{\boldsymbol{k}} + \tilde{\lambda} > 0$ for the diagonalization to work. Together with the more obvious constraint $\omega^2_{\boldsymbol{k}} > 0$, this gives us a lower boundary for the solution of $\tilde{\lambda}$:

$$\tilde{\lambda} > |\gamma^A_{\boldsymbol{k}}| - \gamma^B_{\boldsymbol{k}} \Rightarrow \tilde{\lambda}_{min} \equiv |\gamma^A_{\boldsymbol{k}}| - \gamma^B_{\boldsymbol{k}}, \tag{2.80}$$

which should be taken into account when solving the equation for $\tilde{\lambda}$. The solution of $\tilde{\lambda}$ also rapidly tends towards $\tilde{\lambda}_{min}$, which might cause problems if one does not use high enough precision when solving eq. (2.79).

All parameters converge for systems with a relatively weak next nearest neighbour interaction $j \leq 0.2$. Beyond this point, the values between two following generations start to oscillate back and forth instead of converging within a reasonable amount of time. For the maximal value $j = 0.2$, the number of iterations required to achieve a solution of resolution 10^{-12} varies from 10 for spin values of $S < 15$, and up to 35 iterations for $S = 0.5$. The size N of the system will of course increase the time each iteration takes, so systems with $N > 7056 = 84^2$ will make the solution of the mean field equations takes a long time[9] when calculated on a normal laptop.

The convergence speed seems to be fairly robust when it comes to the choice of initial conditions, as long as it is possible to find a solution for $\tilde{\lambda}_0$. The initial values listed previously will have no issue with convergence for $j \leq 0.2$. The sign of $\mathcal{B}$ was found to be opposite of $\mathcal{A}$ and $\overline{\mathcal{B}}$, so this should be taken into account in the initial conditions. The accuracy of the solution is largely limited by the solution of $\tilde{\lambda}$, which in a worst case scenario will have a resolution of 10^{-12}. This is an issue in the calculations of section 4.4, where some quantities can not be calculated due to the resolution. The implemented way of finding the root is not very efficient, and optimizing this process would speed up the numerical calculation of the mean field equations drastically.

[9] On the time scale of a few hours in a worst case scenario with high j and high S.

3 Sublattice Magnetization

As we already know, the Heisenberg antiferromagnet on the triangular lattice will exhibit a magnetic 120° Néel order for a sufficiently large value of the spin S [6, 9, 10]. However, below the critical spin value S_c, the system is in a spin liquid state. The classical approach to investigate a phase transition from magnetic disorder to magnetic order, is to look at the sublattice magnetization of the system, m. This order parameter is the most intuitive and straight forward choice, as it directly relates to the spatial orientation of the spins in relation to each other.

3.1 Definition

We define m through the equation [3]

$$\left\langle \hat{\mathbf{S}}_0 \cdot \hat{\mathbf{S}}_i \right\rangle \approx m^2 \cos(\upsilon_i), \tag{3.1}$$

where the left hand side represents the correlation between two spins on the lattice, m is the average length of the spin vectors and υ_i is the average angle between them. When the system is magnetically disordered, the correlation between spins that are far apart should rapidly decrease to zero[1], in other words $m \to 0$. When magnetic order occurs, the spins will align in relation to each other in a 120° fashion, and the correlation will obviously be greater than 0. Therefore, we expect an abrupt change in the value of m as we increase the magnitude of S from below to beyond S_c, making m a good choice for an order parameter.

To calculate the local magnetization m, we must look at how the spin correlation behaves in the ground state $|G\rangle$ of the system. Since we have related the ground state to the transformed boson operators $\hat{\eta}_{k\sigma}$ in eq. (2.46), and not to the original Schwinger-bosons, we first attempt to rewrite $\left\langle \hat{\mathbf{S}}_0 \cdot \hat{\mathbf{S}}_i \right\rangle$ in this new basis. The rotational invariance of the original Hamiltonian [15, p. 55] (2.1) means that the spin dot product reduces to:

$$\left\langle \hat{\mathbf{S}}_0 \cdot \hat{\mathbf{S}}_i \right\rangle = 3\left\langle \hat{S}_0^z \cdot \hat{S}_i^z \right\rangle = \frac{3}{4}\left\langle \hat{b}_{0\uparrow}^\dagger \hat{b}_{0\uparrow} \hat{b}_{i\uparrow}^\dagger \hat{b}_{i\uparrow} + \hat{b}_{0\downarrow}^\dagger \hat{b}_{0\downarrow} \hat{b}_{i\downarrow}^\dagger \hat{b}_{i\downarrow} - \hat{b}_{0\uparrow}^\dagger \hat{b}_{0\uparrow} \hat{b}_{i\downarrow}^\dagger \hat{b}_{i\downarrow} - \hat{b}_{0\downarrow}^\dagger \hat{b}_{0\downarrow} \hat{b}_{i\uparrow}^\dagger \hat{b}_{i\uparrow} \right\rangle. \tag{3.2}$$

Transforming into the FT operators $\hat{b}_{k\sigma}$ through eq. (2.18), yields

$$\begin{aligned} \left\langle \hat{\mathbf{S}}_0 \cdot \hat{\mathbf{S}}_i \right\rangle = & \frac{3}{4N^2}\left\langle \sum_{k_1,k_2,k_3,k_4} e^{i(k_4-k_3)\cdot r_i}\left(\hat{b}_{k_1\uparrow}^\dagger \hat{b}_{k_2\uparrow} \hat{b}_{k_3\uparrow}^\dagger \hat{b}_{k_4\uparrow} + \hat{b}_{k_1\downarrow}^\dagger \hat{b}_{k_2\downarrow} \hat{b}_{k_3\downarrow}^\dagger \hat{b}_{k_4\downarrow}\right)\right\rangle \\ & - \frac{3}{4N^2}\left\langle \sum_{k_1,k_2,k_3,k_4} e^{i(k_4-k_3)\cdot r_i}\left(\hat{b}_{k_1\uparrow}^\dagger \hat{b}_{k_2\uparrow} \hat{b}_{k_3\downarrow}^\dagger \hat{b}_{k_4\downarrow} - \hat{b}_{k_1\downarrow}^\dagger \hat{b}_{k_2\downarrow} \hat{b}_{k_3\uparrow}^\dagger \hat{b}_{k_4\uparrow}\right)\right\rangle. \end{aligned} \tag{3.3}$$

[1] A small correlation between neighbouring spins will always be present in numerical calculations, hence the approximation in eq. (3.1).

The transformation to the $\hat{\eta}_{k\sigma}$-operators is given in eq. (2.38), and after adopting the short-hand

$$\begin{aligned} c_i &\equiv \cosh(\theta_{\boldsymbol{k}_i}) \\ s_i &\equiv \sinh(\theta_{\boldsymbol{k}_i}), \end{aligned} \tag{3.4}$$

they read

$$\hat{b}_{\boldsymbol{k}_j\uparrow} = c_j\hat{\eta}_{\boldsymbol{k}_j\uparrow} - s_j\hat{\eta}^\dagger_{\boldsymbol{k}_j\downarrow} \tag{3.5}$$

$$\hat{b}_{\boldsymbol{k}_j\downarrow} = i\left(s_j\hat{\eta}^\dagger_{-\boldsymbol{k}_j\uparrow} + c_j\hat{\eta}_{-\boldsymbol{k}_j\downarrow}\right). \tag{3.6}$$

By applying this to eq. (3.3), as shown in eq. (A.22), we get

$$\left\langle \hat{\boldsymbol{S}}_0 \cdot \hat{\boldsymbol{S}}_i \right\rangle = \frac{3}{8N^2} \sum_{\boldsymbol{k}_1,\boldsymbol{k}_2} e^{i(\boldsymbol{k}_1-\boldsymbol{k}_2)\cdot\boldsymbol{r}_i} \left(\frac{(\gamma^B_{\boldsymbol{k}_1} + \tilde{\lambda})(\gamma^B_{\boldsymbol{k}_2} + \tilde{\lambda}) - \gamma^A_{\boldsymbol{k}_1}\gamma^A_{\boldsymbol{k}_2}}{\omega_{\boldsymbol{k}_1}\omega_{\boldsymbol{k}_2}} - 1 \right). \tag{3.7}$$

The Fourier transform of the left hand side of eq. (3.1) is known as the structure factor $S(\boldsymbol{q})$, and is shown to be

$$S(\boldsymbol{q}) \equiv \sum_i \left\langle \hat{\boldsymbol{S}}_0 \cdot \hat{\boldsymbol{S}}_i \right\rangle e^{-i\boldsymbol{q}\cdot\boldsymbol{r}_i} = \frac{3}{8N} \sum_{\boldsymbol{k}} \left(\frac{(\gamma^B_{\boldsymbol{k}} + \tilde{\lambda})(\gamma^B_{\boldsymbol{k}-\boldsymbol{q}} + \tilde{\lambda}) - \gamma^A_{\boldsymbol{k}}\gamma^A_{\boldsymbol{k}-\boldsymbol{q}}}{\omega_{\boldsymbol{k}}\omega_{\boldsymbol{k}-\boldsymbol{q}}} - 1 \right) \tag{3.8}$$

in eq. (A.23). As it turns out, $S(\boldsymbol{q})$ will diverge for certain wave vectors $\boldsymbol{q} = \pm\boldsymbol{Q}$ if the system is magnetically ordered. This is seen in the numerical analysis, see fig. 3.3. This means we may approximate the inverse transformation of eq. (3.8), and find that[2]

$$\left\langle \hat{\boldsymbol{S}}_0 \cdot \hat{\boldsymbol{S}}_i \right\rangle \equiv \frac{1}{N} \sum_{\boldsymbol{q}} S(\boldsymbol{q}) e^{i\boldsymbol{q}\cdot\boldsymbol{r}_i} \approx \frac{1}{N}\left(S(\boldsymbol{Q}) e^{i\boldsymbol{Q}\cdot\boldsymbol{r}_i} + S(-\boldsymbol{Q}) e^{-i\boldsymbol{Q}\cdot\boldsymbol{r}_i} \right) = \frac{2S(\boldsymbol{Q})}{N} \cos(\boldsymbol{Q}\cdot\boldsymbol{r}_i). \tag{3.9}$$

A quick comparison between eq. (3.1) and eq. (3.9) reveals that

$$v_i = \boldsymbol{Q}\cdot\boldsymbol{r}_i, \tag{3.10}$$

and

$$m = \sqrt{\frac{2S(\boldsymbol{Q})}{N}}. \tag{3.11}$$

[2]The same nodes will be the dominant terms in $S(\boldsymbol{q})$ even if the system is unordered, but naturally the approximation is not as good.

3.2 Numerical Calculations

With the numerical solution of the mean field equations, see section 2.4, it is a simple task to calculate the structure factor $S(\boldsymbol{q})$, from eq. (3.8). Contour plots of $S(\boldsymbol{q})$ with no next nearest neighbour interactions are shown in fig. 3.2 and fig. 3.3. From this picture it is clear that the structure factor has two distinct peaks at $\boldsymbol{q} = \pm\boldsymbol{Q}$, revealing that

$$\boldsymbol{Q} \equiv \frac{q_1}{N_1}\boldsymbol{b}_1 + \frac{q_2}{N_2}\boldsymbol{b}_2 = -\frac{1}{3}\boldsymbol{b}_1 + \frac{1}{3}\boldsymbol{b}_2, \tag{3.12}$$

where $\boldsymbol{b}_1$ and $\boldsymbol{b}_1$ are the basic reciprocal lattice vectors defined in eq. (B.6). This corresponds to the wave vector at the corners of the first Brillouin zone, shown in fig. B.3. Figure fig. 3.1 shows a contour plot of the dispersion relation $\omega_{\boldsymbol{k}}$, which has minimal values for $\boldsymbol{k} = \pm\boldsymbol{Q}$, giving rise to the peaks in $S(\boldsymbol{Q})$.

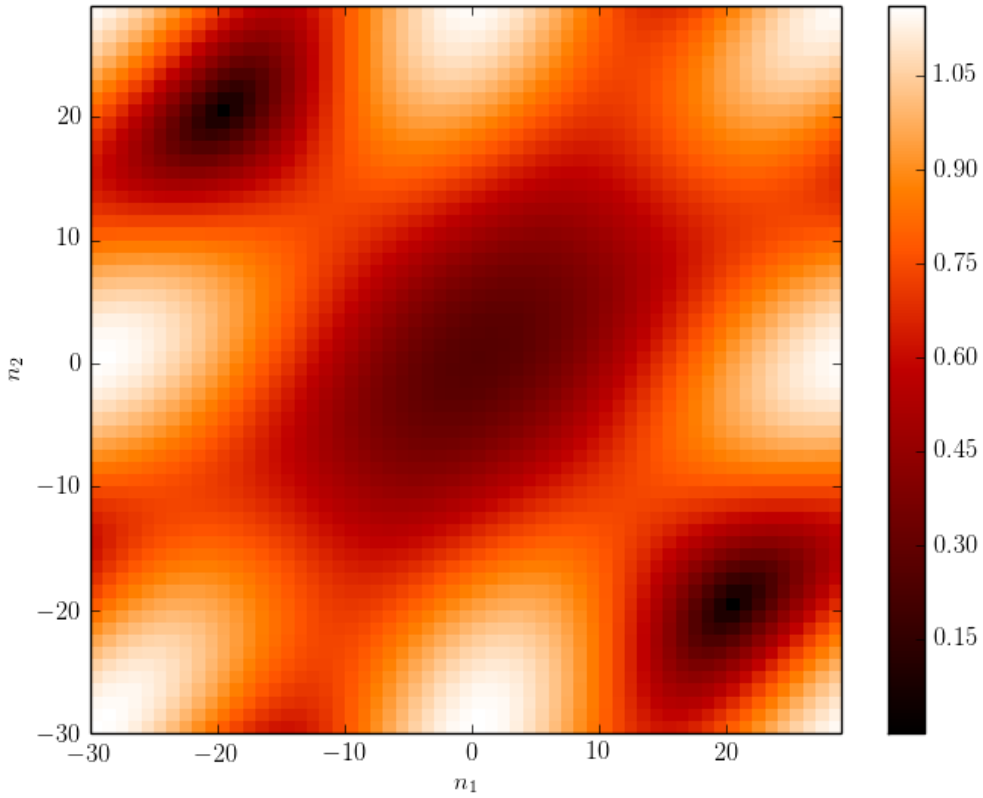

Figure 3.1: A contour plot of the dispersion relation for $S = \frac{1}{2}$, $N = 3600$ and $j = 0$. Every point (n_1, n_2) corresponds to a wave vector in the unit cell of the form given in eq. (B.11). Two "sinks" for $\boldsymbol{k} = \pm\boldsymbol{Q}$ can be seen.

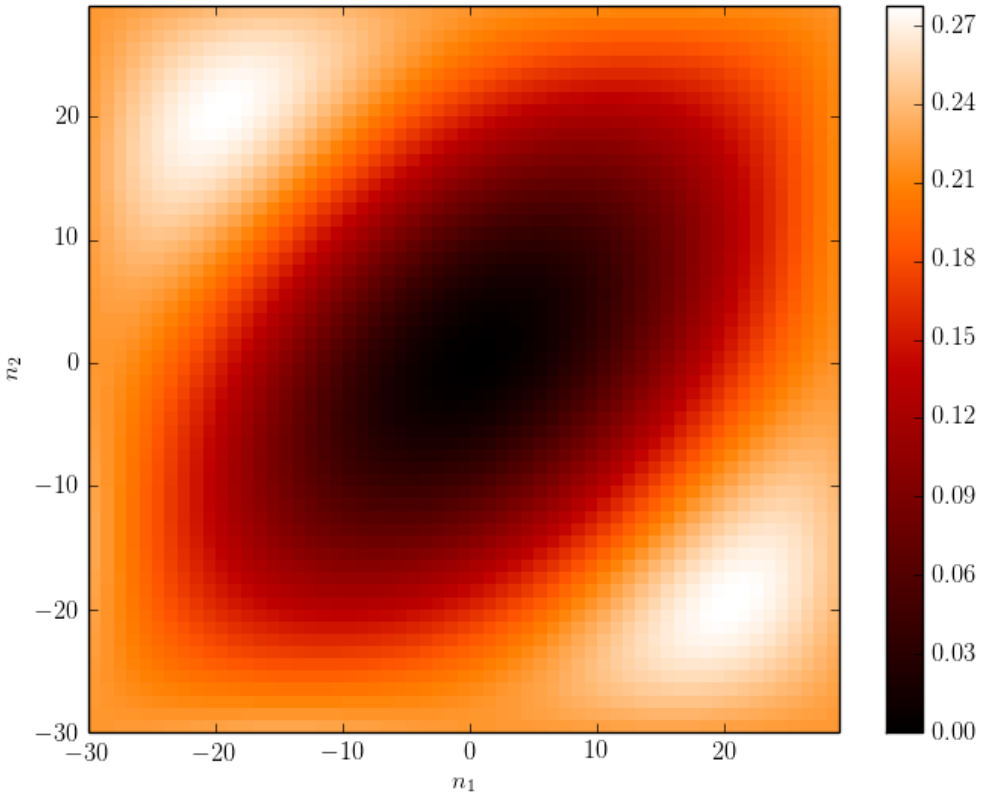

Figure 3.2: A contour plot of the structure factor for $S = 0.1$, $N = 3600$ and $j = 0$. Every point (n_1, n_2) corresponds to a wave vector in the unit cell of the form given in eq. (B.11). The brighter the colour, the higher the value of $S(\boldsymbol{q})$. The two wave vectors $\boldsymbol{q} = \pm\boldsymbol{Q}$ gives the largest values of $S(\boldsymbol{q})$.

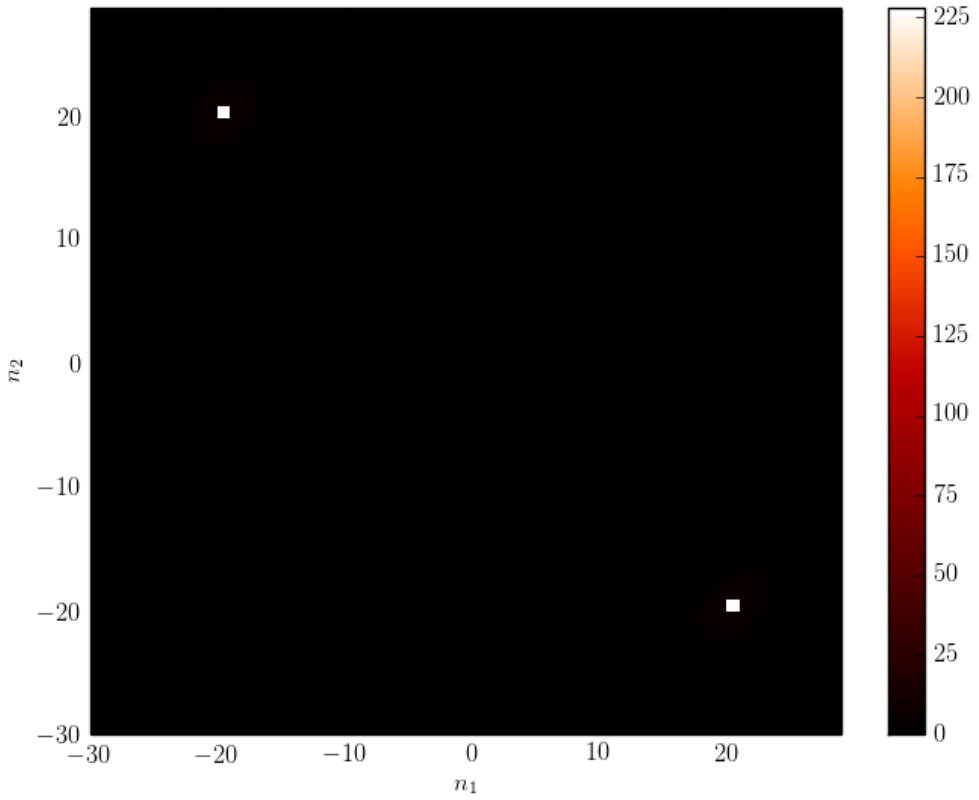

Figure 3.3: A contour plot of the structure factor for $S = \frac{1}{2}$, $N = 3600$ and $j = 0$. Every point (n_1, n_2) corresponds to a wave vector in the unit cell of the form given in eq. (B.11). The brighter the colour, the higher the value of $S(\boldsymbol{q})$. Two peaks for $\boldsymbol{k} = \pm\boldsymbol{Q}$ can be seen.

Now, according to eq. (3.10), the angle between two nearest neighbour spins in a magnetically ordered system will be

$$v_{\delta^x} = \boldsymbol{Q} \cdot \boldsymbol{\delta}^x = \pm 120^\circ, \tag{3.13}$$

where $\boldsymbol{\delta}^x$ is one of the 6 vectors defined in eq. (B.3). So we do indeed have a Néel state when the system is magnetically ordered.

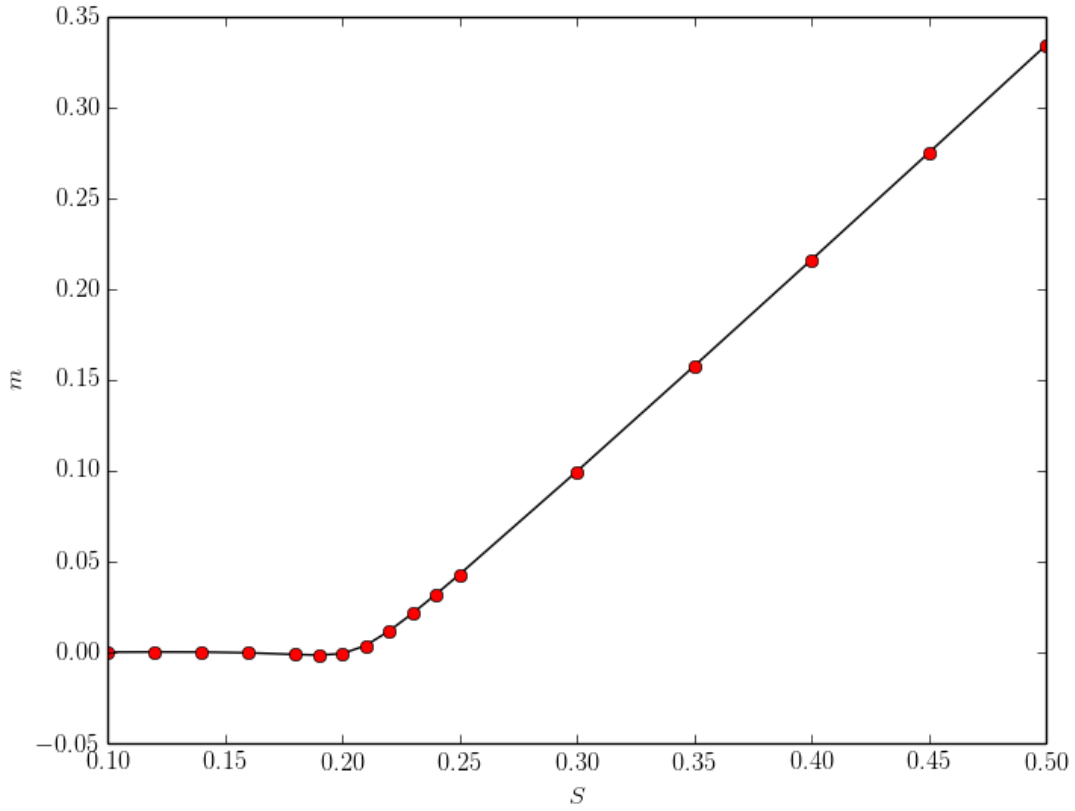

Figure 3.4: The figure shows the calculated values of the order parameter m (red dots) and an extrapolated black line. For small values of S, the order parameter is essentially zero, and the slight deviation can be attributed to numerical noise. After passing the critical value of the spin, $S > S_c$, it becomes non-zero. Since $S_c < \frac{1}{2}$, the system will exhibit an ordered Néel state at $T = 0$K for any physical value of the spin.

We would like to know for what value of S we will transition from a spin liquid state to a magnetically ordered one. To investigate this, we calculate m according to eq. (3.11) for different values of S, and see for which spin value m becomes non-zero. In this calculation, we treat S as a continuous variable to get an estimate of S_c even if it is below the smallest physical spin of $\frac{1}{2}$. We would like to calculate m for an infinite system, but eq. (3.11) refers to a finite system of N lattice sites. To circumvent this problem, we may calculate m for a given S and several values of N, and use regression to write m as a power series of N. According to [16], we should include a term proportional to $\frac{1}{\sqrt{N}}$ due to the symmetries of the Heisenberg Hamiltonian, so our approximation of m is:

$$m \approx m_0 + \frac{m_1}{\sqrt{N}} + \frac{m_2}{N}. \tag{3.14}$$

In the limit $N \to \infty$ only the constant term m_0 survives, which is the term we are interested in. The simple curve fitting function *polyfit* in Python was used to calculate the coefficients in the series expansion. A plot of m_0 is shown in fig. 3.4, where we see that $m \approx 0.33 = 0.66 \cdot S$ for $S = \frac{1}{2}$. The critical value $S_c \approx 0.21$ can clearly be seen in fig. 3.5, which shows an approximation of the derivative $\frac{\Delta m_0}{\Delta S}$.

In paper [9] by Wang and Vishwanath, they calculate a critical spin value of $S_c \approx 0.21$ for $j = 0$ by a minimization of $\omega_{\boldsymbol{k}}$ for $\boldsymbol{k} = \pm \boldsymbol{Q}$, which agrees well with our results. They do however get a different value for the local magnetization at $S = \frac{1}{2}$, $m \approx 0.29$, compared to our calculation. Also Mezio *et al.* get a lower value of $m \approx 0.275$ [10], however there are some errors made in their calculation of $S(\boldsymbol{Q})$, so this value is somewhat questionable[3]. Both agree that the spin-half value of m is overestimated when compared to other methods, probably due to the mean field approximation and the relaxation of the boson number constraint.

[3] Their approximation of $S(\boldsymbol{Q})$ is based on a minimal values of $\omega_{\boldsymbol{k}}$ for $\boldsymbol{k} = \pm \frac{\boldsymbol{Q}}{2}$. This is the case for the square lattice, but not the triangular, as shown in fig. 3.1

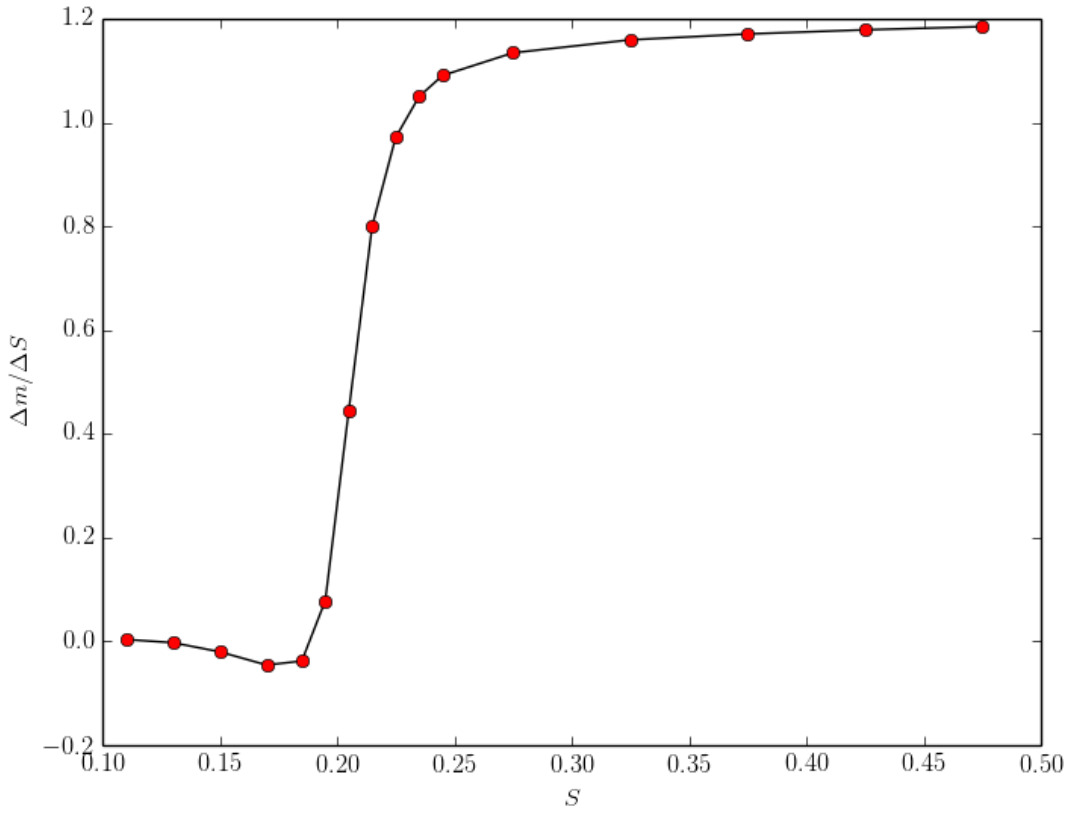

Figure 3.5: The midpoint estimate of the derivative of m with respect to S is shown (red dots) with an extrapolated black line. The critical spin value S_c is the point where a very sharp increase in the derivative occurs, which marks the transition $m = 0 \rightarrow m \neq 0$. From the figure, we can estimate $S_c \approx 0.21$.

The procedure for calculating m is identical when we include next nearest neighbour interactions, that is $j \neq 0$. We see from figs. 3.6 to 3.9 that the critical value has increased to $S_c \approx 0.25$ for $j = 0.1$ and $S_c \approx 0.31$ for $j = 0.2$. The result for $j = 0.2$ is questionable, as other ordered phases than the Néel order which we hav not taken into account might become important somwhere in the region $0.125 < j < 0.2$ [17].

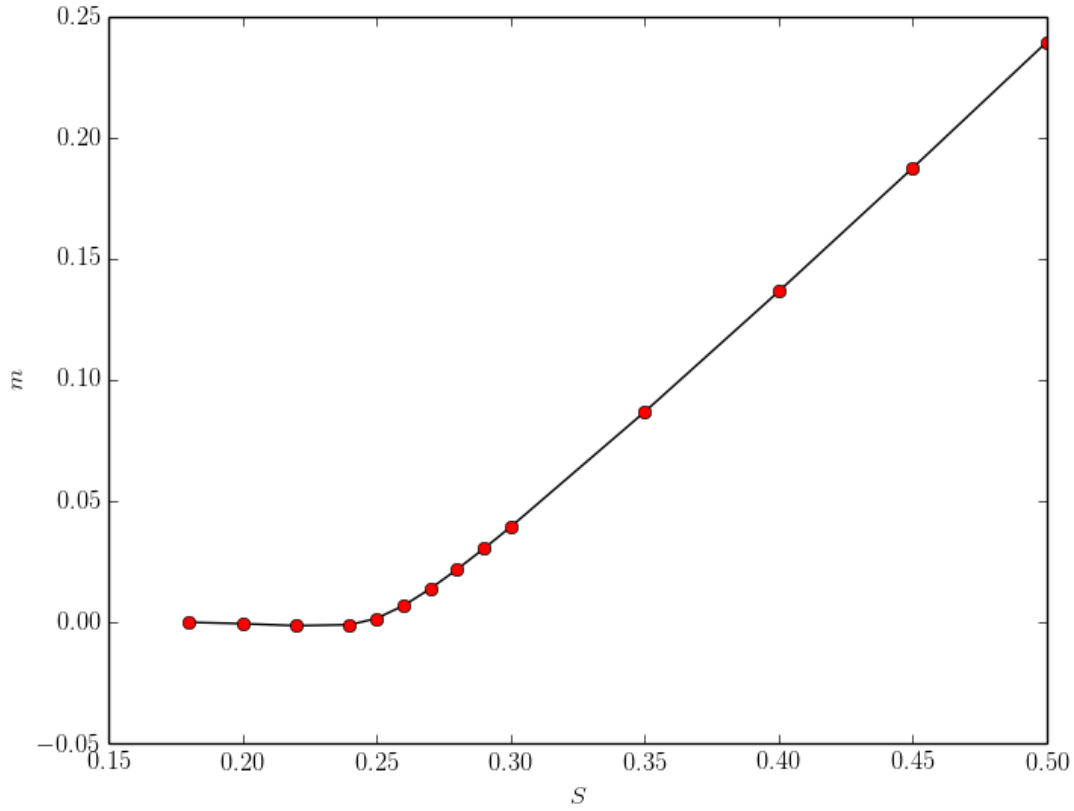

Figure 3.6: The figure shows a plot of m as well as a drawn line between the data points for $j = 0.1$. The critical spin value is shifted towards the right compared to the system with $j = 0$.

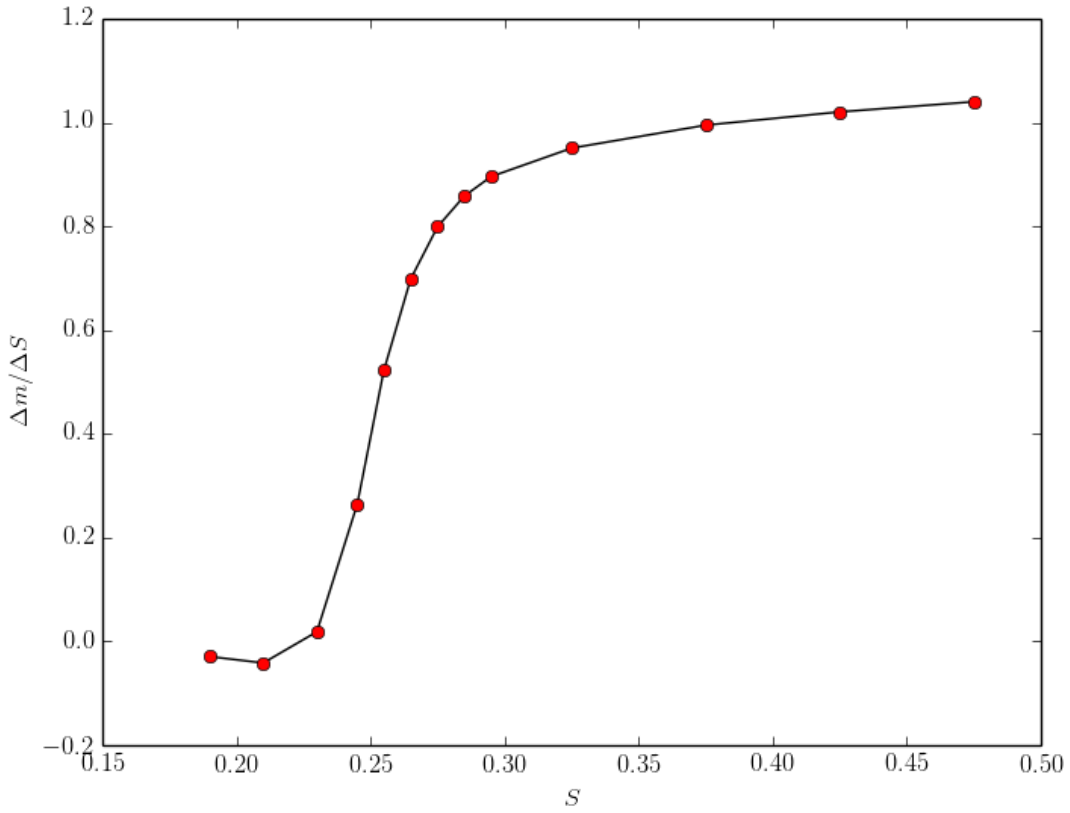

Figure 3.7: The figure shows an approximation of the mid point derivative $\Delta m/\Delta S$ for $j = 0.1$. The critical spin value is estimated to $S_c \approx 0.25$.

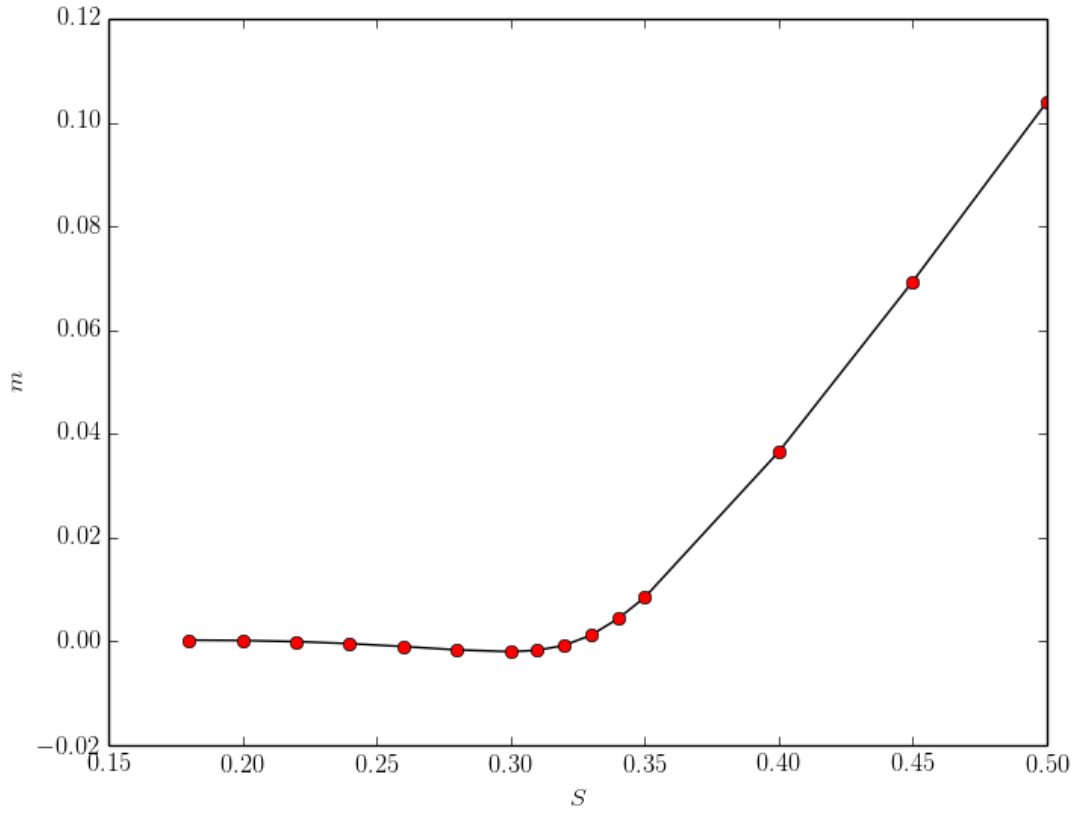

Figure 3.8: The figure shows a plot of m as well as a drawn line between the data points for $j = 0.2$. The critical spin value is shifted towards the right compared to the system with $j = 0.1$. This calculation might be influenced by other ordered states than the Néel state, which makes the numbers uncertain.

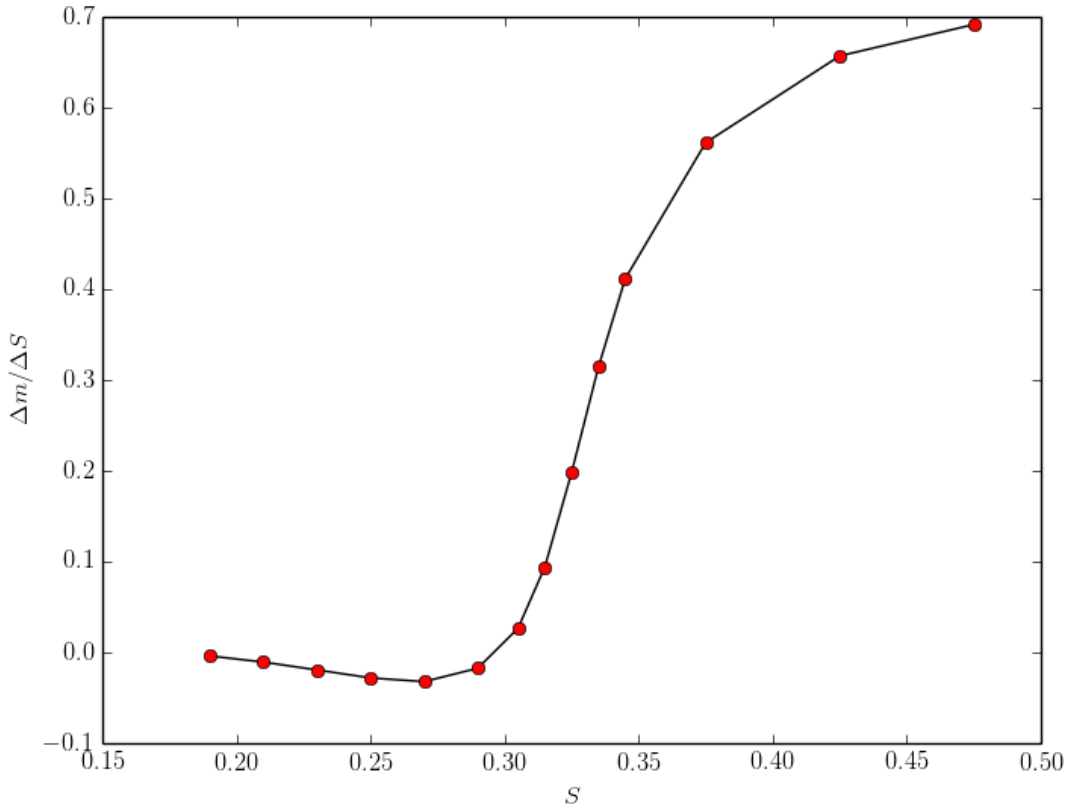

Figure 3.9: The figure shows an approximation of the mid point derivative $\Delta m/\Delta S$ for $j = 0.2$. The critical spin value is estimated to $S_c \approx 0.31$.

4 The Energy Difference between Topologically Ordered States

In this chapter, we will describe the topologically degenerate states of the spin liquid in the formalism of the mean field theory.

4.1 The Toric Code

To better understand the degeneracy which occurs in topologically ordered systems, we will briefly look into a simple topologically ordered system, known as "The Toric Code". This was first proposed by Kitaev [18] in the context of quantum computation, so it is not a physical model. The system consists of spin-$\frac{1}{2}$ particles on a square lattice, and these are placed on the edges instead of the vertices of the grid. The Hamiltonian is given as [19, p. 84]

$$H = -\sum_v \hat{a}_v - \sum_p \hat{b}_p, \tag{4.1}$$

with the operators

$$\hat{a}_v = \prod_{j \in v} \sigma_j^x \tag{4.2}$$

$$\hat{b}_p = \prod_{j \in \partial p} \sigma_j^z. \tag{4.3}$$

Here, σ are the Pauli matrices. The $\hat{a}$ operators are defined on the vertices v of the grid, while the $\hat{b}$ operators operate on the plaquettes p, see fig. 4.1 for an illustration of the system. If we operate in the S_z-basis, σ_i^z will measure the direction of the spin S_i, spin up or spin down, and σ_i^x will flip the spin to point in the other direction. The $\hat{a}$ and $\hat{b}$ operators commute with each other, $\left[\hat{a}_v, \hat{b}_p\right] = 0$, as a vertex and a plaquette overlap with either 0 or 2 spin sites, cancelling any minus sign from a spin flip. Both of the operators square to 1 as $(\sigma^x)^2 = (\sigma^z)^2 = \mathbb{I}$, meaning they have eigen values of ± 1

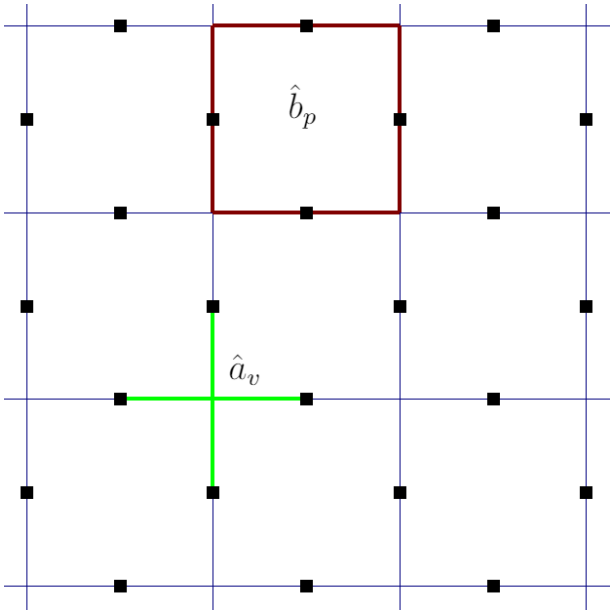

Figure 4.1: An illustration of the system in The Toric Code, where the spin sites (black squares) are located on the edges of the square lattice. The operators $\hat{a}_v$ operate on the four spins closest to the vertex v, here shown in green. $\hat{b}_p$ operates on the four spins on the edges of a given plaquette p, shown as dark red.

Since the operators commute, we can diagonalize the Hamiltonian simultaneously. It is clear that the ground state of the system is given by choosing

$$\hat{a}_v|G\rangle = +|G\rangle \tag{4.4}$$

$$\hat{b}_p|G\rangle = +|G\rangle\,, \tag{4.5}$$

as this minimizes the energy of the system. See [19, p. 84] for the exact form of this ground state, it is not crucial for our purpose. If we define what is known as the flux through a path l as

$$w_l = \prod_{j \in l} \sigma_j^z, \tag{4.6}$$

the restriction on the $\hat{b}_p$ operators means that the flux through every plaquette must be positive. As we will show, this opens up some possibilities for degenerate ground states due to the topology of the system. Consider flipping a single spin when the system is in the ground state. This would cause the plaquette flux of the two neighbouring plaquettes to turn from +1 to −1, raising the energy of the system. This excitation can be thought of as two quasiparticles, sometimes called m anyons or magnetic vortices, being created in the plaquettes with negative flux, see fig. 4.2. Flipping another spin in one of the excited plaquettes will return the plaquette flux back to +1, effectively annihilating the anyon in this plaquette. However, a new anyon will appear in the neighbouring plaquette, and so we have simply moved the anyon. If we move the

leftmost anyon towards the left until it annihilates the other anyon that was created from the first spin flip, we have a system where all plaquette fluxes are back to their initial value +1. The energy of the system is unchanged from the original ground state, and so we have shown that this system has degenerate ground states. This new ground state is characterized by a negative flux through a closed loop perpendicular to the path of the anyons. We could also choose the path of the anyons to be in the vertical direction, creating another degenerate ground state. In total, we can have a flux of ±1 through a loop in the vertical direction and in the horizontal direction, giving us a fourfold degeneracy.

As this two dimensional system is periodic in both directions, we can embed it on a torus in three dimensions. Figure (4.3) shows this torus with the the two non-equivalent paths the anyons can move. The degree of degeneracy is closely linked to the topology of the system, as the genus g of the embedded surface dictates how many non-equivalent paths there exists. It can be shown that we have a degeneracy of 4^g in topologically ordered systems [2]. In the case of the torus, we have $g = 1$ holes and so 4^1 degenerate states, which is what we have just shown.

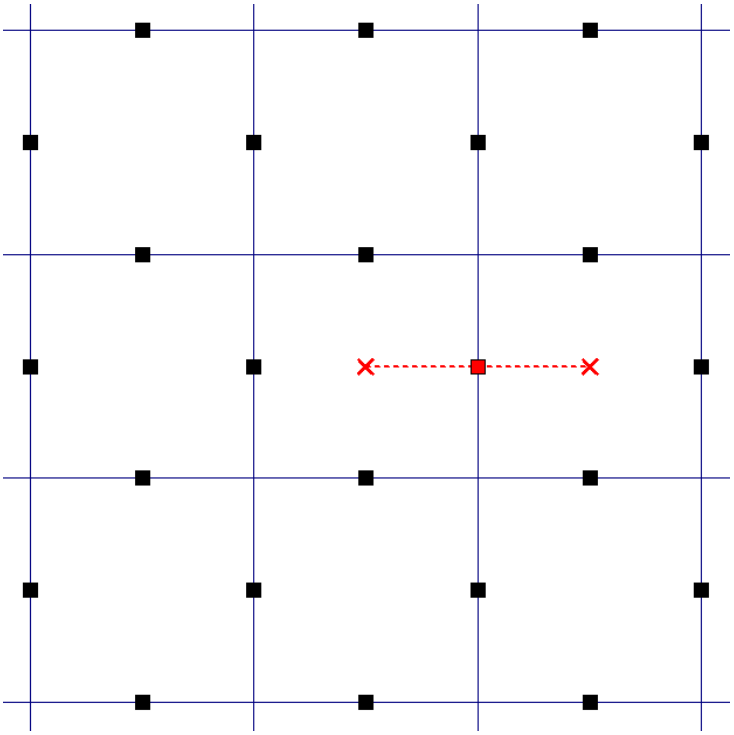

Figure 4.2: Shows two m anyons (red crosses) being created in the neighbouring plaquettes of a flipped spin (red square).

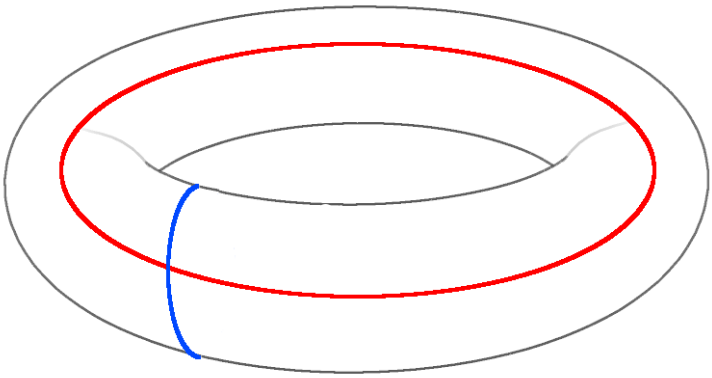

Figure 4.3: The red and blue lines can each have a flux of ±1, resulting in four degenerate ground states: (+1,+1) (+1,−1) (−1,+1) (−1,−1). Illustration from [20].

4.2 Topological Order of the Heisenberg Antiferromagnet on the Triangular Lattice

Just as the system described in The Toric Code, we can embed our triangular lattice on a torus. And as the spin liquid state is topologically ordered, we would expect to find $4^1 = 4$ degenerate ground states for the Heisenberg antiferromagnet. To shed some light on these degenerate states, we will revisit our initial analysis in section 2.3 of the gauge freedom and symmetries we have in our system, with a slightly more general approach. As we have previously discussed, we may transform the Scwinger-bosons in the following way

$$\hat{b}_{j\sigma} \rightarrow e^{-i\phi_j}\hat{b}_{j\sigma} \equiv z_j\hat{b}_{j\sigma} \tag{4.7}$$

without changing the physical quantities of the system[1]. This gauge transformation transforms the $\hat{A}_{ij}$ and $\hat{B}_{ij}$ operators,

$$\begin{aligned}\hat{A}_{ij} &\rightarrow z_i z_j \hat{A}_{ij} \\ \hat{B}_{ij} &\rightarrow z_i^* z_j \hat{B}_{ij},\end{aligned} \tag{4.8}$$

and the mean field values are of course transformed in the same way. Now we consider a one dimensional chain of spins with only nearest neighbour interactions. For simplicity, we will only consider a small chain of length $N = 4$ with connected ends, see fig. 4.4.

[1] The minus sign in the exponent of the gauge transformation is chosen out of convenience.

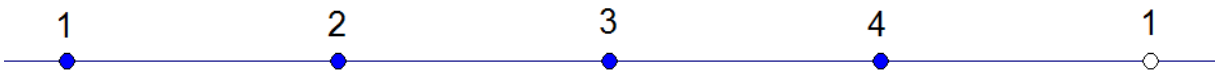

Figure 4.4: A one dimensional spin system with four lattice sites and connected endpoints.

Translating the system to the right by one grid constant and then performing the gauge transformation should leave us in the same state as before the translation:

$$\left(\mathcal{A}_{12},\mathcal{A}_{23},\mathcal{A}_{34},\mathcal{A}_{41}\right) \overset{T}{\Rightarrow} \left(\mathcal{A}_{41},\mathcal{A}_{12},\mathcal{A}_{23},\mathcal{A}_{34}\right) \overset{z_i z_j}{\Longrightarrow} \left(z_1 z_2 \mathcal{A}_{41}, z_2 z_3 \mathcal{A}_{12}, z_3 z_4 \mathcal{A}_{23}, z_4 z_1 \mathcal{A}_{34}\right). \tag{4.9}$$

This gives us the relations between the parameters,

$$\mathcal{A}_{12} = z_1 z_2 \mathcal{A}_{41} \ , \mathcal{A}_{23} = z_2 z_3 \mathcal{A}_{12} \ , \mathcal{A}_{34} = z_3 z_4 \mathcal{A}_{23} \ , \mathcal{A}_{41} = z_4 z_1 \mathcal{A}_{34}, \tag{4.10}$$

which implies that

$$|\mathcal{A}_{12}| = |\mathcal{A}_{23}| = |\mathcal{A}_{34}| = |\mathcal{A}_{41}|. \tag{4.11}$$

We have similar relations for the B field. The relations between the A field parameters may be written in a compact matrix form:

$$M\vec{\mathcal{A}} = \vec{\mathcal{A}} \ \Rightarrow \ (M - \mathbb{I})\vec{\mathcal{A}} = 0, \tag{4.12}$$

where we have defined

$$\vec{\mathcal{A}} \equiv \left(\mathcal{A}_{12},\mathcal{A}_{23},\mathcal{A}_{34},\mathcal{A}_{41}\right)^T \tag{4.13}$$

and

$$M \equiv \begin{pmatrix} 0 & 0 & 0 & z_1 z_2 \\ z_2 z_3 & 0 & 0 & 0 \\ 0 & z_3 z_4 & 0 & 0 \\ 0 & 0 & z_4 z_1 & 0 \end{pmatrix}. \tag{4.14}$$

This equation has a non-trivial solution if $\det(M - \mathbb{I}) = 0$, which gives us a restriction on the gauge transformation:

$$(z_1 z_2 z_3 z_4)^2 = 1 \ \Rightarrow \ \prod_i z_i = \pm 1. \tag{4.15}$$

The same calculation done for the B field yields $\prod_i |z_i|^2 = 1$, which is always satisfied when $z_j = e^{-i\phi_j}$. There are an infinite amount of choices to achieve $\prod_i z_i = \pm 1$, but which of these choices

are gauge equivalent? More precisely put: if we have a system described by the parameters $\{\mathcal{A}_{ij}\}$ and phase factors $\{z_i\}$, and then perform a gauge transformation to a system with different parameters $\{\tilde{\mathcal{A}}_{ij}\}$ and $\{\tilde{z}_i\}$, what is the connection between the two sets of phase factors? First of all, we note that the gauge transformation

$$\tilde{\mathcal{A}}_{ij} = \tilde{z}_i \tilde{z}_j \mathcal{A}_{ij} \tag{4.16}$$

preserves the absolute value $\left|\tilde{\mathcal{A}}_{ij}\right| = \left|\mathcal{A}_{ij}\right|$. Now we introduce what is known as the flux of the system, analogous of the flux defined in The Toric Code,

$$\mathcal{A}_{12}\mathcal{A}^*_{23}\mathcal{A}_{34}\mathcal{A}^*_{41}, \tag{4.17}$$

which is a gauge invariant quantity. Every lattice index appears in two factors in the flux, one of which is complex conjugated, resulting in a cancellation of any gauge transformation of the form given in eq. (4.8). This flux is related to $\prod_i z_i$, which can be seen by inserting eq. (4.10) into eq. (4.17):

$$\mathcal{A}_{12}\mathcal{A}^*_{23}\mathcal{A}_{34}\mathcal{A}^*_{41} = \mathcal{A}_{12}\cdot z_2^* z_3^* \mathcal{A}^*_{12}\cdot z_2 (z_3)^2 z_4 \mathcal{A}_{12}\cdot z_1 z_2 \mathcal{A}^*_{12} = |\mathcal{A}_{12}|^4 \prod_i z_i. \tag{4.18}$$

As the flux is gauge invariant, we know that

$$|\mathcal{A}_{12}|^4 \prod_i z_i = \left|\tilde{\mathcal{A}}_{12}\right|^4 \prod_i \tilde{z}_i. \tag{4.19}$$

Since the gauge transformation leaves the absolute value of the mean field parameters unchanged, we conclude that we must have $\prod_i z_i = \prod_i \tilde{z}_i$ for the systems to be gauge equivalent. This means that we have two classes of systems with either positive or negative flux, and all gauge choices leaving $\prod_i z_i$ unchanged are physically equivalent. We will from here on use the convention

$$z_i = +1 \qquad \text{for } \prod_i z_i = +1 \tag{4.20}$$

$$z_1 = -1\ ,\ z_{i\neq 1} = +1 \text{ for } \prod_i z_i = -1, \tag{4.21}$$

for the two different classes. A flux of +1 results in $\mathcal{A}_{ij} \equiv \mathcal{A}$ and $\mathcal{B}_{ij} \equiv \mathcal{B}$ which is what we found in our initial analysis in section 2.3. This can be seen by inserting $z_i = +1$ in eq. (4.9)[2]. However, a negative flux results in a flip of the sign of the 4-1 bond[3] for both the A and B field. The two situations are illustrated in figs. 4.5a and 4.5b, where the arrows indicate the positive direction of the bonds.

Now we will connect two chains with nearest neighbour interactions as shown in fig. 4.6. We choose the flux to be -1 on both these chains, and see what consequences this has for the

[2]Note that this equation is also valid for the B field as we chose all z_i to be real numbers.

[3]With our convention for the choice of z_i.

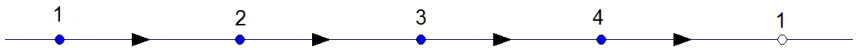

(a)

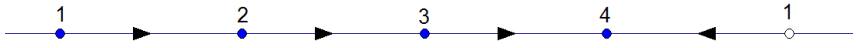

(b)

Figure 4.5: Illustration of two one dimensional chains with $N = 4$ lattice sites and different choices for the flux $\prod_i z_i$. The system in figure (a) has a flux of +1, while (b) has a negative flux of -1. The arrows point in the positive direction of each bond.

direction on the bonds connecting the two chains. With our convention, we choose the first lattice points of each chain, (1,1) and (2,1), to have a gauge phases[4] $z_{11} = z_{21} = -1$, and set the other $z_{ij} = +1$. We first concentrate on the bonds marked 1-4 in fig. 4.6, and translate and gauge transform the system:

$$\left(\mathcal{A}_1,\mathcal{A}_2,\mathcal{A}_3,\mathcal{A}_4\right)\overset{T}{\Rightarrow}\left(\mathcal{A}_4,\mathcal{A}_1,\mathcal{A}_2,\mathcal{A}_3\right)\overset{z_iz_j}{\Longrightarrow}\left(z_{21}z_{12}\mathcal{A}_4,z_{22}z_{13}\mathcal{A}_1,z_{23}z_{14}\mathcal{A}_2,z_{24}z_{11}\mathcal{A}_3\right)=\left(-\mathcal{A}_4,\mathcal{A}_1,\mathcal{A}_2,-\mathcal{A}_3\right)$$

$$\Rightarrow\mathcal{A}_1=\mathcal{A}_2=\mathcal{A}_3=-\mathcal{A}_4 \tag{4.22}$$

Again, this is also valid for the B field. We see that the last of these bonds, bond 4, will be flipped. This is not the case for the remaining (unnumbered) bonds connecting the two chains, which can be shown in a similar way. As they connect the two lattice points with negative gauge phases, point (1,1) and (2,1), to each other, the minus signs are cancelled. We are left with the system illustrated in fig. 4.7, where we have flipped all the bonds along the path marked by the red striped line. It is worth noting that all chains must have the same flux, as connecting chains with different fluxes will only give the trivial solution $\mathcal{A}_{ij} = \mathcal{B}_{ij} = 0$ on the lattice. These results still hold true if we scale up our system in either direction. Note that we have not shown any relation between the mean field parameters on the three different types of nearest neighbour bonds. This can be done by using the rotational and reflection symmetries of the grid, see the

[4]The notation z_{ij} refers to lattice point ij in fig. 4.6.

analysis in section 2.3. The results from this chapter are unchanged, except for the change of sign for the flipped bonds.

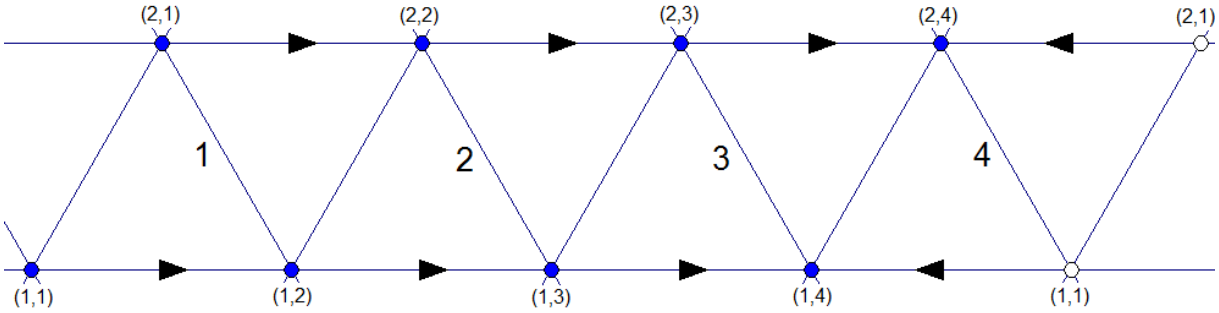

Figure 4.6: Two chains with negative flux connected with nearest neighbour interactions.

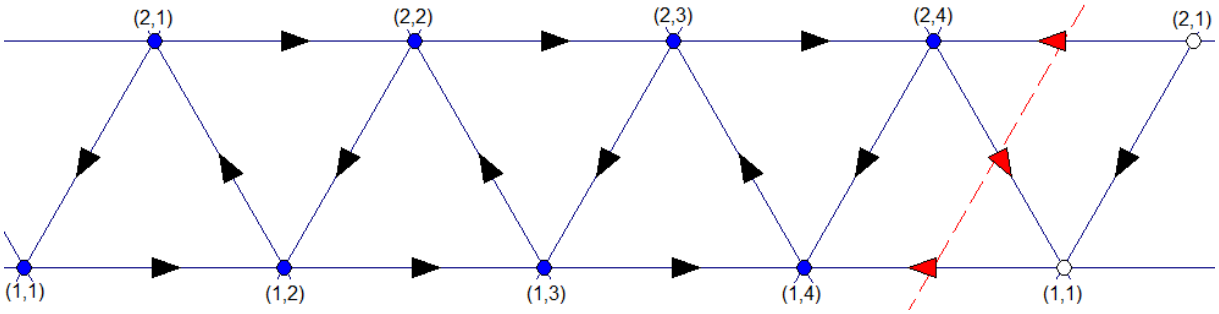

Figure 4.7: Shows the state of the system when a negative flux in all of the horizontal chains is introduced. We have here chosen the positive direction of the arrows to be the same as in the analysis in section 2.3. All bonds crossing the red striped line are flipped.

We have achieved to generate a new system state with a flux of -1 through any horizontal closed loop around the system, which should be energetically degenerate with the ground state in the limit $N \to \infty$. Analogous to the system in The Toric Code, we can make four different states in this way by choosing a flux of either ± 1 in the two principal directions of the lattice. We may also think of the flipping of the bonds as creating two quasiparticles and moving them in opposite directions to annihilate each other. To figure out what happens to the next nearest neighbour bonds, we apply the same method we used for nearest neighbour interactions. The analysis shows that all of these bonds crossing the red striped line in fig. 4.7 are also flipped. Note that two of the bonds shown in fig. 4.8 actually cross the red line.

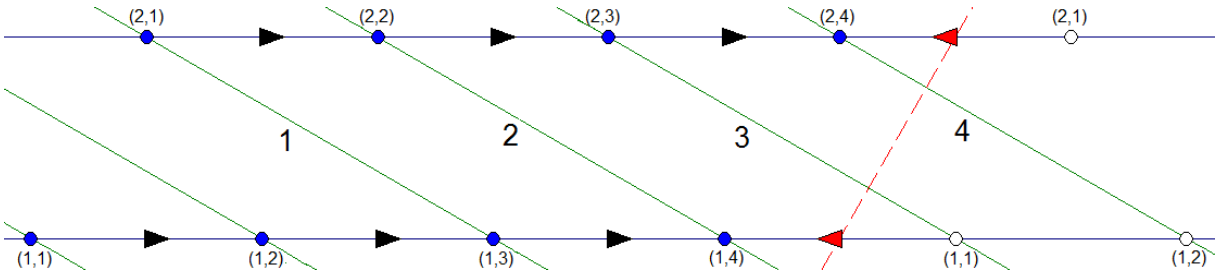

Figure 4.8: Both of the next nearest neighbour bonds crossing the same red striped line as shown in fig. 4.7 will be flipped. Note that bond 4 is flipped even though it is not connected to any negative z_{ij}.

We expect the four ground states that exist to be energetically degenerate in an infinite system, and we wish to calculate the energy difference in our finite system. First we need to solve the mean field equations for a system with a negative flux in one or both directions of the grid, which can be done by changing the boundary conditions. Previously we have used periodic boundary conditions in both directions, but an antiperiodic boundary in for instance the horizontal direction, will flip all bonds connected to the lattice points at the start of the chains. The analysis in appendix B.2 shows that the shape and form of the mean field equations are not changed in any way by introducing antiperiodic boundaries, the only difference will be a shift in the values of the $\boldsymbol{k}$ vectors in the first Brillouin zone. However, there is one catch. As fig. 4.8 shows, bond 4 is flipped without being connected to either of the starting points $(1,1)$ or $(2,1)$. This means that we will not be able to flip this bond in our calculations by introducing antiperiodic boundaries, introducing an error into our numerical results when $j \neq 0$.

4.3 Energy Difference by Small S Expansion

In an infinite system, the four states with different boundary conditions will be degenerate with an energy difference of zero when we are in the spin liquid state. With a finite number of lattice points, we expect the energy difference to rapidly decrease as a function of the system size. We first attempt to find an analytical expression for this dependence of N, and expand the mean field equations for small values of the spin S. For simplicity, we will set the next nearest neighbour interaction to zero, $j = 0$, and use the scale $J_1 = 1$. We then define the new scaled parameters

$$\alpha \equiv \mathcal{A}/\tilde{\lambda} \tag{4.23}$$
$$\beta \equiv \mathcal{A}/\tilde{\lambda} \tag{4.24}$$
$$\Omega_{\boldsymbol{k}} \equiv \omega_{\boldsymbol{k}}/\tilde{\lambda}. \tag{4.25}$$

Using the geometric factors $\Gamma^A_{\boldsymbol{k}}$ and $\Gamma^B_{\boldsymbol{k}}$ defined in eq. (2.68), we see that

$$\gamma_k^A = \mathcal{A}\Gamma_k^A = \tilde{\lambda}\alpha\Gamma_k^A \tag{4.26}$$
$$\gamma_k^B = \mathcal{B}\Gamma_k^B = \tilde{\lambda}\beta\Gamma_k^B \tag{4.27}$$
$$\Omega_k = \sqrt{(\beta\Gamma_k^B + 1)^2 - \alpha^2(\Gamma_k^A)^2}. \tag{4.28}$$

The two equations (2.69) and (2.70) can now be written as

$$\tilde{\lambda} = \frac{1}{6N}\sum_k \frac{(\Gamma_k^A)^2}{\Omega_k} \tag{4.29}$$
$$\tilde{\lambda} = \frac{1}{6N}\sum_k \frac{1}{\beta}\frac{(\beta\Gamma_k^B + 1)\Gamma_k^B}{\Omega_k}, \tag{4.30}$$

and equating them gives us the condition

$$\sum_k \frac{\beta(\Gamma_k^A)^2 - (\beta\Gamma_k^B + 1)\Gamma_k^B}{\Omega_k} = 0. \tag{4.31}$$

In addition, eq. (2.72) reads

$$\frac{1}{2} + S = \frac{1}{2N}\sum_k \frac{\beta\Gamma_k^B + 1}{\Omega_k}. \tag{4.32}$$

We would like to approximately solve these equations for small S, so we write the parameters α and β as a series expansion in S:

$$\alpha^2 = \alpha_1^2 S + \alpha_2^2 S^2 + ... \tag{4.33}$$
$$\beta = \beta_1 S + \beta_2 S^2 + ... \tag{4.34}$$

We have here set $\alpha_0^2 = \beta_0 = 0$ since the A and B fields are zero when the spin of the interacting particles vanish. We now insert these expressions in the modified mean field equations to find the expansion parameters. Expanding eq. (4.32) up to order S^2 gives

$$\begin{aligned}\frac{1}{2} + S &= \frac{1}{2N}\sum_k \frac{\beta\Gamma_k^B + 1}{\Omega_k} = \frac{1}{2N}\sum_k \left(1 + \beta_1\Gamma_k^B \cdot S + \beta_2\Gamma_k^B \cdot S^2 + \mathcal{O}(S^3)\right)\cdot \frac{1}{\Omega_k} \\ &= \frac{1}{2N}\sum_k \left(1 + \frac{1}{2}\alpha_1^2(\Gamma_k^A)^2 \cdot S + \left(\frac{1}{2}\alpha_2^2(\Gamma_k^A)^2 - \beta_1\alpha_1^2\Gamma_k^B(\Gamma_k^A)^2 + \frac{3}{8}\alpha_1^4(\Gamma_k^A)^4\right)\cdot S^2 + \mathcal{O}(S^3)\right),\end{aligned} \tag{4.35}$$

where we have used eq. (A.26) in the expansion of $1/\Omega_k$. Comparing the coefficients of the polynomials in S on both sides of the equation gives us the two equations

$$1=\frac{1}{2N}\sum_{k}\frac{1}{2}\alpha_1^2(\Gamma_k^A)^2 \tag{4.36}$$

$$0=\frac{1}{2N}\sum_{k}\left(\frac{1}{2}\alpha_2^2(\Gamma_k^A)^2-\beta_1\alpha_1^2\Gamma_k^B(\Gamma_k^A)^2+\frac{3}{8}\alpha_1^4(\Gamma_k^A)^4\right), \tag{4.37}$$

Where the zeroth term,

$$\frac{1}{2}=\frac{1}{2N}\sum_{k}1, \tag{4.38}$$

is automatically satisfied. Another two equations can be obtained from eq. (4.31) in the same way:

$$0=\sum_{k}\left(\beta_1(\Gamma_k^A)^2-\frac{1}{2}\alpha_1^2\Gamma_k^B(\Gamma_k^A)^2\right) \tag{4.39}$$

$$0=\sum_{k}\left(\beta_2(\Gamma_k^A)^2-\frac{1}{2}\alpha_2^2\Gamma_k^B(\Gamma_k^A)^2+\beta_1\alpha_1^2(\Gamma_k^B)^2(\Gamma_k^A)^2+\frac{1}{2}\beta_1\alpha_1^2(\Gamma_k^A)^4-\beta_1^2\Gamma_k^B(\Gamma_k^A)^2-\frac{3}{8}\alpha_1^4\Gamma_k^B(\Gamma_k^A)^4\right). \tag{4.40}$$

We introduce the sum

$$R_{m,n}\equiv\frac{1}{N}\sum_{k}(\Gamma_k^A)^m(\Gamma_k^B)^n, \tag{4.41}$$

and rewrite the four previous equations to get the expansion factors:

$$\alpha_1^2=\frac{4}{R_{2,0}} \tag{4.42}$$

$$\beta_1=2\cdot\frac{R_{2,1}}{(R_{2,0})^2} \tag{4.43}$$

$$\alpha_2^2=16\cdot\frac{(R_{2,1})^2}{(R_{2,0})^4}-12\cdot\frac{R_{4,0}}{(R_{2,0})^3} \tag{4.44}$$

$$\beta_2=12\cdot\frac{(R_{2,1})^3}{(R_{2,0})^5}-2\cdot\frac{R_{2,1}}{(R_{2,0})^4}\left(5\cdot R_{4,0}+4\cdot R_{2,2}\right)+6\cdot\frac{R_{4,1}}{(R_{2,0})^3}. \tag{4.45}$$

Here is where we would expect to find a numerical difference between systems with periodic boundaries and systems with at least one antiperiodic boundary. As shown in appendix B.2, the $\boldsymbol{k}$ vectors are slightly shifted when we introduce antiperiodic boundaries, and so one would expect that the factors $R_{m,n}$ would also shift. However, numerically computing the sums $R_{m,n}$ that are part of the coefficients above, we find that they are simple fractions,

$$\begin{aligned} R_{2,0} &= \frac{3}{2} \\ R_{2,1} &= -\frac{3}{2} \\ R_{2,2} &= \frac{15}{8} \\ R_{4,0} &= \frac{45}{8} \\ R_{4,1} &= -\frac{27}{4}, \end{aligned} \tag{4.46}$$

and that they are identical for both periodic and antiperiodic boundary conditions. This gives an energy difference of exactly zero, which should not be the case for systems of finite size. This means that the energy difference is not analytic in the parameter S, which is in itself an interesting observation. But this forces us to give up on the approximate calculation, and instead we have to calculate the total energy of the systems in the different degenerate states to investigate the energy difference.

4.4 Energy Difference by Direct Calculation

We are left with the straight forward option of a direct calculation of the system energy. We will compare the energy between three systems, one with periodic boundaries in both directions, one with antiperiodic boundaries in both directions, and one where there is one of each boundary. It turns out that the energy of the doubly antiperiodic and the mixed boundary systems are equal when the system is chosen to be quadratic, in the sense that $N_1 = N_2 = \sqrt{N}$, which we use in all our calculations. However, we do observe a difference between these systems and the doubly periodic system. The interesting questions here are: How does the energy difference scale with the system size N, and what happens to this scaling when we undergo a phase transition to a magnetically ordered phase? By calculating the energy difference for many different values of N for each spin value S, we find that it scales as

$$\ln(\Delta E) \approx a + C_{exp}\sqrt{N} \Rightarrow \Delta E \propto e^{C_{exp}\sqrt{N}} \tag{4.47}$$

for spin values $S < S_c$, shown in fig. 4.9. A simiar behaviour has been discovered in fractional quantum hall states, which are another example of topological ordered states [21]. For $S > S_c$, it decreases algebraically:

$$\ln(\Delta E) \approx \tilde{a} + C_{log}\ln(N) \Rightarrow \Delta E \propto N^{C_{log}}, \tag{4.48}$$

shown in fig. 4.10. By a simple linear curve fit, it turns out that $C_{log} \to -1$ in the magnetically ordered region, while C_{exp} is a function of S in the spin liquid phase. Calculating these parameters outside their respective regions might seem pointless as ΔE scales in a different way, but this shows up as an obvious break point in their value, reminiscent of the magnetization in fig. 3.4.

In figs. 4.11 and 4.12, we see what happens to the linear regression when we try to calculate C_{exp} and C_{log} outside their respective phase. The plots of C_{exp} and C_{log} as functions of S are shown in fig. 4.13 and fig. 4.14 for a system with $j = 0$, and these order parameters predict a critical spin value of $S_c \approx 0.21$, which is what found in chapter 3. Note that the value of ΔE for small S and large N is small enough to contest the resolution of the solution of the mean field equations. As mentioned in section 2.4, the calculation of $\tilde{\lambda}$ is the limiting factor when it comes to the numeric accuracy, with a precision of 10^{-12} in a worst case scenario. In fig. 4.15, the last 9 of the points have a value less than 10^{-12}, and are not counted in the linear curve fitting as they are simply numerical noise. This limits the accuracy of the curve fit for small values of S, typically $S < 0.15$.

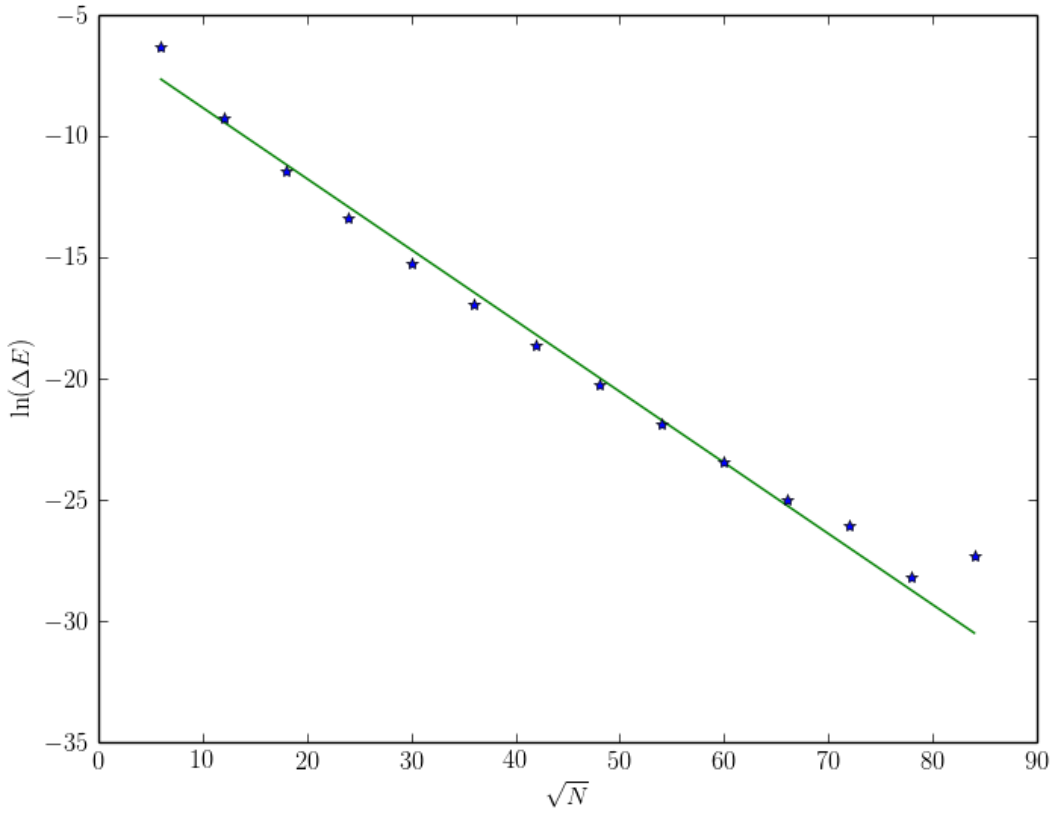

Figure 4.9: Plot of the logarithm of the energy difference as a function of $\sqrt{N}$ for $S = 0.16 < S_c$ and $j = 0$. The figure also shows the linear regression curve with slope C_{exp}.

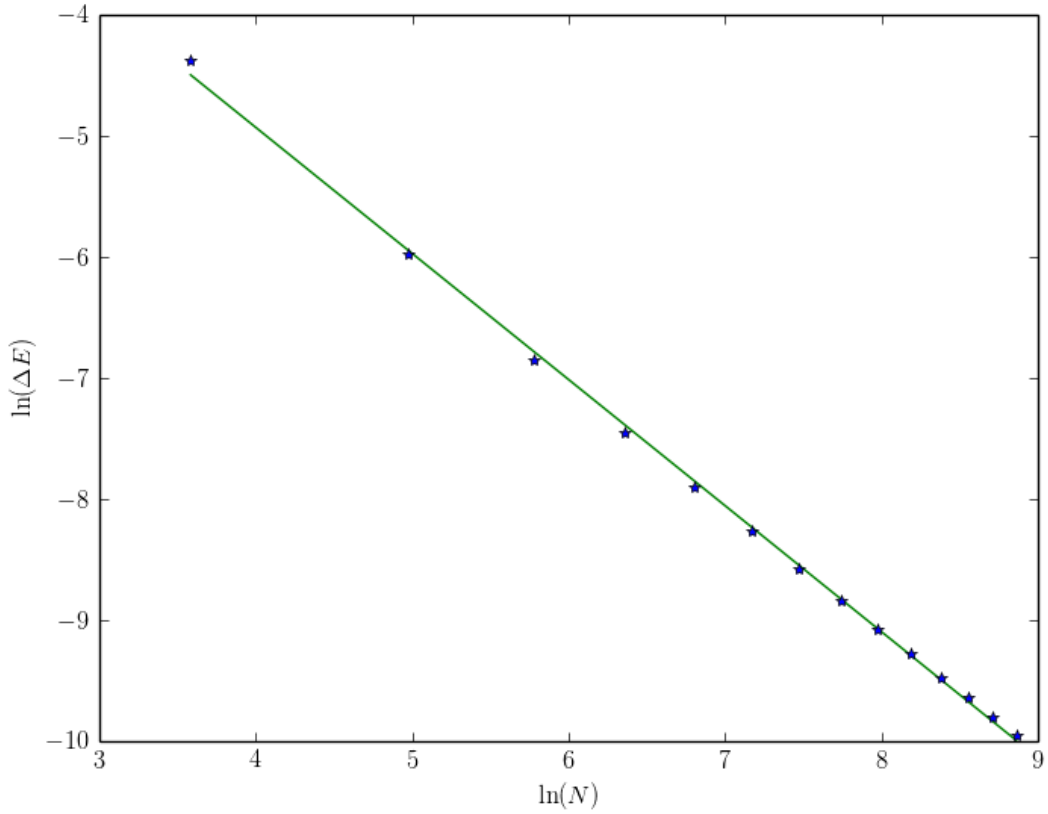

Figure 4.10: Plot of the logarithm of the energy difference as a function of $\ln(N)$ for $S = 0.3 > S_c$ and $j = 0$. The figure also shows the linear regression curve with slope $C_{log} = -1$, which is a very good approximation in this case.

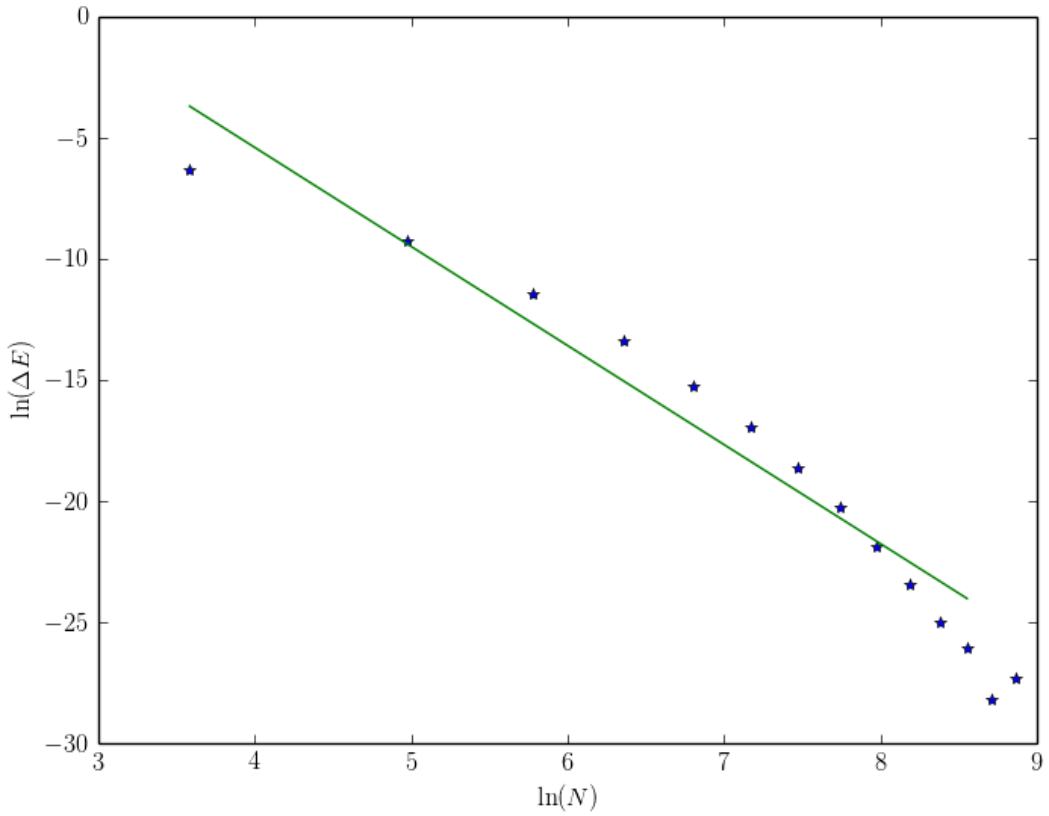

Figure 4.11: Plot of the logarithm of the energy difference as a function of $\ln(N)$ for $S = 0.16 < S_c$ and $j = 0$. The figure also shows the linear regression curve with slope C_{log}. There is clarely no linear dependence between $\ln(\Delta E)$ and $\ln(N)$ in this region.

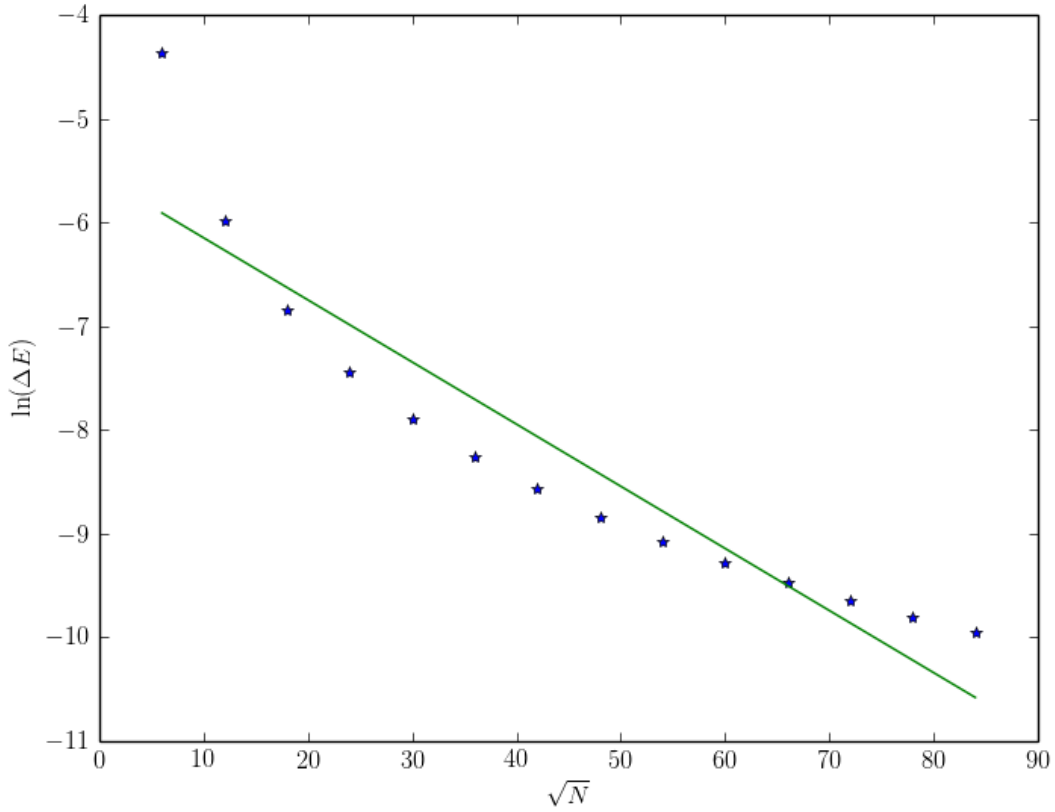

Figure 4.12: Plot of the logarithm of the energy difference as a function of $\sqrt{N}$ for $S = 0.3 > S_c$ and $j = 0$. The figure also shows the linear regression curve with slope C_{exp}. There is clarely no linear dependence between $\ln(\Delta E)$ and $\sqrt{N}$ in this region.

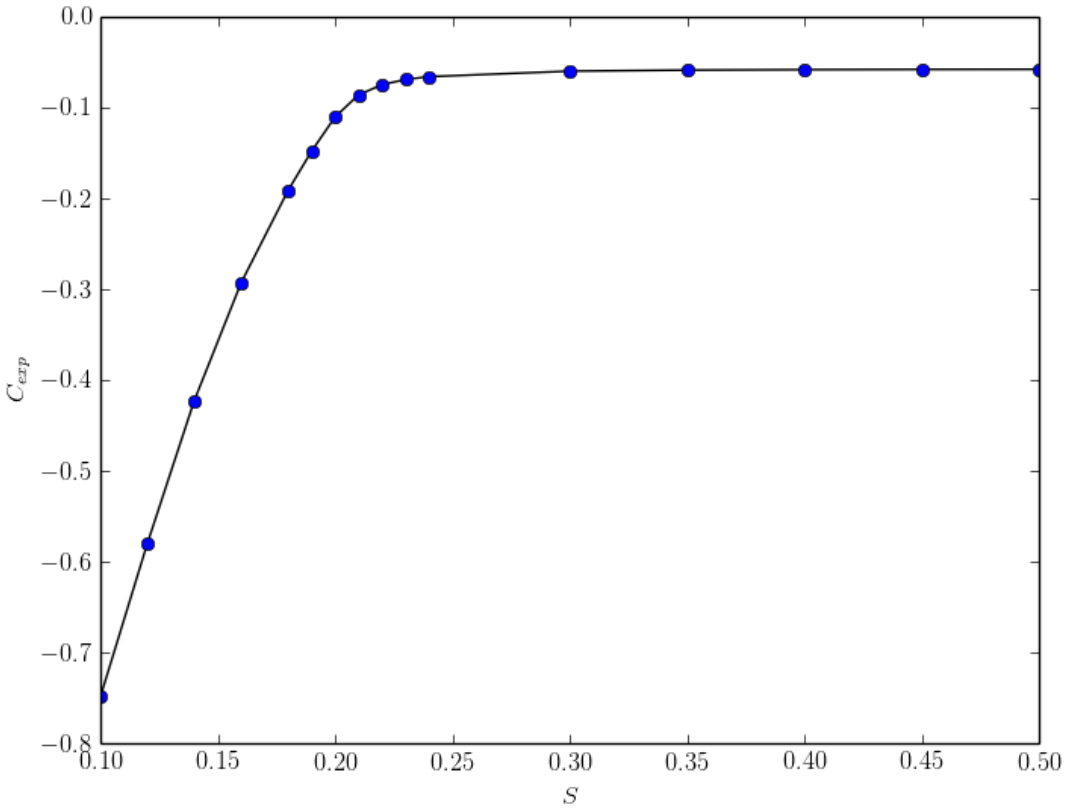

Figure 4.13: The figure shows the values of the parameter C_{exp} for $j = 0$. C_{exp} increases linearly in the spin liquid phase, and flattens out for $S > S_c = 0.21$ as ΔE scales in a different manner in this region.

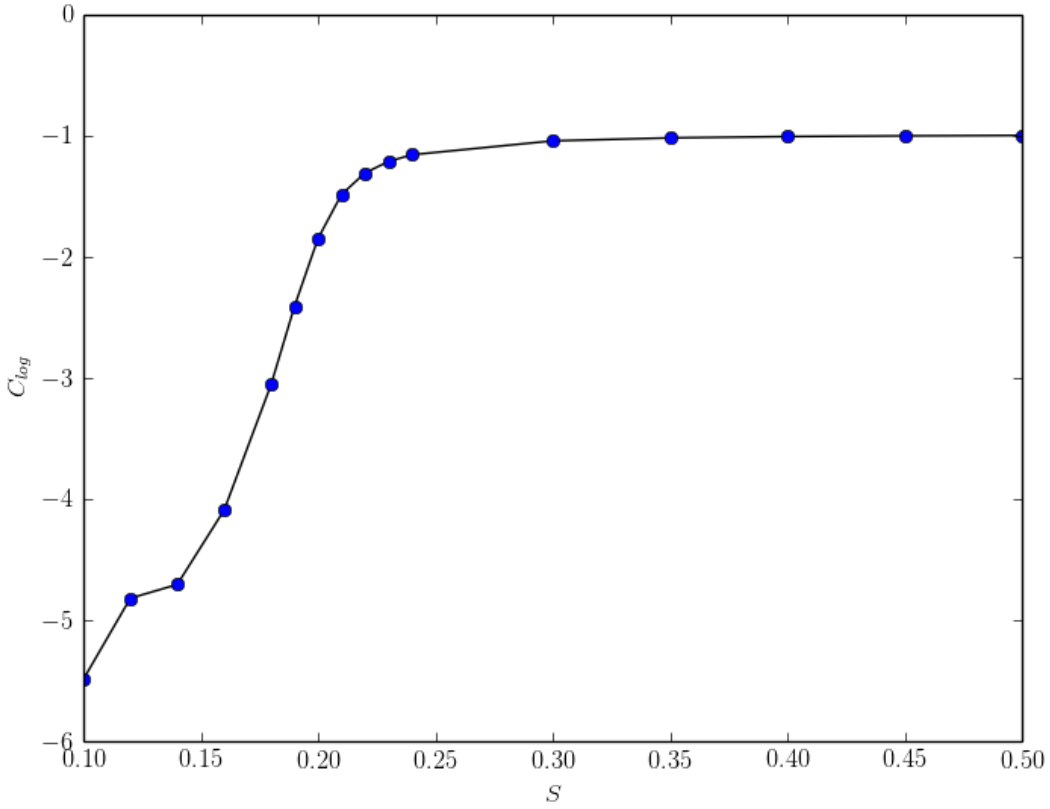

Figure 4.14: The figure shows the values of the parameter C_{log} for $j = 0$. C_{log} rapidly tends towards -1 in the magnetically ordered region of $S > S_c = 0.21$, and is significantly lower in the spin liquid phase.

These order parameters also seem to work for $j \neq 0$, even though the antiperiodic boundary conditions do not flip all of the next nearest neighbours bond in the right way. We would not expect this to introduce a large error into our calculations for small values of j, as it is only one bond that is not flipped correctly. The plot for $j = 0.1$ is shown in figs. 4.16 and 4.17, which again agrees with our findings in chapter 3 of $S_c \approx 0.25$. When $j = 0.2$ we see in figs. 4.18 and 4.19 that the curves are smoother and without an obvious break point, making it hard to estimate the critical spin value. Therefore, our estimate of $S_c \approx 0.35$ is not precise. This is a higher value than was estimated for the sublattice magnetization order parameter, but other ordered phases than the Néel state might again be influencing our results.

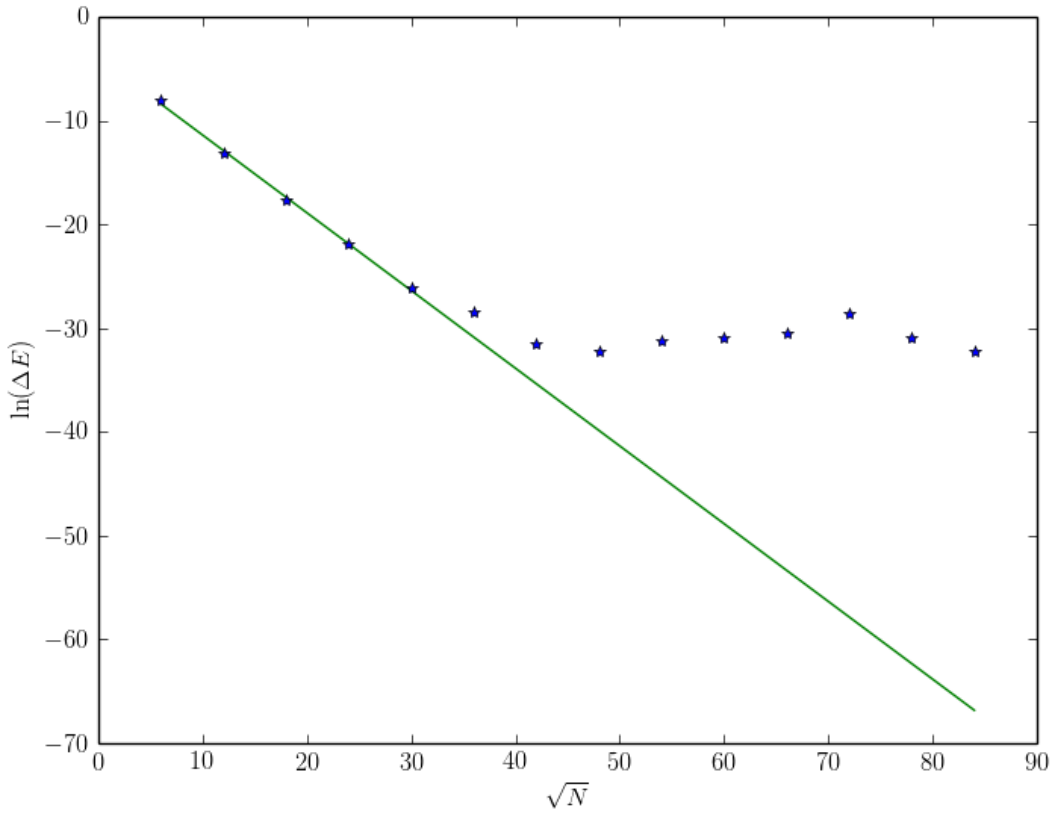

Figure 4.15: In this case of $S = 0.10$ and $j = 0$, the numerical resolution of the mean field parameters is too low to calculate the energy difference ΔE for $N > 900$. The last 9 points are numerical noise and not considered in the curve fitting.

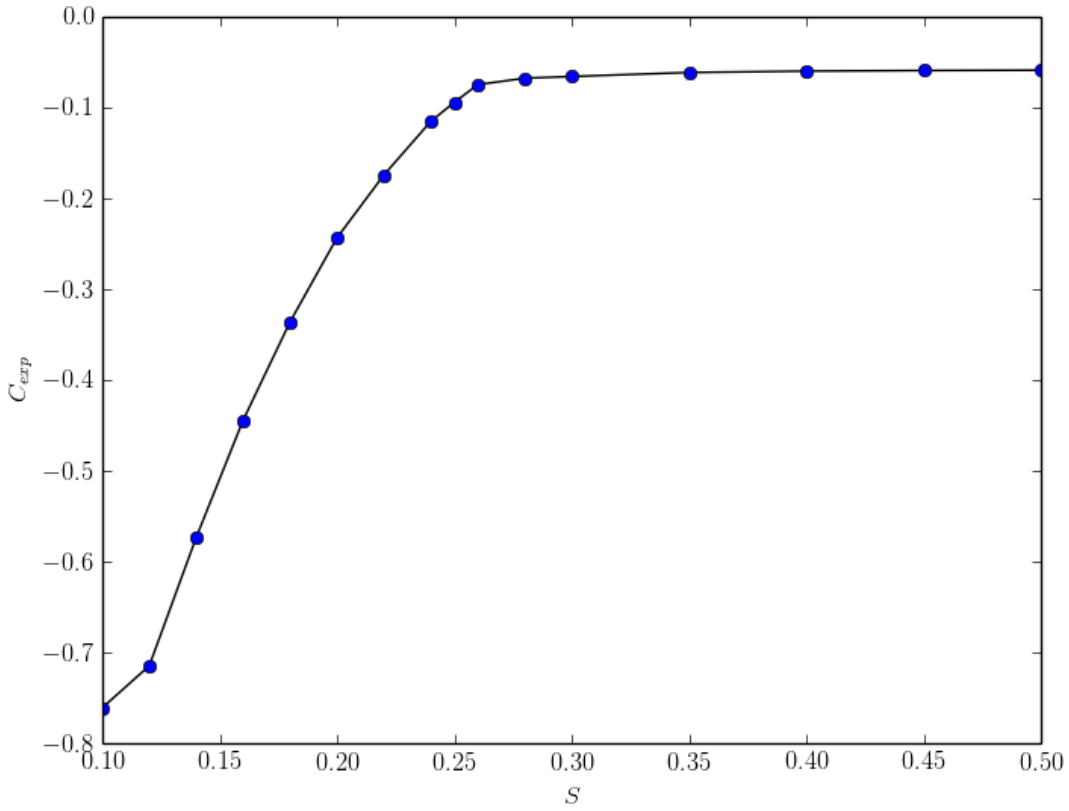

Figure 4.16: The figure shows C_{exp} for $j = 0.1$, with a critical value estimated at $S_c \approx 0.25$.

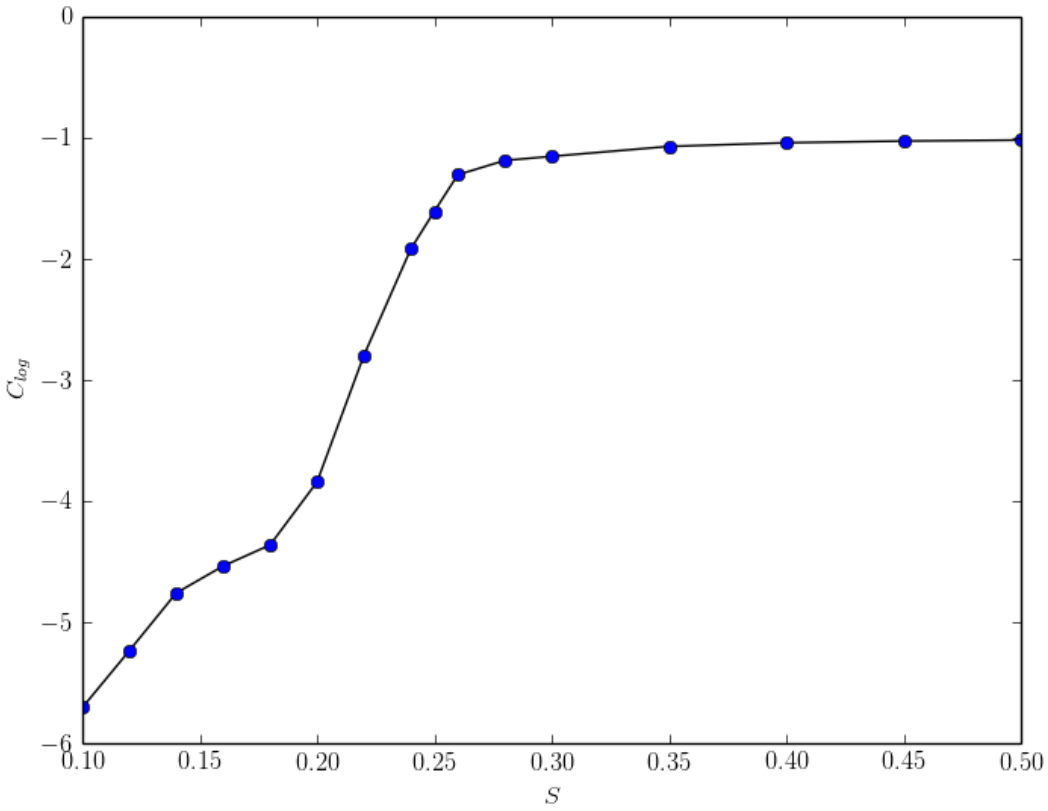

Figure 4.17: The figure shows C_{log} for $j = 0.1$, with a critical value estimated at $S_c \approx 0.25$.

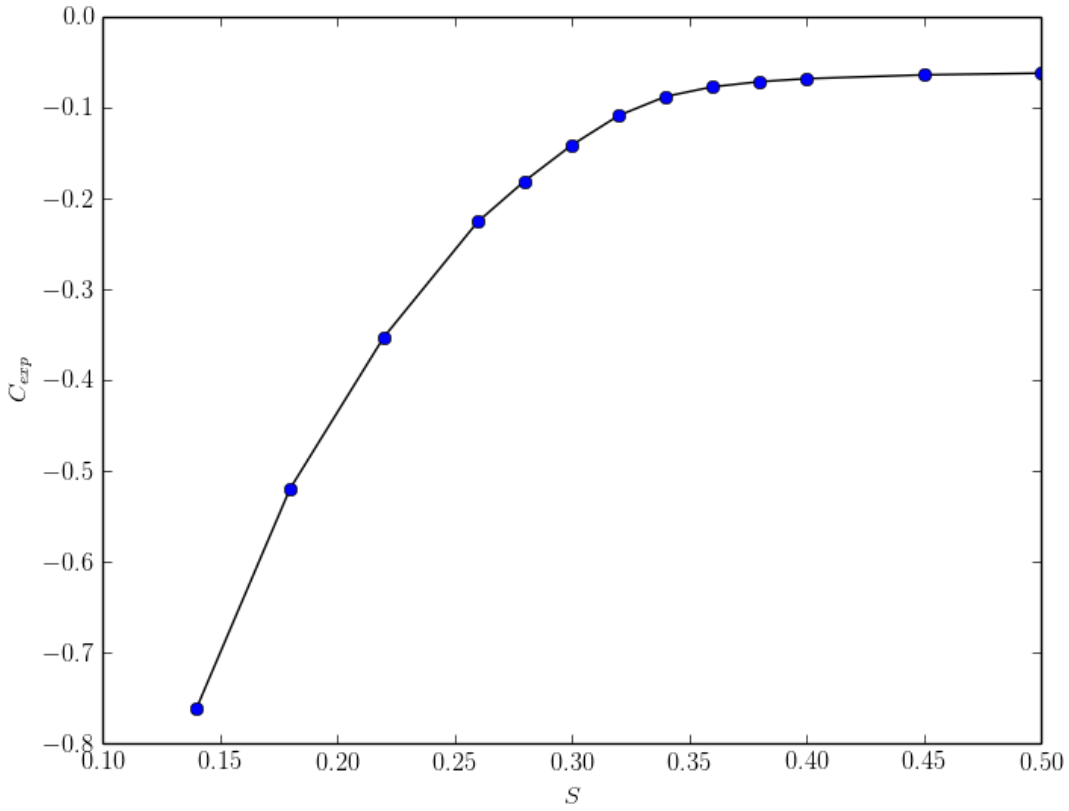

Figure 4.18: The figure shows C_{exp} for $j = 0.2$, with a critical value estimated at $S_c \approx 0.35$. It is hard to make a good estimation of the critical value as the curve is much smoother compared to lower values of j.

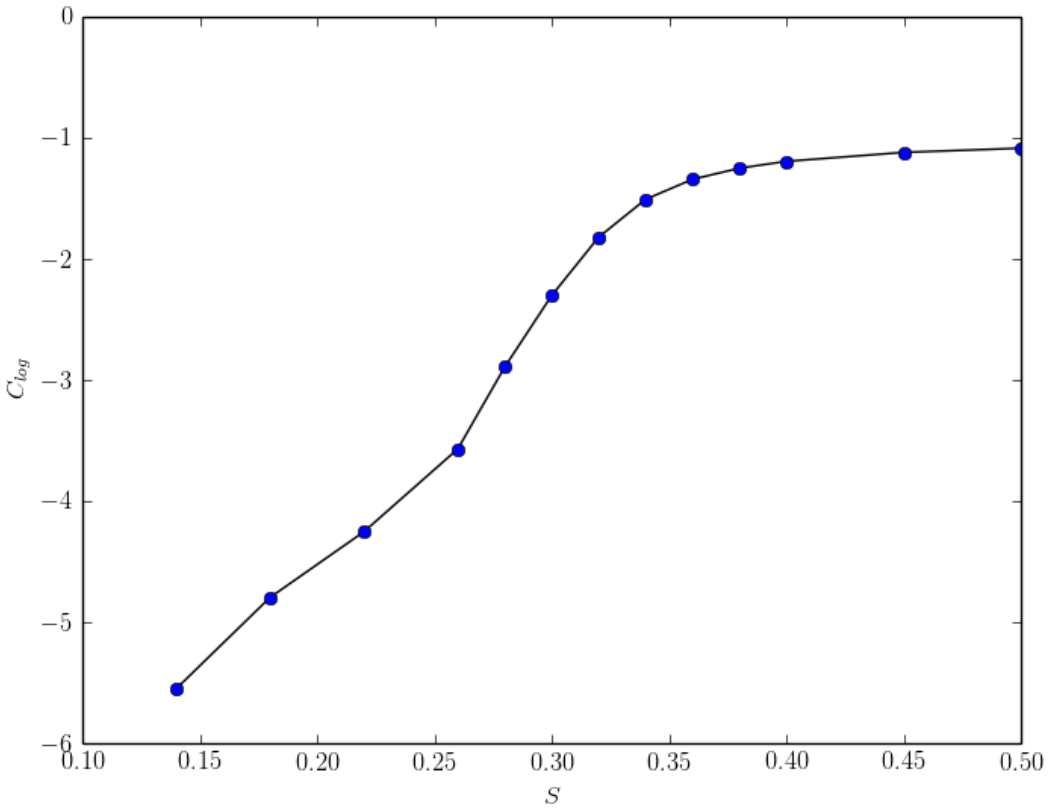

Figure 4.19: The figure shows C_{log} for $j = 0.2$, with a critical value estimated at $S_c \approx 0.35$. It is hard to make a good estimation of the critical value as the curve is much smoother compared to lower values of j.

5 Quantum Fidelity

We have one more method of investigating the phase transition between the topologically ordered spin liquid state and the magnetically ordered Néel state that we will take a look at. It is known as the quantum fidelity, or simply just the fidelity, and it measures the closeness or overlap of two quantum states. Originally an offspring of quantum information theory, the fidelity approach requires no knowledge of which, if any, symmetries are broken in the phase transition [11]. This stands in clear opposition to the method employed in chapter 4, which is purely a product of the symmetries of the spin liquid state and the triangular grid. It is therefore an appealing tool for exploring this quantum phase transition, as it brings a new and quite different perspective to the problem. From the definition of the fidelity [11]

$$f = \left|\left\langle \Psi' \middle| \Psi \right\rangle\right|, \tag{5.1}$$

we see that $0 < f < 1$ if the states are normalized. A fidelity of 1 signifies that the states are identical, and $f = 0$ occurs for two orthonormal states. A phase transition brings about a radical change of the system state, so the fidelity of two states on opposite sides of this transition should be much smaller compared to the fidelity of two states in the same phase. So by slowly moving the system from the spin liquid state over to the magnetically ordered state, we should see a drop in the fidelity when we reach the phase transition.

5.1 Ground State

First of all, we need an explicit expression for the ground state $|G\rangle$ defined in eq. (2.46). Motivated by paper [22], we try a ground state of the form:

$$|G\rangle = C \cdot \exp\left(\sum_{ij} h_{ij} \hat{A}^\dagger_{ij}\right)|0\rangle_b\,, \tag{5.2}$$

where $|0\rangle_b$ is the vacuum state for the original Schwinger-bosons, C is a noramilzation coefficient and

$$h_{ij} = \frac{1}{N}\sum_{\boldsymbol{k}} h_{\boldsymbol{k}} e^{i(\boldsymbol{r}_i - \boldsymbol{r}_j)\cdot \boldsymbol{k}}, \tag{5.3}$$

where $h_{\boldsymbol{k}}$ is assumed to be an antisymmetric function of $\boldsymbol{k}$ we will determine. Rewriting the exponent in eq. (5.2) in terms of the Fourier transformed boson operators, we get

$$\sum_{ij} h_{ij} \hat{A}^\dagger_{ij} = \sum_{\boldsymbol{k}} h_{\boldsymbol{k}} \hat{b}^\dagger_{\boldsymbol{k}\uparrow} \hat{b}^\dagger_{-\boldsymbol{k}\downarrow}, \tag{5.4}$$

as shown in eq. (A.27). For eq. (5.2) to represent a ground state for our system, we must have

$$\hat{\eta}_{k\sigma}|G\rangle = C\hat{\eta}_{k\sigma}\exp\left(\sum_k h_k \hat{b}^\dagger_{k\uparrow}\hat{b}^\dagger_{-k\downarrow}\right)|0\rangle_b = 0, \tag{5.5}$$

as this is our definition of a ground state. Let us first choose $\sigma = \uparrow$, and use eq. (2.38) to write

$$\hat{\eta}_{k\uparrow} = c_k \hat{b}_{k\uparrow} + is_k \hat{b}^\dagger_{-k\downarrow}, \tag{5.6}$$

where $c_k \equiv \cosh\theta_k$ and $s_k \equiv \sinh\theta_k$ given through eqs. (2.41) and (2.42). Defining the operator

$$\hat{L} \equiv \sum_k h_k \hat{b}^\dagger_{k\uparrow}\hat{b}^\dagger_{-k\downarrow}, \tag{5.7}$$

we rewrite the left hand side of eq. (5.5):

$$\begin{aligned}\hat{\eta}_{k\sigma}|G\rangle =& C\left(c_k\hat{b}_{k\uparrow} + is_k\hat{b}^\dagger_{-k\downarrow}\right)e^{\hat{L}}|0\rangle_b \\ =& Ce^{\hat{L}}\cdot e^{-\hat{L}}\left(c_k\hat{b}_{k\uparrow} + is_k\hat{b}^\dagger_{-k\downarrow}\right)e^{\hat{L}}|0\rangle_b \\ =& Ce^{\hat{L}}\cdot\left(c_k\cdot e^{-\hat{L}}\hat{b}_{k\uparrow}e^{\hat{L}} + is_k\cdot e^{-\hat{L}}\hat{b}^\dagger_{-k\downarrow}e^{\hat{L}}\right)|0\rangle_b .\end{aligned} \tag{5.8}$$

We now make use of what is known as the Baker-Hausdorff theorem [23]:

$$e^{-\hat{B}}\hat{A}e^{\hat{B}} = \hat{A} + \left[\hat{A},\hat{B}\right] + \frac{1}{2!}\left[\left[\hat{A},\hat{B}\right],\hat{B}\right] + \ldots = \sum_{n=0}^{\infty}\frac{1}{n!}\left[\hat{A},\hat{B}\right]_n, \tag{5.9}$$

where $\hat{A}$ and $\hat{B}$ are operators and $\left[\hat{A},\hat{B}\right]_n$ is the nested commutator defined as

$$\left[\hat{A},\hat{B}\right]_0 \equiv \hat{A} \tag{5.10}$$

$$\left[\hat{A},\hat{B}\right]_n \equiv \left[\left[\hat{A},\hat{B}\right]_{n-1},\hat{B}\right], \; n > 0. \tag{5.11}$$

Theorem (5.9) shows that the second term in eq. (5.8) is

$$e^{-\hat{L}}\hat{b}^\dagger_{-k\downarrow}e^{\hat{L}} = \hat{b}^\dagger_{-k\downarrow}, \tag{5.12}$$

since $\hat{L}$ and $\hat{b}^\dagger_{-k\downarrow}$ commute. To calculate the first term in eq. (5.8), we see that

$$\left[\hat{b}_{k\uparrow},\hat{L}\right] = \left[\hat{b}_{k\uparrow},\sum_{k'}h_{k'}\hat{b}^\dagger_{k'\uparrow}\hat{b}^\dagger_{-k'\downarrow}\right] = \sum_{k'}h_{k'}\hat{b}^\dagger_{-k'\downarrow}\left[\hat{b}_{k\uparrow},\hat{b}^\dagger_{k'\uparrow}\right] = \sum_{k'}h_{k'}\hat{b}^\dagger_{-k'\downarrow}\delta_{k,k'} = h_k\hat{b}^\dagger_{-k\downarrow}, \tag{5.13}$$

which makes all higher nested commutator terms $\left[\hat{b}_{k\uparrow},\hat{L}\right]_n$ vanish. This leaves us with

$$\hat{\eta}_{k\sigma}|G\rangle = Ce^{\hat{L}} \cdot \left(c_k\left(\hat{b}_{k\uparrow} + h_k\hat{b}^\dagger_{-k\downarrow}\right) + is_k\hat{b}^\dagger_{-k\downarrow}\right)|0\rangle_b = Ce^{\hat{L}} \cdot \left(c_k\hat{b}_{k\uparrow} + \left(c_k h_k + is_k\right)\hat{b}^\dagger_{-k\downarrow}\right)|0\rangle_b . \tag{5.14}$$

The annihilation operators $\hat{b}_{k\sigma}$ are a sum of the original annihilation operators $\hat{b}_{i\sigma}$ according to eq. (2.19), so

$$c_k\hat{b}_{k\uparrow}|0\rangle_b = 0. \tag{5.15}$$

However, we must force the second term to be zero by choosing

$$h_k = -i\frac{s_k}{c_k} \tag{5.16}$$

to satisfy condition (5.5). The same expression for h_k is needed to satisfy $\hat{\eta}_{k\downarrow}|G\rangle = 0$, and we see that our assumption $h_{-k} = -h_k$ indeed is true. We note that

$$c_k = = \frac{1}{\sqrt{2}}\sqrt{\cosh 2\theta_k + 1} = \frac{1}{\sqrt{2}}\sqrt{\frac{\gamma^B_k + \tilde{\lambda}}{\omega_k} + 1} \tag{5.17}$$

$$s_k = \pm\frac{1}{\sqrt{2}}\sqrt{\cosh 2\theta_k - 1} = \pm\frac{1}{\sqrt{2}}\sqrt{\frac{\gamma^B_k + \tilde{\lambda}}{\omega_k} - 1}, \tag{5.18}$$

and since

$$\sinh\theta_k = \frac{1}{2}\cdot\frac{\sinh 2\theta_k}{\cosh\theta_k}, \tag{5.19}$$

the sign of s_k is

$$\operatorname{sgn}(s_k) = \operatorname{sgn}(\sinh 2\theta_k) = -\operatorname{sgn}(\gamma^A_k). \tag{5.20}$$

We finally end up with the expression for h_k as

$$h_k = i\operatorname{sgn}(\gamma^A_k)\sqrt{\frac{(\gamma^B_k + \tilde{\lambda})/\omega_k - 1}{(\gamma^B_k + \tilde{\lambda})/\omega_k + 1}}. \tag{5.21}$$

5.2 Susceptibility of the Fidelity

Now we can calculate the expression of the fidelity between two ground states, $|G\rangle$ and $|G'\rangle$, at different points in parameter space. As shown in eq. (A.28), we get

$$f = \left|\langle G'|G\rangle\right| = CC' \cdot \prod_k \frac{1}{\left|1 + h'_k h_k\right|}. \tag{5.22}$$

From this and the normalization condition $\langle G|G\rangle = 1$, we find that the constant C is

$$\frac{1}{C^2} = \prod_k \frac{1}{1+h_k^2} = \prod_k \left(1 - \left(\mathrm{sgn}(\gamma_k^A)\right)^2 \frac{(\gamma_k^B+\tilde{\lambda})/\omega_k - 1}{(\gamma_k^B+\tilde{\lambda})/\omega_k + 1}\right)^{-1}$$
$$= \prod_k \frac{1}{2}\left(\frac{\gamma_k^B+\tilde{\lambda}}{\omega_k} + 1\right). \tag{5.23}$$

It is more practical to calculate the logarithm of the normalization constant

$$\ln(C) = \frac{N}{2}\ln(2) - \frac{1}{2}\sum_k \ln\left(\frac{\gamma_k^B+\tilde{\lambda}}{\omega_k} + 1\right), \tag{5.24}$$

and the fidelity

$$\ln(f) = \ln(C) + \ln(C') - \sum_k \ln\left(\left|1 + h_k h_k'\right|\right), \tag{5.25}$$

to avoid problems with the accuracy of the numerical calculations. This far, we have not put any restrictions on the two arbitrary ground states except from the form of h_k. However, for the fidelity to be of any use to us, we will only be looking at ground states separated by a small distance in parameter space. And to make calculations simple, we will only be changing one parameter at a time, keeping everything else constant. The two clear candidates for parameters to vary are the value of the spin S and the relative interaction strength j. For now, we will vary the generic parameter p, so that $|G\rangle = \left|G(p)\right\rangle$ and $|G'\rangle = \left|G(p+\delta p)\right\rangle$. This lets us calculate what is known as the susceptibility of the fidelity [11]:

$$\chi_f = \lim_{\delta p \to 0} \frac{-2\ln(f)}{(\delta p)^2} = -\frac{\partial^2 f}{\partial(\delta p)^2}. \tag{5.26}$$

This is the leading term in the series expansion of the fidelity around the parameter p, which is a measure of the response of the fidelity to a small change δp. As the fidelity will be at a local minimum with $f < 1$ at the point of a phase transition, χ_f will exhibit a local maximum at the same spot.

We start by looking at the fidelity when we let p be the relative interaction strength j. For $S = 0.1$, deep inside the spin liquid region when $j = 0$, χ_f has the monotonically decreasing form shown in fig. 5.1. It is clear that there is no phase transition for this spin value in the region $0 < j < 0.2$, as χ_f has no local maxima. The story is different for $S = 0.21$, which is shown in fig. 5.2. The maximal value, and therefore the phase transition, occurs for $j \approx 0.015$. This is fairly consistent with what we have found in previous chapters, where the critical spin value is $S_c \approx 0.21$ for $j = 0$. Similarly we found that $j = 0.1$ resulted in $S_c \approx 0.25$, which is in agreement with fig. 5.3. When we increase the spin value further to $S > 0.35$, we see that the local maximum of χ_f turns into a saddle point, which means we can no longer detect a phase transition in the region $0 < j < 0.2$, and as in the previous chapters the results might be influenced by ordered states different from the Néel state. Our previous results for the critical spin value at $j = 0.2$ is $S_c \approx 0.31$ in chapter 3

and $S_c \approx 0.35$ in chapter 4.

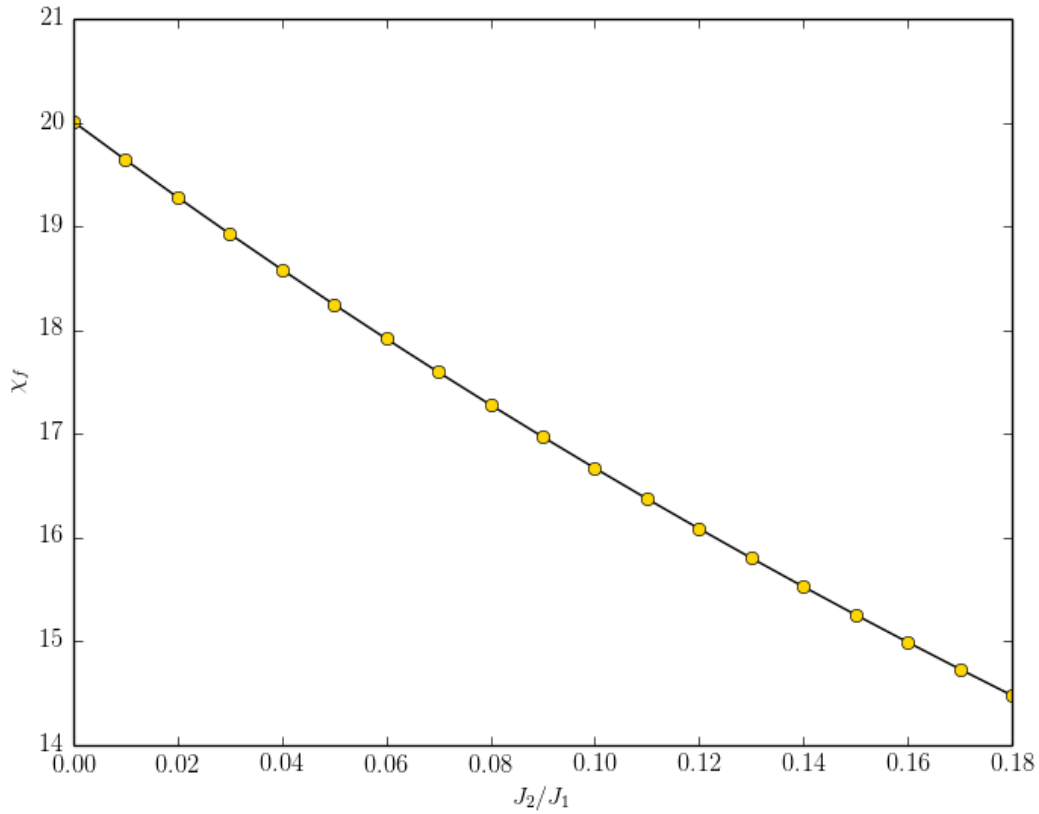

Figure 5.1: The figure shows the susceptibility for $S = 0.1$, $\delta j = 0.02$ and $N = 3600$. There is no local maxima, and so no phase transition is visible.

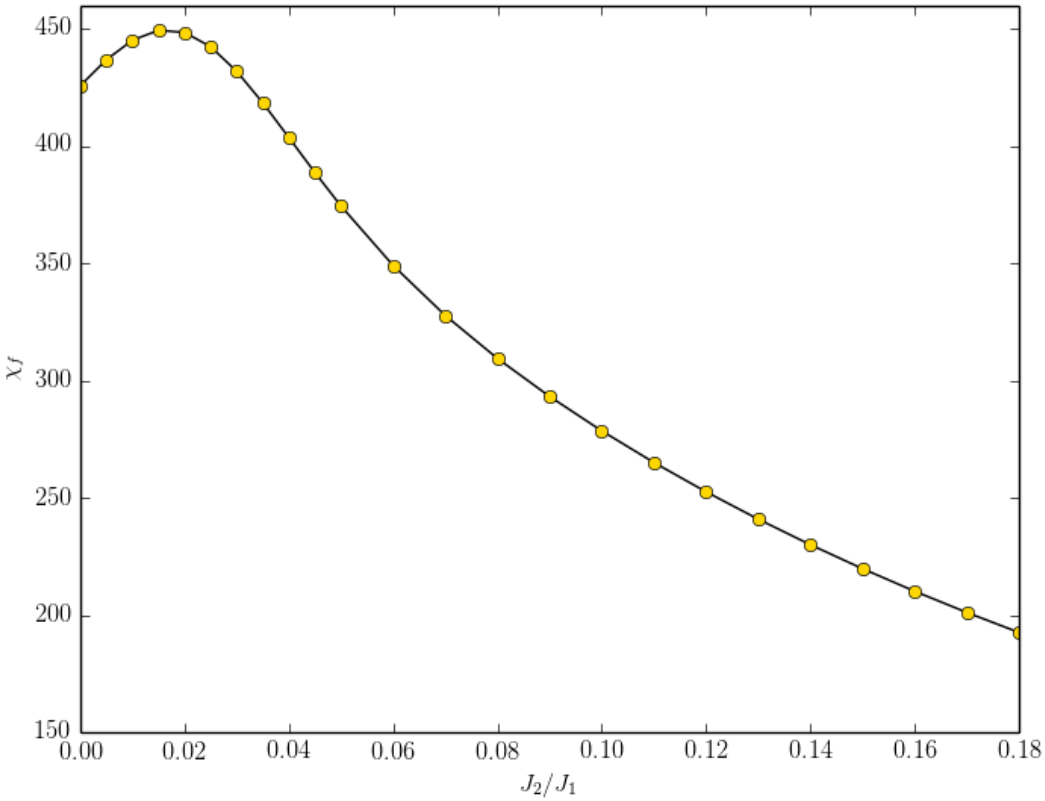

Figure 5.2: The figure shows the susceptibility for $S = 0.21$, $\delta j = 0.02$ and $N = 3600$. We see a phase transition for $j \approx 0.015$.

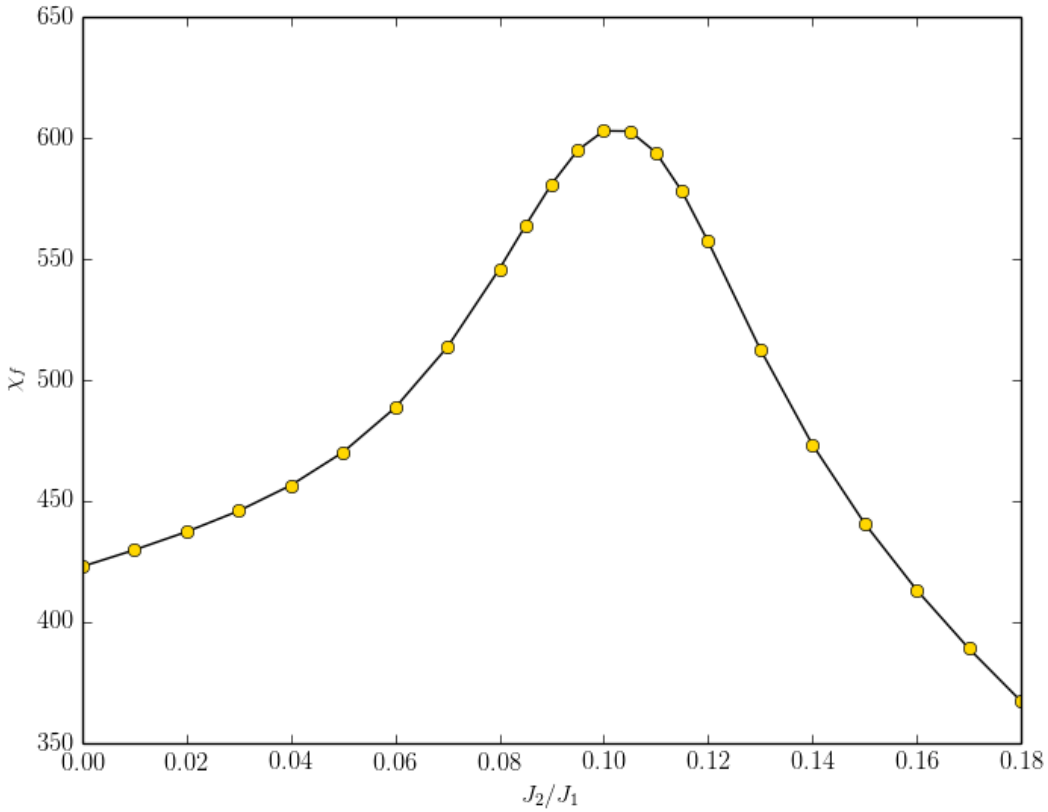

Figure 5.3: The figure shows the susceptibility for $S = 0.25$, $\delta j = 0.02$ and $N = 3600$. The top at $j \approx 0.105$ signifies a phase transition.

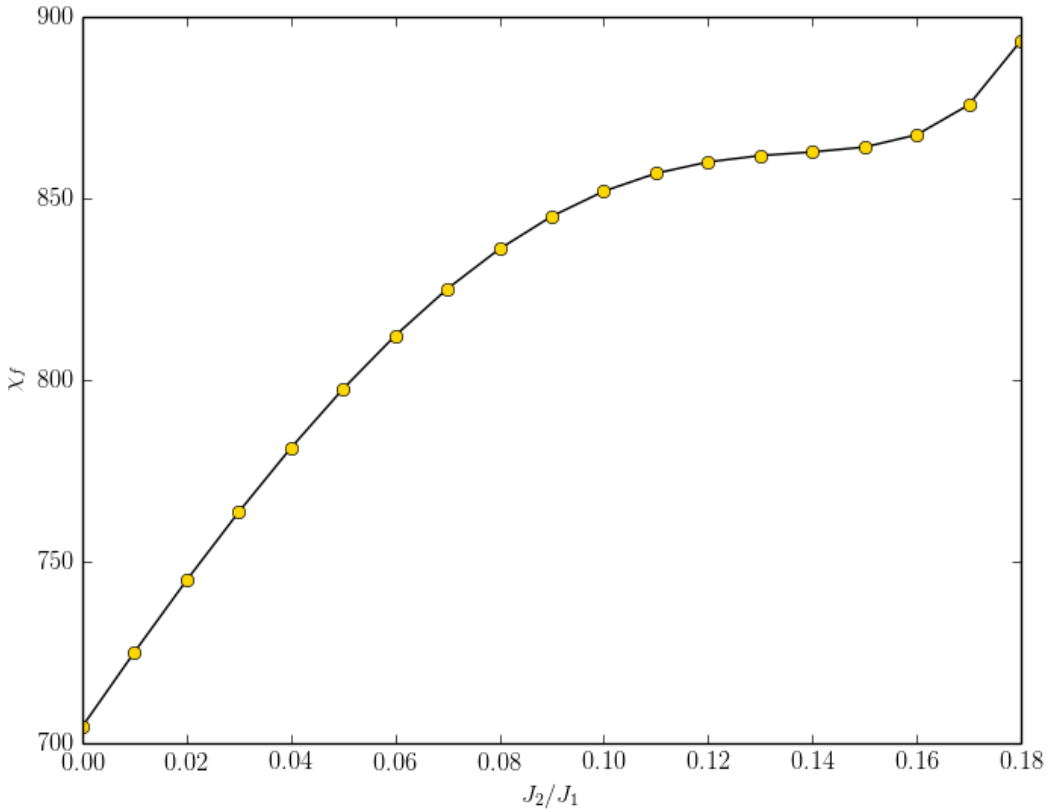

Figure 5.4: The figure shows the susceptibility for $S = 0.36$, $\delta j = 0.02$ and $N = 3600$. There is no local maxima, only a saddle point, so we detect no phase transition in this region.

In these calculations we have used $\delta j = 0.02$ and $N = 3600$. The effect of changing δj is shown in fig. 5.5, and fig. 5.6 shows the effect of changing the system size. As we can see, a smaller δj shifts the top of χ_f towards the higher values of j, while the opposite is true for increasing the system size. These effects are definitely important when it comes to precisely identifying the point of the phase transition, so the accuracy of the calculations shown in figs. 5.2 to 5.4 is not very high. The effects pulling in opposite directions is a saving grace, as it will correct some of the error.

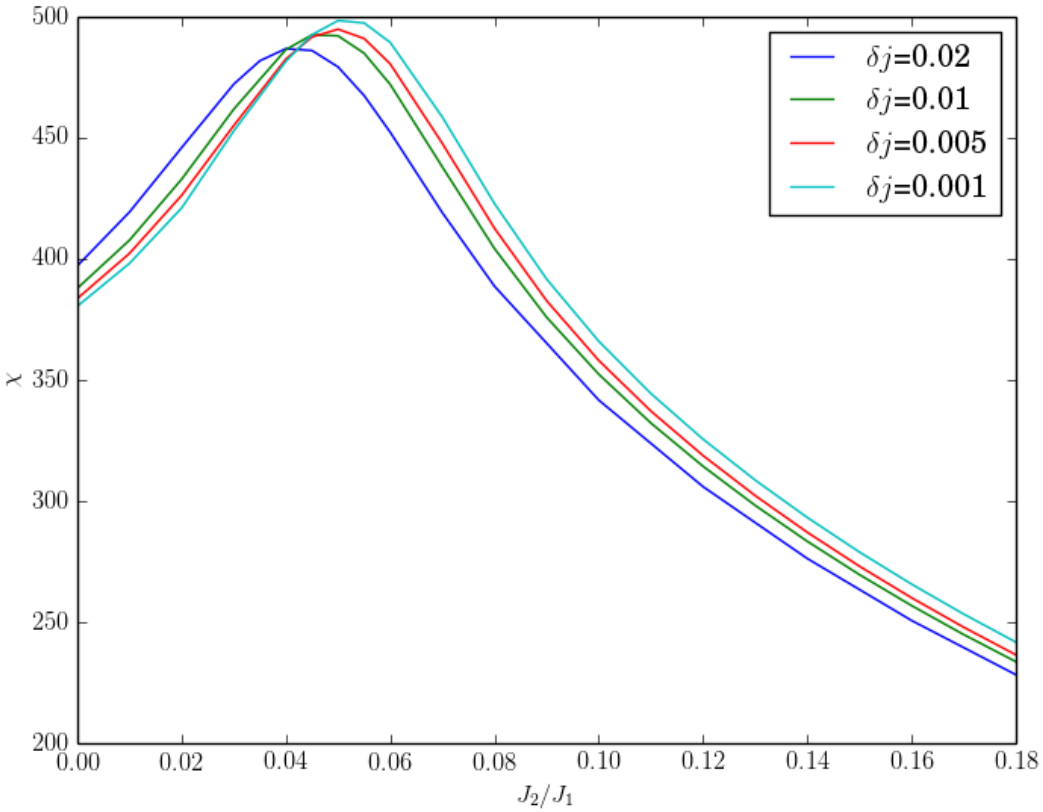

Figure 5.5: The figure shows the effect of changing δj for a system with $N = 3600$ and $S = 0.22$.

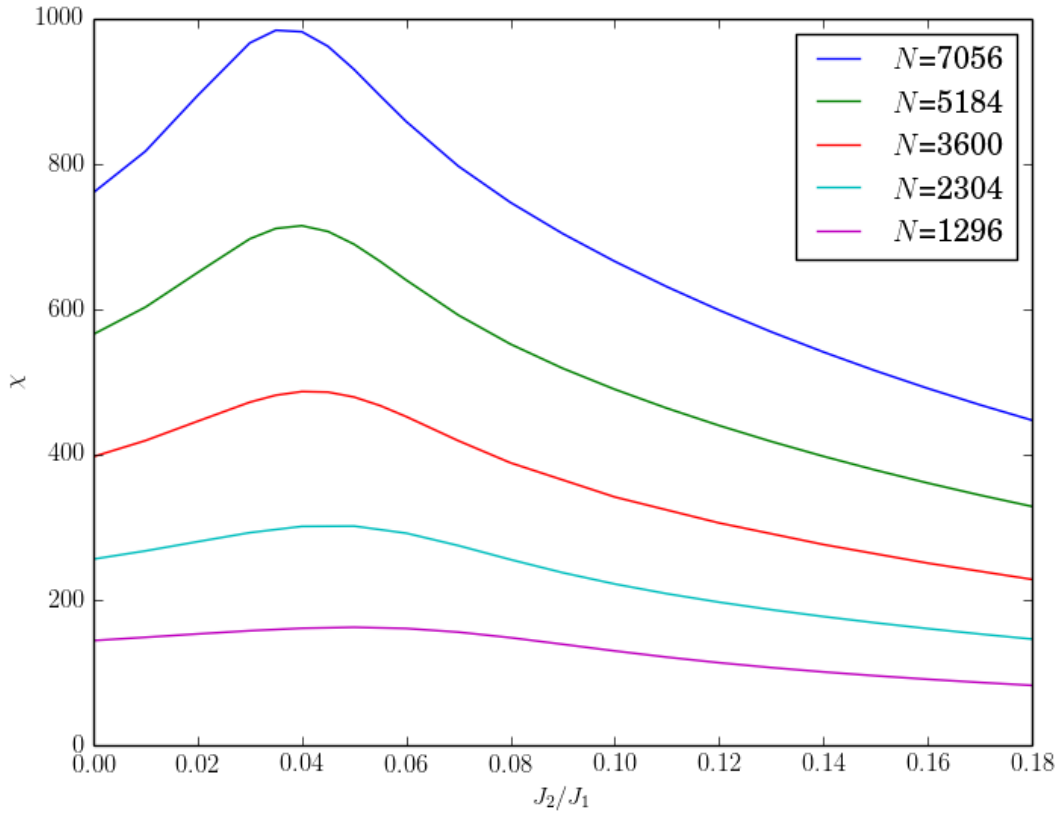

Figure 5.6: The figure shows the effect of changing N for a system with $\delta j = 0.02$ and $S = 0.22$.

Figure (5.7) shows a low resolution contour plot of χ_f in j-S parameter space, where each strip of constant S has been calculated separately. The white line visible indicates the location of the phase transition, and we can see that it compares with figure 8 from paper [9].

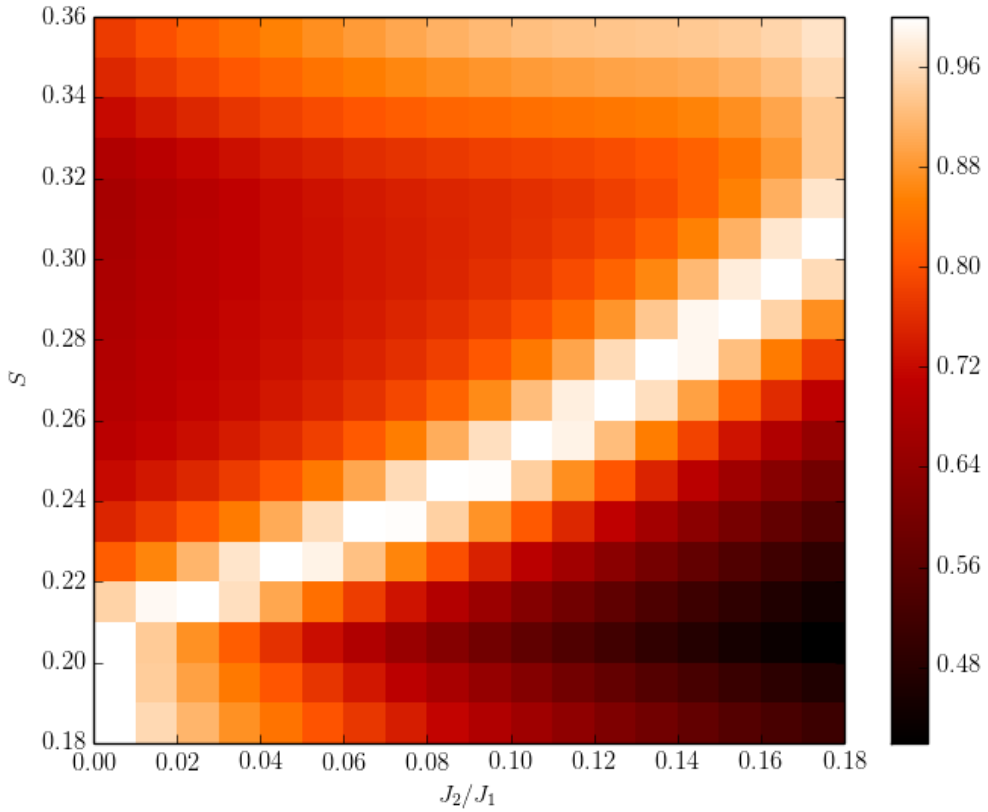

Figure 5.7: The figure shows a contour plot of the susceptibility χ_f in S-j parameter space for $N = 3600$ and $\delta j = 0.02$. Each horizontal line is calculated separately, and normalized by its maximal value for visual purposes. For $S < 0.21$ the maximal value of each strip is located at $j = 0$, as they resemble fig. 5.1. No phase tansition has occurred in this region. For $0.21 < S < 0.36$, we see the phase tansition as the white line curving upwards, and each strip resembles fig. 5.3. Above this region, we have the case illustrated in fig. 5.4, with no phase tansition. Note that the resolution of the plot is low, and is intended mainly for illustrative purposes.

As it turns out, varying S and keeping j constant does not produce similar results for the fidelity calculations. Figure (5.8) shows that the phase transition at $j = 0.1$ and $S \approx 0.25$ is not present. This is surprising, and we do not have a good answer for this behaviour. It could possibly be related to the fact that we are treating the half-integer parameter S a continuous, even though this works well for the sublattice magnetization.

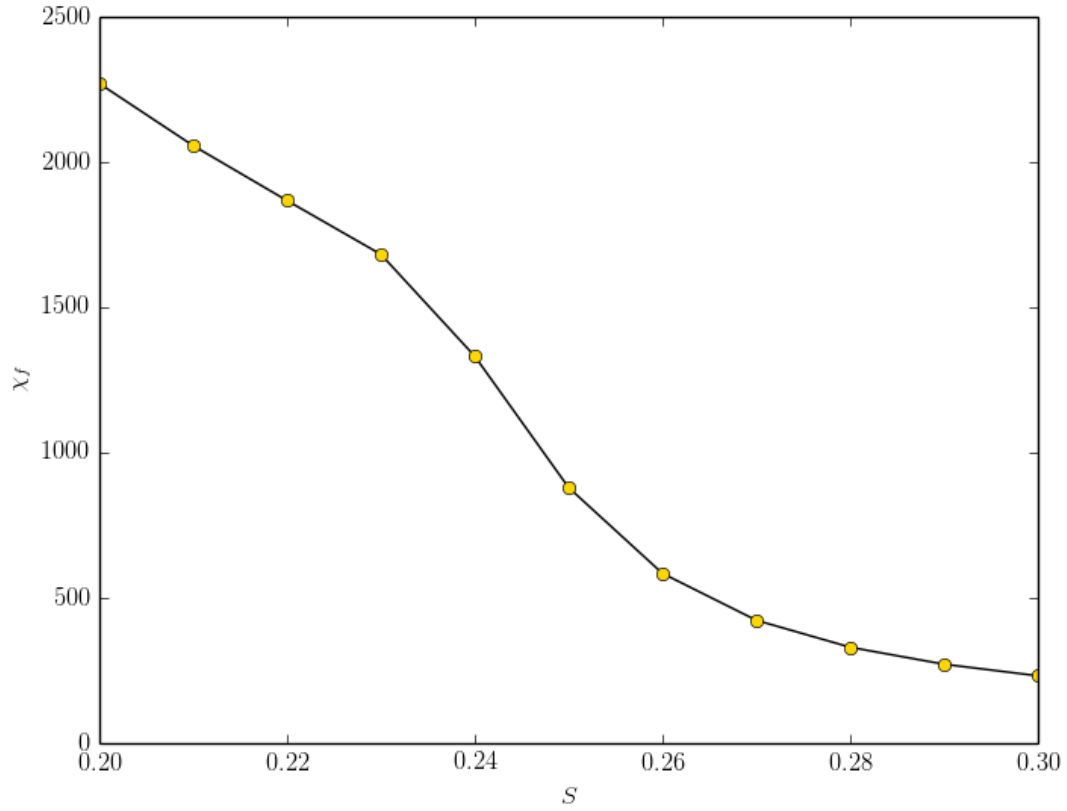

Figure 5.8: Shows χ_f when $j = 0.1$ is constant and S is varied from 0.2 to 0.3 with $\delta S = 0.01$. We would expect to see a phase transition at $S \approx 0.25$, but this it not present in the plot.

6 Conclusion

Based on the variety of the methods we have used and the results in [9], we can say with little doubt that the critical spin value of the phase transition from spin liquid to Néel order is $S_c \approx 0.21$ for $j = 0$ in the mean field approximation of the Heisenberg antiferromagnet. The methods also agree that $S_c \approx 0.25$ for $j = 0.1$, but as the strength of the next nearest neighbour interactions increase, S_c is harder to precisely establish. The parameters we are plotting seem to undergo a smoother transition from the spin liquid phase to the magnetically ordered one, especially close to $j = 0.2$. The three different methods have quite a gap in their predictions for this value of j, ranging from $S_c \approx 0.31$ for the sublattice magnetization calculation, to $S_c \approx 0.35$ for the topologically degenerate states energy difference and the fidelity. This is might be due to the existence of other phases than the spin liquid and Néel order somewhere in the region $0.125 < j < 0.2$ [17] that we have not taken into account in our numerical analysis, so our calculations should not be trusted blindly in this region.

The conclusion of our analysis is that all of the three presented methods are able to detect the quantum phase shift from spin liquid to Néel order in the mean field triangular Heisenberg antiferromagnet. These methods are based on different principles and phenomena, so it is a compelling result when the estimates of S_c from all three methods agree. However, there are some issues related to the methods, for instance that not all next nearest neighbour bonds are flipped correctly in our calculation of ΔE and that the fidelity does not seem to pick up a signal of a phase transition when we treat S as a continuous variable. We should also restrict our region of validity for these methods to $j < 0.125$, as we are uncertain of how the other ordered magnetic states interfere with our calculations.

A Appendix: Details of Calculations

Since nothing is more frustrating than reading an article where several pages of calculations have gone missing between a few lines of text, this appendix was added.

A.1 Commutator relations

Our first aim is to prove eq. (2.3). We define a general state $\left|n_1, n_2, ..., n_\nu, ..., n_\mu, ...\right\rangle \equiv \left|n_\nu, n_\mu\right\rangle$, where n_j is the number of bosons in state j. The creation and annihilation boson operators will work on such a state in the following way [13]:

$$\hat{b}_\mu \left|n_\nu, n_\mu\right\rangle = \sqrt{n_\mu}\left|n_\nu, n_\mu - 1\right\rangle \tag{A.1}$$

$$\hat{b}_\mu^\dagger \left|n_\nu, n_\mu\right\rangle = \sqrt{n_\mu + 1}\left|n_\nu, n_\mu + 1\right\rangle. \tag{A.2}$$

Now, assume first that $\nu \neq \mu$, and let the boson commutator operate on the general state:

$$\begin{aligned}\left[\hat{b}_\mu, \hat{b}_\nu^\dagger\right]\left|n_\nu, n_\mu\right\rangle &\equiv \left(\hat{b}_\mu \hat{b}_\nu^\dagger - \hat{b}_\nu^\dagger \hat{b}_\mu\right)\left|n_\nu, n_\mu\right\rangle \\ &= \left(\sqrt{(n_\nu + 1)(n_\mu - 1)} - \sqrt{(n_\mu - 1)(n_\nu + 1)}\right)\left|n_\nu + 1, n_\mu - 1\right\rangle = 0.\end{aligned} \tag{A.3}$$

However, if $\nu = \mu$, we get

$$\left[\hat{b}_\mu, \hat{b}_\mu^\dagger\right]\left|n_\mu\right\rangle = \left(\sqrt{(n_\mu + 1)^2} - \sqrt{n_\mu^2}\right)\left|n_\mu\right\rangle = 1 \cdot \left|n_\mu\right\rangle, \tag{A.4}$$

resulting in the commutator relation

$$\left[\hat{b}_\mu, \hat{b}_\nu^\dagger\right] = \delta_{\mu,\nu}. \tag{A.5}$$

The rest of the commutator relations eq. (2.3) may be shown in a similar way.

The Fourier transformed operators $\hat{b}_{\boldsymbol{k}\sigma}$ follow the same commutator relation eq. (2.3):

$$\begin{aligned}\left[\hat{b}_{\boldsymbol{k}\sigma}, \hat{b}_{\boldsymbol{k}'\sigma}^\dagger\right] &= \hat{b}_{\boldsymbol{k}\sigma}\hat{b}_{\boldsymbol{k}'\sigma}^\dagger - \hat{b}_{\boldsymbol{k}'\sigma}^\dagger \hat{b}_{\boldsymbol{k}\sigma} = \frac{1}{N}\sum_i e^{-i\boldsymbol{k}\cdot\boldsymbol{r}_i}\hat{b}_{i\sigma}\sum_j e^{i\boldsymbol{k}'\cdot\boldsymbol{r}_j}\hat{b}_{j\sigma}^\dagger - \frac{1}{N}\sum_j e^{i\boldsymbol{k}'\cdot\boldsymbol{r}_j}\hat{b}_{j\sigma}^\dagger \sum_i e^{-i\boldsymbol{k}\cdot\boldsymbol{r}_i}\hat{b}_{i\sigma} \\ &= \frac{1}{N}\sum_{ij} e^{i(\boldsymbol{k}'\cdot\boldsymbol{r}_j - \boldsymbol{k}\cdot\boldsymbol{r}_i)}\left(\hat{b}_{i\sigma}\hat{b}_{j\sigma}^\dagger - \hat{b}_{j\sigma}^\dagger\hat{b}_{i\sigma}\right) = \frac{1}{N}\sum_{ij} e^{i(\boldsymbol{k}'\cdot\boldsymbol{r}_j - \boldsymbol{k}\cdot\boldsymbol{r}_i)}\left[\hat{b}_{i\sigma}, \hat{b}_{j\sigma}^\dagger\right] \\ &= \frac{1}{N}\sum_{ij} e^{i(\boldsymbol{k}'\cdot\boldsymbol{r}_j - \boldsymbol{k}\cdot\boldsymbol{r}_i)}\delta_{i,j} = \frac{1}{N}\sum_i e^{i(\boldsymbol{k}'-\boldsymbol{k})\cdot\boldsymbol{r}_i} = \delta_{\boldsymbol{k},\boldsymbol{k}'}\end{aligned} \tag{A.6}$$

where we have used eq. (B.15) and eq. (A.5). Again, the other commutator relations follow in a similar way.

Finally, the commutator of the Bogoliubov transformed operators $\hat{\eta}_{k\uparrow}$ and $\hat{\eta}^{\dagger}_{k'\uparrow}$ is

$$\begin{aligned}\left[\hat{\eta}_{k\uparrow},\hat{\eta}^{\dagger}_{k'\uparrow}\right]&=\left[u_k\hat{b}_{k\uparrow}+iv_k\hat{b}^{\dagger}_{-k\downarrow}\,,\,u_{k'}\hat{b}^{\dagger}_{k'\uparrow}-iv_{k'}\hat{b}_{-k'\downarrow}\right]\\&=\left[u_k\hat{b}_{k\uparrow},u_{k'}\hat{b}^{\dagger}_{k'\uparrow}\right]+\left[iv_k\hat{b}^{\dagger}_{-k\downarrow},-iv_{k'}\hat{b}_{-k'\downarrow}\right]\\&=\left(u_ku_{k'}-v_kv_{k'}\right)\delta_{k,k'},\end{aligned}\tag{A.7}$$

where we have used eq. (A.6) and some general properties of the commutator brackets. For $\boldsymbol{k}=\boldsymbol{k}'$, we get $\left[\hat{\eta}_{k\uparrow},\hat{\eta}^{\dagger}_{k'\uparrow}\right]=u_k^2-v_k^2$. To keep the commutator on the same form as eq. (2.3), we must choose $u_k^2-v_k^2=1$. The rest of the constraints in (2.35) can be shown in a similar way by using the other two equations in (2.34).

A.2 The spin dot product expressed by Scwinger-bosons

The spin dot product between two different lattice sites i and j, using the definition (2.2), is

$$\begin{aligned}\hat{\boldsymbol{S}}_i\cdot\hat{\boldsymbol{S}}_j&=\hat{S}_i^x\hat{S}_j^x+\hat{S}_i^y\hat{S}_j^y+\hat{S}_i^z\hat{S}_j^z\\&=\frac{1}{2}\left(\hat{b}^{\dagger}_{i\uparrow}\hat{b}_{i\downarrow}\hat{b}^{\dagger}_{j\downarrow}\hat{b}_{j\uparrow}+\hat{b}^{\dagger}_{i\downarrow}\hat{b}_{i\uparrow}\hat{b}^{\dagger}_{j\uparrow}\hat{b}_{j\downarrow}\right)+\frac{1}{4}\left(\hat{b}^{\dagger}_{i\uparrow}\hat{b}_{i\uparrow}-\hat{b}^{\dagger}_{i\downarrow}\hat{b}_{i\downarrow}\right)\left(\hat{b}^{\dagger}_{j\uparrow}\hat{b}_{j\uparrow}-\hat{b}^{\dagger}_{j\downarrow}\hat{b}_{j\downarrow}\right)\\&=\frac{1}{4}\left(\hat{b}^{\dagger}_{i\uparrow}\hat{b}_{i\uparrow}\hat{b}^{\dagger}_{j\uparrow}\hat{b}_{j\uparrow}+\hat{b}^{\dagger}_{i\downarrow}\hat{b}_{i\downarrow}\hat{b}^{\dagger}_{j\downarrow}\hat{b}_{j\downarrow}-\hat{b}^{\dagger}_{i\uparrow}\hat{b}_{i\uparrow}\hat{b}^{\dagger}_{j\downarrow}\hat{b}_{j\downarrow}-\hat{b}^{\dagger}_{i\downarrow}\hat{b}_{i\downarrow}\hat{b}^{\dagger}_{j\uparrow}\hat{b}_{j\uparrow}+2\hat{b}^{\dagger}_{i\uparrow}\hat{b}_{i\downarrow}\hat{b}^{\dagger}_{j\downarrow}\hat{b}_{j\uparrow}+2\hat{b}^{\dagger}_{i\downarrow}\hat{b}_{i\uparrow}\hat{b}^{\dagger}_{j\uparrow}\hat{b}_{j\downarrow}\right).\end{aligned}\tag{A.8}$$

From the definitions of the A and B field, see eq. (2.4), we may compute the product

$$\begin{aligned}\hat{A}^{\dagger}_{ij}\hat{A}_{ij}&=\frac{1}{4}\left(\hat{b}^{\dagger}_{i\uparrow}\hat{b}^{\dagger}_{j\downarrow}-\hat{b}^{\dagger}_{i\downarrow}\hat{b}^{\dagger}_{j\uparrow}\right)\left(\hat{b}_{i\uparrow}\hat{b}_{j\downarrow}-\hat{b}_{i\downarrow}\hat{b}_{j\uparrow}\right)\\&=\frac{1}{4}\left(\hat{b}^{\dagger}_{i\uparrow}\hat{b}_{i\uparrow}\hat{b}^{\dagger}_{j\downarrow}\hat{b}_{j\downarrow}+\hat{b}^{\dagger}_{i\downarrow}\hat{b}_{i\downarrow}\hat{b}^{\dagger}_{j\uparrow}\hat{b}_{j\uparrow}-\hat{b}^{\dagger}_{i\uparrow}\hat{b}_{i\downarrow}\hat{b}^{\dagger}_{j\downarrow}\hat{b}_{j\uparrow}-\hat{b}^{\dagger}_{i\downarrow}\hat{b}_{i\uparrow}\hat{b}^{\dagger}_{j\uparrow}\hat{b}_{j\downarrow}\right),\end{aligned}\tag{A.9}$$

and

$$\begin{aligned}
\hat{B}_{ij}^\dagger \hat{B}_{ij} =& \frac{1}{4}\left(\hat{b}_{i\uparrow}^\dagger \hat{b}_{j\uparrow} + \hat{b}_{i\downarrow}^\dagger \hat{b}_{j\downarrow}\right)\left(\hat{b}_{i\uparrow}\hat{b}_{j\uparrow}^\dagger + \hat{b}_{i\downarrow}\hat{b}_{j\downarrow}^\dagger\right) \\
=& \frac{1}{4}\left(\hat{b}_{i\uparrow}^\dagger \hat{b}_{i\uparrow}\hat{b}_{j\uparrow}\hat{b}_{j\uparrow}^\dagger + \hat{b}_{i\downarrow}^\dagger \hat{b}_{i\downarrow}\hat{b}_{j\downarrow}\hat{b}_{j\downarrow}^\dagger + \hat{b}_{i\uparrow}^\dagger \hat{b}_{i\downarrow}\hat{b}_{j\downarrow}^\dagger \hat{b}_{j\uparrow} + \hat{b}_{i\downarrow}^\dagger \hat{b}_{i\uparrow}\hat{b}_{j\uparrow}^\dagger \hat{b}_{j\downarrow}\right) \\
=& \frac{1}{4}\left(\hat{b}_{i\uparrow}^\dagger \hat{b}_{i\uparrow}(1+\hat{b}_{j\uparrow}^\dagger \hat{b}_{j\uparrow}) + \hat{b}_{i\downarrow}^\dagger \hat{b}_{i\downarrow}(1+\hat{b}_{j\downarrow}^\dagger \hat{b}_{j\downarrow}) + \hat{b}_{i\uparrow}^\dagger \hat{b}_{i\downarrow}\hat{b}_{j\downarrow}^\dagger \hat{b}_{j\uparrow} + \hat{b}_{i\downarrow}^\dagger \hat{b}_{i\uparrow}\hat{b}_{j\uparrow}^\dagger \hat{b}_{j\downarrow}\right) \\
=& \frac{1}{4}\left(\hat{b}_{i\uparrow}^\dagger \hat{b}_{i\uparrow}\hat{b}_{j\uparrow}^\dagger \hat{b}_{j\uparrow} + \hat{b}_{i\downarrow}^\dagger \hat{b}_{i\downarrow}\hat{b}_{j\downarrow}^\dagger \hat{b}_{j\downarrow} + \hat{b}_{i\uparrow}^\dagger \hat{b}_{i\downarrow}\hat{b}_{j\downarrow}^\dagger \hat{b}_{j\uparrow} + \hat{b}_{i\downarrow}^\dagger \hat{b}_{i\uparrow}\hat{b}_{j\uparrow}^\dagger \hat{b}_{j\downarrow}\right) + \frac{1}{4}\left(\hat{b}_{i\uparrow}^\dagger \hat{b}_{i\uparrow} + \hat{b}_{i\downarrow}^\dagger \hat{b}_{i\downarrow}\right) \\
\equiv& :\hat{B}_{ij}^\dagger \hat{B}_{ij}: + \frac{1}{4}\left(\hat{b}_{i\uparrow}^\dagger \hat{b}_{i\uparrow} + \hat{b}_{i\downarrow}^\dagger \hat{b}_{i\downarrow}\right).
\end{aligned} \tag{A.10}$$

Comparing these directly with eq. (A.8), we see that

$$\hat{\mathbf{S}}_i \cdot \hat{\mathbf{S}}_j = :\hat{B}_{ij}^\dagger \hat{B}_{ij}: - \hat{A}_{ij}^\dagger \hat{A}_{ij} = \hat{B}_{ij}^\dagger \hat{B}_{ij} - \hat{A}_{ij}^\dagger \hat{A}_{ij} - \frac{1}{4}\left(\hat{b}_{i\uparrow}^\dagger \hat{b}_{i\uparrow} + \hat{b}_{i\downarrow}^\dagger \hat{b}_{i\downarrow}\right), \tag{A.11}$$

where we have defined $:\hat{B}_{ij}^\dagger \hat{B}_{ij}: = \frac{1}{4}\left(\hat{b}_{i\uparrow}^\dagger \hat{b}_{i\uparrow}\hat{b}_{j\uparrow}^\dagger \hat{b}_{j\uparrow} + \hat{b}_{i\downarrow}^\dagger \hat{b}_{i\downarrow}\hat{b}_{j\downarrow}^\dagger \hat{b}_{j\downarrow} + \hat{b}_{i\uparrow}^\dagger \hat{b}_{i\downarrow}\hat{b}_{j\downarrow}^\dagger \hat{b}_{j\uparrow} + \hat{b}_{i\downarrow}^\dagger \hat{b}_{i\uparrow}\hat{b}_{j\uparrow}^\dagger \hat{b}_{j\downarrow}\right)$. Using the definitions eq. (2.6) and eq. (2.7), we rewrite eq. (A.11) as

$$\begin{aligned}
\hat{\mathbf{S}}_i \cdot \hat{\mathbf{S}}_{ij} =& \left(\mathcal{B}_{ij} + \delta\hat{B}_{ij}^\dagger\right)\left(\mathcal{B}_{ij} + \delta\hat{B}_{ij}\right) - \left(\mathcal{A}_{ij} + \delta\hat{A}_{ij}^\dagger\right)\left(\mathcal{A}_{ij} + \delta\hat{A}_{ij}\right) - \frac{1}{4}\left(\hat{b}_{i\uparrow}^\dagger \hat{b}_{i\uparrow} + \hat{b}_{i\downarrow}^\dagger \hat{b}_{i\downarrow}\right) \\
=& \mathcal{B}_{ij}^2 + \mathcal{B}_{ij}\left(\delta\hat{B}_{ij}^\dagger + \delta\hat{B}_{ij}\right) - \mathcal{A}_{ij}^2 - \mathcal{A}_{ij}\left(\delta\hat{A}_{ij}^\dagger + \delta\hat{A}_{ij}\right) - \frac{1}{4}\left(\hat{b}_{i\uparrow}^\dagger \hat{b}_{i\uparrow} + \hat{b}_{i\downarrow}^\dagger \hat{b}_{i\downarrow}\right) + \mathcal{O}(\delta^2) \\
=& \mathcal{A}_{ij}^2 - \mathcal{B}_{ij}^2 + \mathcal{B}_{ij}\hat{B}_{ij} + \mathcal{B}_{ij}\hat{B}_{ij}^\dagger - \mathcal{A}_{ij}\hat{A}_{ij} - \mathcal{A}_{ij}\hat{A}_{ij}^\dagger - \frac{1}{4}\left(\hat{b}_{i\uparrow}^\dagger \hat{b}_{i\uparrow} + \hat{b}_{i\downarrow}^\dagger \hat{b}_{i\downarrow}\right) + \mathcal{O}(\delta^2).
\end{aligned} \tag{A.12}$$

The square of the spin operator on a lattice site i is

$$\begin{aligned}
\hat{\mathbf{S}}_i \cdot \hat{\mathbf{S}}_i =& \frac{1}{4}\left(2\hat{b}_{i\uparrow}^\dagger \hat{b}_{i\uparrow}\hat{b}_{i\downarrow}\hat{b}_{i\downarrow}^\dagger + 2\hat{b}_{i\uparrow}\hat{b}_{i\uparrow}^\dagger \hat{b}_{i\downarrow}^\dagger \hat{b}_{i\downarrow} + \hat{b}_{i\uparrow}^\dagger \hat{b}_{i\uparrow}\hat{b}_{i\uparrow}^\dagger \hat{b}_{i\uparrow} + \hat{b}_{i\downarrow}^\dagger \hat{b}_{i\downarrow}\hat{b}_{i\downarrow}^\dagger \hat{b}_{i\downarrow} - 2\hat{b}_{i\uparrow}^\dagger \hat{b}_{i\uparrow}\hat{b}_{i\downarrow}^\dagger \hat{b}_{i\downarrow}\right) \\
=& \frac{1}{4}\left(2\hat{n}_{i\uparrow}(1+\hat{n}_{i\downarrow}) + 2\hat{n}_{i\downarrow}(1+\hat{n}_{i\uparrow}) + \hat{n}_{i\uparrow}\hat{n}_{i\uparrow} + \hat{n}_{i\downarrow}\hat{n}_{i\downarrow} - 2\hat{n}_{i\uparrow}\hat{n}_{i\downarrow}\right) \\
=& \frac{1}{4}\left((\hat{n}_{i\uparrow} + \hat{n}_{i\downarrow})^2 + 2(\hat{n}_{i\uparrow} + \hat{n}_{i\downarrow})\right) \\
=& \left(\frac{1}{2}\hat{n}_i\right)^2 + \frac{1}{2}\hat{n}_i,
\end{aligned} \tag{A.13}$$

where we have used the definition of the number operator $\hat{n}_i \equiv \sum_\sigma \hat{n}_{i\sigma} \equiv \sum_\sigma \hat{b}_{i\sigma}^\dagger \hat{b}_{i\sigma}$ [13] and the commutator relations (2.3). The eigenvalue of this equation must be equal to $S^2 + S$ to complete the spin algebra, which is satisfied when

$$\hat{n}_i |\Psi\rangle = 2S|\Psi\rangle. \tag{A.14}$$

A.3 Fourier transformation of the A and B fields and the mean field equations

When Fourier transforming the A and B fields, we find that

$$\begin{aligned}\sum_i \hat{A}_{i,i+\boldsymbol{d}} &= \frac{1}{2}\sum_i \left(\hat{b}_{i+\boldsymbol{d}\downarrow}\hat{b}_{i\uparrow} - \hat{b}_{i+\boldsymbol{d}\uparrow}\hat{b}_{i\downarrow}\right) \\ &= \frac{1}{2N}\sum_i \sum_{\boldsymbol{k},\boldsymbol{k}'} \left(e^{i\boldsymbol{k}'\cdot(\boldsymbol{r}_i+\boldsymbol{d})}e^{i\boldsymbol{k}\cdot\boldsymbol{r}_i}\hat{b}_{\boldsymbol{k}'\downarrow}\hat{b}_{\boldsymbol{k}\uparrow} - e^{i\boldsymbol{k}'\cdot(\boldsymbol{r}_i+\boldsymbol{d})}e^{i\boldsymbol{k}\cdot\boldsymbol{r}_i}\hat{b}_{\boldsymbol{k}'\uparrow}\hat{b}_{\boldsymbol{k}\downarrow}\right) \\ &= \frac{1}{2}\sum_{\boldsymbol{k}} e^{-i\boldsymbol{k}\cdot\boldsymbol{d}}\left(\hat{b}_{-\boldsymbol{k}\downarrow}\hat{b}_{\boldsymbol{k}\uparrow} - \hat{b}_{-\boldsymbol{k}\uparrow}\hat{b}_{\boldsymbol{k}\downarrow}\right),\end{aligned} \tag{A.15}$$

where we have used eq. (B.15). In a similar way:

$$\sum_i \hat{B}_{i,i+\boldsymbol{d}} = \frac{1}{2}\sum_{\boldsymbol{k}} e^{-i\boldsymbol{k}\cdot\boldsymbol{d}}\left(\hat{b}^\dagger_{\boldsymbol{k}\uparrow}\hat{b}_{\boldsymbol{k}\uparrow} + \hat{b}^\dagger_{\boldsymbol{k}\downarrow}\hat{b}_{\boldsymbol{k}\downarrow}\right). \tag{A.16}$$

In our calculations, we also come across the sum

$$\begin{aligned}\sum_{\boldsymbol{k}} \gamma^B_{\boldsymbol{k}} &= \sum_{\boldsymbol{k},\boldsymbol{d}} J_{\boldsymbol{d}}\mathcal{B}_{\boldsymbol{d}}\cos(\boldsymbol{k}\cdot\boldsymbol{d}) = \sum_{\boldsymbol{k},\boldsymbol{d}} J_{\boldsymbol{d}}\mathcal{B}_{\boldsymbol{d}}\cdot\frac{1}{2}\left(e^{i\boldsymbol{k}\cdot\boldsymbol{d}} + e^{-i\boldsymbol{k}\cdot\boldsymbol{d}}\right) \\ &= \sum_{\boldsymbol{d}} J_{\boldsymbol{d}}\mathcal{B}_{\boldsymbol{d}}\cdot\frac{N}{2}\left(\delta_{\boldsymbol{d},0} + \delta_{-\boldsymbol{d},0}\right) = 0,\end{aligned} \tag{A.17}$$

where we have used eq. (B.19) and the fact that $\boldsymbol{d} \neq 0$.

The mean field equations (2.49) are defined through differentiation of the ground state energy E_0 given in eq. (2.47). Performing the differentiation with respect to $\mathcal{A}_{\boldsymbol{d}}$:

$$\begin{aligned}\frac{\partial E_0}{\partial \mathcal{A}_{\boldsymbol{d}}} &= NJ_{\boldsymbol{d}}\mathcal{A}_{\boldsymbol{d}} + \sum_{\boldsymbol{k}}\frac{\partial\omega_{\boldsymbol{k}}}{\partial\mathcal{A}_{\boldsymbol{d}}} = 0 \\ \Rightarrow NJ_{\boldsymbol{d}}\mathcal{A}_{\boldsymbol{d}} &= -\sum_{\boldsymbol{k}}\frac{-\gamma^A_{\boldsymbol{k}}\frac{1}{2}J_{\boldsymbol{d}}\sin(\boldsymbol{k}\cdot\boldsymbol{d})}{\omega_{\boldsymbol{k}}} \\ \Rightarrow \quad \mathcal{A}_{\boldsymbol{d}} &= \frac{1}{2N}\sum_{\boldsymbol{k}}\frac{\gamma^A_{\boldsymbol{k}}}{\omega_{\boldsymbol{k}}}\sin(\boldsymbol{k}\cdot\boldsymbol{d}),\end{aligned} \tag{A.18}$$

and the rest of the equations may be derived in the same way.
The contracted version of the mean field equations are easily derived from the original ones by performing a sum over either $\boldsymbol{\delta}$ or $\boldsymbol{\Delta}$. For instance:

$$\sum_{\delta}\mathcal{A}=\sum_{\delta}\mathrm{sgn}(\mathcal{A}_\delta)\mathcal{A}_\delta=\frac{1}{2N}\sum_{\delta}\sum_{k}\frac{\gamma_k^A}{\omega_k}\mathrm{sgn}(\mathcal{A}_\delta)\sin(\boldsymbol{k}\cdot\boldsymbol{\delta})=\frac{1}{N}\sum_{k}\frac{\gamma_k^A}{\omega_k}\Gamma_k^A$$
$$\Rightarrow\quad \mathcal{A}=\frac{1}{6N}\sum_{k}\frac{\gamma_k^A}{\omega_k}\Gamma_k^A. \tag{A.19}$$

The other eqs. (2.70) to (2.72) follow in a similar way.

A.4 The structure factor

The first term in eq. (3.3) is

$$\left\langle\hat{b}^\dagger_{k_1\uparrow}\hat{b}_{k_2\uparrow}\hat{b}^\dagger_{k_3\uparrow}\hat{b}_{k_4\uparrow}\right\rangle=\left\langle(c_1\hat{\eta}^\dagger_{k_1\uparrow}-s_1\hat{\eta}_{k_1\downarrow})(c_2\hat{\eta}_{k_2\uparrow}-s_2\hat{\eta}^\dagger_{k_2\downarrow})(c_3\hat{\eta}^\dagger_{k_3\uparrow}-s_3\hat{\eta}_{k_3\downarrow})(c_4\hat{\eta}_{k_4\uparrow}-s_4\hat{\eta}^\dagger_{k_4\downarrow})\right\rangle. \tag{A.20}$$

Due to commutator relation and the definition of the ground state eq. (2.46), the only non-zero terms in the equation above will involve two creation and two annihilation operators. Relation eq. (2.46) also eliminates the terms starting with $\hat{\eta}^\dagger_{k_1\uparrow}$ and/or ending with $\hat{\eta}_{k_4\uparrow}$.

$$\begin{aligned}\left\langle\hat{b}^\dagger_{k_1\uparrow}\hat{b}_{k_2\uparrow}\hat{b}^\dagger_{k_3\uparrow}\hat{b}_{k_4\uparrow}\right\rangle=&\left\langle s_1c_2c_3s_4\hat{\eta}_{k_1\downarrow}\hat{\eta}_{k_2\uparrow}\hat{\eta}^\dagger_{k_3\uparrow}\hat{\eta}^\dagger_{k_4\downarrow}+s_1s_2s_3s_4\hat{\eta}_{k_1\downarrow}\hat{\eta}^\dagger_{k_2\downarrow}\hat{\eta}_{k_3\downarrow}\hat{\eta}^\dagger_{k_4\downarrow}\right\rangle\\
=&s_1c_2c_3s_4\left\langle(\delta_{k_2,k_3}+\hat{\eta}^\dagger_{k_3\uparrow}\hat{\eta}_{k_2\uparrow})(\delta_{k_1,k_4}+\hat{\eta}^\dagger_{k_4\downarrow}\hat{\eta}_{k_1\downarrow})\right\rangle\\
+&s_1s_2s_3s_4\left\langle(\delta_{k_1,k_2}+\hat{\eta}^\dagger_{k_2\downarrow}\hat{\eta}_{k_1\downarrow})(\delta_{k_3,k_4}+\hat{\eta}^\dagger_{k_4\downarrow}\hat{\eta}_{k_3\downarrow})\right\rangle\\
=&s_1c_2c_3s_4\delta_{k_2,k_3}\delta_{k_1,k_4}+s_1s_2s_3s_4\delta_{k_1,k_2}\delta_{k_3,k_4}.\end{aligned} \tag{A.21}$$

Similarly, the other three terms may be reduced in this way. Inserting eq. (A.21), together with the three other terms, into eq. (3.3), we get the correlation between the spins in the ground state:

$$\begin{aligned}\left\langle\hat{\boldsymbol{S}}_0\cdot\hat{\boldsymbol{S}}_i\right\rangle=&\frac{3}{2N^2}\sum_{k_1,k_2,k_3,k_4}e^{i(k_4-k_3)\cdot r_i}s_1c_2c_3s_4\left(\delta_{k_2,k_3}\delta_{k_1,k_4}+\delta_{k_1,k_{-3}}\delta_{k_2,k_{-4}}\right)\\
=&\frac{3}{2N^2}\sum_{k_1,k_2}e^{i(k_1-k_2)\cdot r_i}\left(s_1^2c_2^2+s_1c_2c_{-1}s_{-2}\right)\\
=&\frac{3}{8N^2}\sum_{k_1,k_2}e^{i(k_1-k_2)\cdot r_i}\Big(\big(\cosh(2\theta_{k_1})-1\big)\big(\cosh(2\theta_{k_2})+1\big)-\sinh(2\theta_{k_1})\sinh(2\theta_{k_2})\Big)\\
=&\frac{3}{8N^2}\sum_{k_1,k_2}e^{i(k_1-k_2)\cdot r_i}\left(\frac{\gamma^B_{k_1}+\tilde{\lambda}}{\omega_{k_1}}\cdot\frac{\gamma^B_{k_2}+\tilde{\lambda}}{\omega_{k_2}}-\frac{\gamma^A_{k_1}}{\omega_{k_1}}\cdot\frac{\gamma^A_{k_2}}{\omega_{k_2}}+\frac{\gamma^B_{k_1}+\tilde{\lambda}}{\omega_{k_1}}-\frac{\gamma^B_{k_2}+\tilde{\lambda}}{\omega_{k_2}}-1\right)\\
=&\frac{3}{8N^2}\sum_{k_1,k_2}e^{i(k_1-k_2)\cdot r_i}\left(\frac{(\gamma^B_{k_1}+\tilde{\lambda})(\gamma^B_{k_2}+\tilde{\lambda})-\gamma^A_{k_1}\gamma^A_{k_2}}{\omega_{k_1}\omega_{k_2}}-1\right),\end{aligned} \tag{A.22}$$

where we have used eq. (2.41), eq. (2.42) and eq. (2.43). The structure factor is then

$$\begin{aligned}
S(\boldsymbol{q}) \equiv & \sum_i \left\langle \hat{\mathbf{S}}_0 \cdot \hat{\mathbf{S}}_i \right\rangle e^{-i\boldsymbol{q}\cdot\boldsymbol{r}_i} = \frac{3}{8N^2} \sum_{k_1,k_2} \sum_i e^{i(k_1-k_2-q)\cdot r_i} \left(\frac{(\gamma^B_{k_1}+\tilde{\lambda})(\gamma^B_{k_2}+\tilde{\lambda}) - \gamma^A_{k_1}\gamma^A_{k_2}}{\omega_{k_1}\omega_{k_2}} - 1 \right) \\
= & \frac{3}{8N^2} \sum_{k_1,k_2} \sum_{\boldsymbol{K}} \delta_{\boldsymbol{K},k_1-k_2-q} \left(\frac{(\gamma^B_{k_1}+\tilde{\lambda})(\gamma^B_{k_2}+\tilde{\lambda}) - \gamma^A_{k_1}\gamma^A_{k_2}}{\omega_{k_1}\omega_{k_2}} - 1 \right) \\
= & \frac{3}{8N^2} \sum_{k_1,k_2} \left(\frac{(\gamma^B_{k_1}+\tilde{\lambda})(\gamma^B_{k_1-q-\boldsymbol{K}}+\tilde{\lambda}) - \gamma^A_{k_1}\gamma^A_{k_1-q-\boldsymbol{K}}}{\omega_{k_1}\omega_{k_1-q-\boldsymbol{K}}} - 1 \right) \\
= & \frac{3}{8N^2} \sum_{k_1,k_2} \left(\frac{(\gamma^B_{k_1}+\tilde{\lambda})(\gamma^B_{k_1-q}+\tilde{\lambda}) - \gamma^A_{k_1}\gamma^A_{k_1-q}}{\omega_{k_1}\omega_{k_1-q}} - 1 \right) \\
= & \frac{3}{8N} \sum_{k} \left(\frac{(\gamma^B_{k}+\tilde{\lambda})(\gamma^B_{k-q}+\tilde{\lambda}) - \gamma^A_{k}\gamma^A_{k-q}}{\omega_{k}\omega_{k-q}} - 1 \right),
\end{aligned} \tag{A.23}$$

where $\boldsymbol{K}$ is a reciprocal lattice vector. We have used eq. (A.22) and a more general version of eq. (B.15). The fact that

$$\gamma^A_{k'+\boldsymbol{K}} = \frac{1}{2} \sum_{\boldsymbol{d}} J_{\boldsymbol{d}} \mathcal{A}_{\boldsymbol{d}} \sin(\boldsymbol{k}'\cdot\boldsymbol{d} + \boldsymbol{K}\cdot\boldsymbol{d}) = \frac{1}{2} \sum_{\boldsymbol{d}} J_{\boldsymbol{d}} \mathcal{A}_{\boldsymbol{d}} \sin(\boldsymbol{k}'\cdot\boldsymbol{d} + 2\pi m) = \gamma^A_{k'} \tag{A.24}$$

$$\gamma^B_{k'+\boldsymbol{K}} = \gamma^B_{k'} \tag{A.25}$$

was also used.

A.5 Expansion of $1/\Omega_k$

We will now find the expansion of $1/\Omega_k$ for small S:

$$\begin{aligned}
1/\Omega_k = & \left((\beta\Gamma^B_k + 1)^2 - \alpha^2 (\Gamma^A_k)^2 \right)^{-1/2} = \left((1 + \beta_1\Gamma^B_k S + \beta_2 \Gamma^B_k S^2 + \mathcal{O}(S^3))^2 - (\alpha_1^2 S + \alpha_2^2 S^2 + \mathcal{O}(S^3))(\Gamma^A_k)^2 \right)^{-1/2} \\
= & \left(1 + \left(2\beta_1\Gamma^B_k - \alpha_1^2 (\Gamma^A_k)^2 \right) \cdot S + \left(2\beta_2\Gamma^B_k + \beta_1^2 (\Gamma^B_k)^2 - \alpha_2^2 (\Gamma^A_k)^2 \right) \cdot S^2 + \mathcal{O}(S^3) \right)^{-1/2} \\
= & 1 + \left(\frac{1}{2}\alpha_1^2 (\Gamma^A_k)^2 - \beta_1 \Gamma^B_k \right) \cdot S + \left(\frac{1}{2}\alpha_2^2 (\Gamma^A_k)^2 - \beta_2 \Gamma^B_k - \frac{3}{2}\beta_1\alpha_1^2 \Gamma^B_k (\Gamma^A_k)^2 + \beta_1^2 (\Gamma^B_k)^2 + \frac{3}{8}\alpha_1^4 (\Gamma^A_k)^4 \right) \cdot S^2 \\
& + \mathcal{O}(S^3).
\end{aligned} \tag{A.26}$$

A.6 Fidelity

We simplify the expression

$$\begin{aligned}
\sum_{ij} h_{ij}\hat{A}^\dagger_{ij} &= \frac{1}{2N^2}\sum_{ij}\sum_{\boldsymbol{k}_1,\boldsymbol{k}_2,\boldsymbol{k}_3} h_{\boldsymbol{k}_1} e^{i(\boldsymbol{r}_i-\boldsymbol{r}_j)\cdot\boldsymbol{k}_1}\cdot e^{-i(\boldsymbol{r}_i\cdot\boldsymbol{k}_2+\boldsymbol{r}_j\cdot\boldsymbol{k}_3)}\left(\hat{b}^\dagger_{\boldsymbol{k}_2\uparrow}\hat{b}^\dagger_{\boldsymbol{k}_3\downarrow}-\hat{b}^\dagger_{\boldsymbol{k}_2\downarrow}\hat{b}^\dagger_{\boldsymbol{k}_3\uparrow}\right)\\
&= \frac{1}{2N^2}\sum_{ij}\sum_{\boldsymbol{k}_1,\boldsymbol{k}_2,\boldsymbol{k}_3} h_{\boldsymbol{k}_1} e^{i(\boldsymbol{k}_1-\boldsymbol{k}_2)\cdot\boldsymbol{r}_i}\cdot e^{-i(\boldsymbol{k}_1+\boldsymbol{k}_3)\boldsymbol{r}_j}\left(\hat{b}^\dagger_{\boldsymbol{k}_2\uparrow}\hat{b}^\dagger_{\boldsymbol{k}_3\downarrow}-\hat{b}^\dagger_{\boldsymbol{k}_2\downarrow}\hat{b}^\dagger_{\boldsymbol{k}_3\uparrow}\right)\\
&= \frac{1}{2}\sum_{\boldsymbol{k}_1,\boldsymbol{k}_2,\boldsymbol{k}_3} h_{\boldsymbol{k}_1}\delta_{\boldsymbol{k}_1,\boldsymbol{k}_2}\delta_{\boldsymbol{k}_1,-\boldsymbol{k}_3}\left(\hat{b}^\dagger_{\boldsymbol{k}_2\uparrow}\hat{b}^\dagger_{\boldsymbol{k}_3\downarrow}-\hat{b}^\dagger_{\boldsymbol{k}_2\downarrow}\hat{b}^\dagger_{\boldsymbol{k}_3\uparrow}\right)\\
&= \frac{1}{2}\sum_{\boldsymbol{k}} h_{\boldsymbol{k}}\left(\hat{b}^\dagger_{\boldsymbol{k}\uparrow}\hat{b}^\dagger_{-\boldsymbol{k}\downarrow}-\hat{b}^\dagger_{\boldsymbol{k}\downarrow}\hat{b}^\dagger_{-\boldsymbol{k}\uparrow}\right)\\
&= \frac{1}{2}\sum_{\boldsymbol{k}} h_{\boldsymbol{k}}\hat{b}^\dagger_{\boldsymbol{k}\uparrow}\hat{b}^\dagger_{-\boldsymbol{k}\downarrow}-\frac{1}{2}\sum_{-\boldsymbol{k}} h_{-\boldsymbol{k}}\hat{b}^\dagger_{-\boldsymbol{k}\downarrow}\hat{b}^\dagger_{\boldsymbol{k}\uparrow}\\
&= \sum_{\boldsymbol{k}} h_{\boldsymbol{k}}\hat{b}^\dagger_{\boldsymbol{k}\uparrow}\hat{b}^\dagger_{-\boldsymbol{k}\downarrow},
\end{aligned} \tag{A.27}$$

where we have used eq. (B.15) and the assumption that $h_{\boldsymbol{k}}$ is antisymmetric in $\boldsymbol{k}$.

The normalized inner product of two ground states $|G\rangle$ and $|G'\rangle$ on the form given in eq. (5.2), can be written as

$$
\begin{aligned}
\frac{1}{CC'}\Big\langle G'\Big|G\Big\rangle &= \langle 0|\exp\Big(\sum_{k'} h'^{\dagger}_{k'}\hat{b}_{k'\uparrow}\hat{b}_{-k'\downarrow}\Big)\exp\Big(\sum_{k} h_k\hat{b}^{\dagger}_{k\uparrow}\hat{b}^{\dagger}_{-k\downarrow}\Big)|0\rangle_b \\
&= \langle 0|\prod_{k'}\exp\Big(-h'_{k'}\hat{b}_{k'\uparrow}\hat{b}_{-k'\downarrow}\Big)\prod_{k}\exp\Big(h_k\hat{b}^{\dagger}_{k\uparrow}\hat{b}^{\dagger}_{-k\downarrow}\Big)|0\rangle_b \\
&= \prod_{k}\langle 0|\exp\Big(-h'_k\hat{b}_{k\uparrow}\hat{b}_{-k\downarrow}\Big)\exp\Big(h_k\hat{b}^{\dagger}_{k\uparrow}\hat{b}^{\dagger}_{-k\downarrow}\Big)|0\rangle_b \\
&= \prod_{k}\sum_{nm}\frac{1}{(n!)(m!)}(-h'_k)^m(h_k)^n\langle 0|\Big(\hat{b}_{k\uparrow}\hat{b}_{-k\downarrow}\Big)^m\Big(\hat{b}^{\dagger}_{k\uparrow}\hat{b}^{\dagger}_{-k\downarrow}\Big)^n|0\rangle_b \\
&= \prod_{k}\sum_{n}\frac{1}{(n!)^2}(-h'_k h_k)^n\langle 0|\Big(\hat{b}_{k\uparrow}\hat{b}_{-k\downarrow}\Big)^n\Big(\hat{b}^{\dagger}_{k\uparrow}\hat{b}^{\dagger}_{-k\downarrow}\Big)^n|0\rangle_b \\
&= \prod_{k}\sum_{n}\frac{1}{(n!)^2}(-h'_k h_k)^n\langle 0|\Big(\hat{b}_{k\uparrow}\Big)^n\Big(\hat{b}^{\dagger}_{k\uparrow}\Big)^n|0\rangle_b\langle 0|\Big(\hat{b}_{-k\downarrow}\Big)^n\Big(\hat{b}^{\dagger}_{-k\downarrow}\Big)^n|0\rangle_b \\
&= \prod_{k}\sum_{n}\frac{1}{(n!)^2}(-h'_k h_k)^n(n!)^2\Big\langle n\Big|n\Big\rangle\cdot\Big\langle n\Big|n\Big\rangle \\
&= \prod_{k}\sum_{n}(-h'_k h_k)^n \\
&= \prod_{k}\frac{1}{1+h'_k h_k},
\end{aligned}
\tag{A.28}
$$

where we have used eq. (A.27), the Taylor series expansion $e^x = \sum_{n=0}^{\infty}\frac{1}{n!}x^n$, and the repeated use of the boson relations from eq. (A.1): $\left(\hat{b}^{\dagger}_{\mu}\right)^n|0\rangle = \sqrt{n!}\,|n\rangle$.

B Appendix: The Fourier Transform and Reciprocal Space

B.1 Definition

When defining our Fourier transformation of the Schwinger-boson operators, see eq. (2.18) and eq. (2.19), we move from operators in real space to operators defined in reciprocal space. To explore this reciprocal space, we must first characterize the real triangular lattice by a set of linearly independent basic lattice vectors. In two dimensions, we may choose the vectors

$$\begin{aligned} \boldsymbol{a}_1 &= \left(1, 0\right) \\ \boldsymbol{a}_2 &= \frac{1}{2}\left(1, \sqrt{3}\right), \end{aligned} \tag{B.1}$$

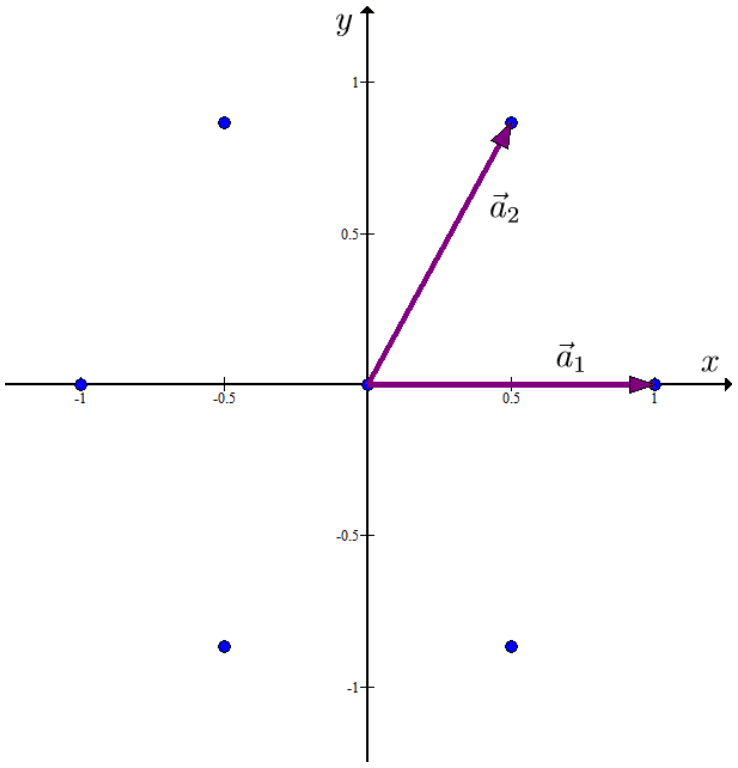

Figure B.1: Illustration of the triangular lattice. Only the lattice point in the origin and its 6 closest neighbours are shown.

shown in fig. B.1, as our basic lattice vectors. Here we have scaled the distance between two

neighbouring lattice points to 1. Any lattice point can be reached by an integer linear combination of these two vectors, where the resulting vector is known as a lattice vector[1]:

$$\boldsymbol{R} = p_1\boldsymbol{a}_1 + p_2\boldsymbol{a}_2. \tag{B.2}$$

From the basic lattice vectors, we also construct the set of nearest neighbour vectors $\boldsymbol{\delta}$ of length 1:

$$\begin{aligned} \{\boldsymbol{\delta}\} &= \left\{\pm\boldsymbol{\delta}^-, \pm\boldsymbol{\delta}^0, \pm\boldsymbol{\delta}^+\right\} \\ \boldsymbol{\delta}^- &= \boldsymbol{a}_1 - \boldsymbol{a}_2 = \frac{1}{2}\left(1, -\sqrt{3}\right) \\ \boldsymbol{\delta}^0 &= \boldsymbol{a}_1 = \left(1, 0\right) \\ \boldsymbol{\delta}^+ &= \boldsymbol{a}_2 = \frac{1}{2}\left(1, \sqrt{3}\right), \end{aligned} \tag{B.3}$$

and the next nearest neighbour vectors[2] $\boldsymbol{\Delta}$ of length $\sqrt{3}$:

$$\begin{aligned} \{\boldsymbol{\Delta}\} &= \left\{\pm\boldsymbol{\Delta}^-, \pm\boldsymbol{\Delta}^0, \pm\boldsymbol{\Delta}^+\right\} \\ \boldsymbol{\Delta}^- &= \boldsymbol{\delta}^0 + \boldsymbol{\delta}^- = \frac{1}{2}\left(3, -\sqrt{3}\right) \\ \boldsymbol{\Delta}^0 &= \boldsymbol{\delta}^0 + \boldsymbol{\delta}^+ = \frac{1}{2}\left(3, \sqrt{3}\right) \\ \boldsymbol{\Delta}^+ &= \boldsymbol{\delta}^+ - \boldsymbol{\delta}^- = \left(0, \sqrt{3}\right). \end{aligned} \tag{B.4}$$

The reciprocal space of the triangular grid is similarly spanned by the basic reciprocal lattice vectors $\boldsymbol{b}_1$ and $\boldsymbol{b}_2$. They are defined through the relation [24, p. 87]

$$\boldsymbol{a}_i \cdot \boldsymbol{b}_j = 2\pi\delta_{ij}, \tag{B.5}$$

and for our choice of $\boldsymbol{a}_1$ and $\boldsymbol{a}_2$, these vectors are:

$$\begin{aligned} \boldsymbol{b}_1 &= 2\pi\left(1, -\tfrac{1}{\sqrt{3}}\right) \\ \boldsymbol{b}_2 &= 2\pi\left(0, \tfrac{2}{\sqrt{3}}\right), \end{aligned} \tag{B.6}$$

[1] In the report we use $\boldsymbol{r}_j$ as the lattice vector of site j.

[2] Not to be confused the Kronecker delta δ_{ab}!

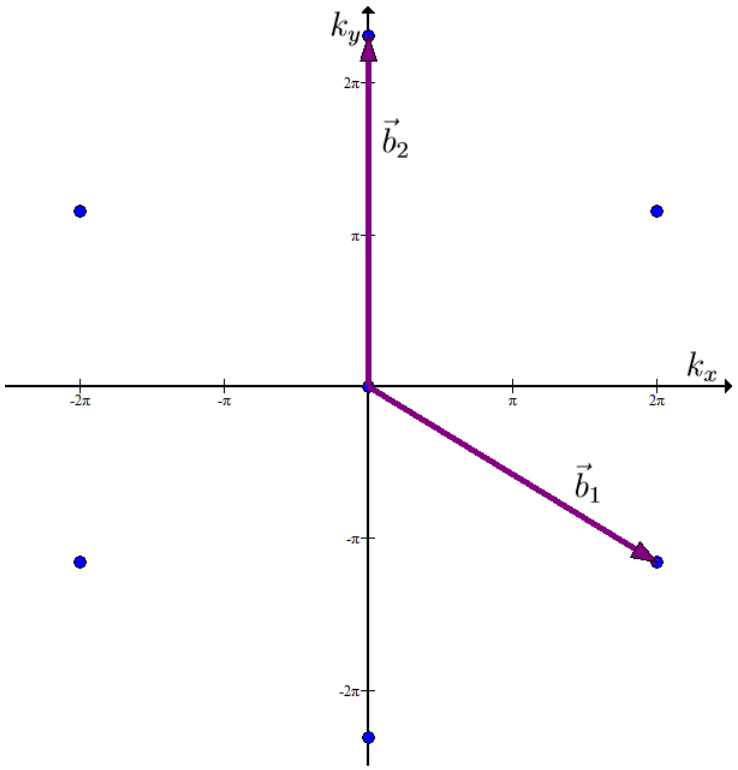

Figure B.2: Illustration of the reciprocal space of the triangular lattice.

shown in fig. B.2. Note that these basic reciprocal vectors have a length of $\frac{4\pi}{\sqrt{3}}$, unlike the basic lattice vectors. The reciprocal analogue to vectors in real space are the wave vectors $\boldsymbol{k}$. We may expand the wave vectors in the $\boldsymbol{b}_1 - \boldsymbol{b}_2$ basis, so that

$$\boldsymbol{k} = m_1\boldsymbol{b}_1 + m_2\boldsymbol{b}_2, \tag{B.7}$$

where m_1, m_2 are real numbers. By definition, the reciprocal lattice vector $\boldsymbol{K}$ has the property

$$e^{i\boldsymbol{K}\cdot\boldsymbol{R}} = 1. \tag{B.8}$$

Expanding $\boldsymbol{K}$ as shown above, we get

$$e^{i\boldsymbol{K}\cdot\boldsymbol{R}} = e^{i(m_1\boldsymbol{b}_1+m_2\boldsymbol{b}_2)\cdot(p_1\boldsymbol{a}_1+p_2\boldsymbol{a}_2)} = e^{2\pi i(m_1p_1+m_2p_2)} \equiv 1, \tag{B.9}$$

which is satisfied in general when m_1 and m_2 are integers.

B.2 Periodicity

B.2.1 Periodic Boundary Conditions

Our grid in real space is normally periodical in both the $\boldsymbol{a}_i$-directions, in the sense that $\hat{b}_{(\boldsymbol{R}+N_i\boldsymbol{a}_i)\sigma} = \hat{b}_{\boldsymbol{R}\sigma}$, where N_i is the number lattice sites in $\boldsymbol{a}_i$-direction. This periodicity carries over

into reciprocal space through the Fourier transform in eq. (2.18), and we require that

$$e^{i\boldsymbol{k}\cdot(\boldsymbol{R}+N_i\boldsymbol{a}_i)} = e^{i\boldsymbol{k}\cdot\boldsymbol{R}} \tag{B.10}$$

to satisfy the spatial symmetry. Equation (B.9) implies that this holds if $N_i\boldsymbol{k}$ is a reciprocal lattice vector, so we may write $m_i = \frac{n_i}{N_i}$ where n_i is an integer.

Now, since adding a reciprocal lattice vector $\boldsymbol{K}$ to the wave vector $\boldsymbol{k}$ has no effect on the exponential phase factor $e^{i\boldsymbol{k}\cdot\boldsymbol{R}}$ in the Fourier transformation, we may restrict ourselves to keep the wave vectors within what is known as the first Brillouin zone. This zone is the area of reciprocal space that is closer to a certain reciprocal lattice point than any other point in the lattice [24, p. 89], and is shown in fig. B.3. A wave vector outside the first Brillouin zone will be equivalent to a vector inside it, this can be seen by simply adding and subtracting reciprocal lattice vectors. For the triangular lattice, the it has a rather cumbersome hexagonal shape. Luckily, an equivalent unit cell in the simpler shape of a rhombus can be constructed, also shown in fig. B.3. In this rhombic unit cell, the triangles 1, 2, 3 and 4 do not overlap with the original first Brillouin zone. But by adding/subtracting either $\boldsymbol{b}_1$ or $\boldsymbol{b}_2$, we can project all the exterior triangles 1-4 to the interior triangles a-d (1 →a and so on). Therefore, there are no "missing" wave vectors in the rhombic unit cell, and we may use it instead of the hexagonal one.

The wave vectors contained in this unit cell can be written as

$$\begin{aligned}\boldsymbol{k} &= \frac{n_1}{N_1}\boldsymbol{b}_1 + \frac{n_2}{N_2}\boldsymbol{b}_2 \\ n_1 &\in \left\{-\frac{N_1}{2}, -\frac{N_1}{2}+1, \ldots, \frac{N_1}{2}-1\right\} \\ n_2 &\in \left\{-\frac{N_2}{2}, -\frac{N_2}{2}+1, \ldots, \frac{N_2}{2}-1\right\},\end{aligned} \tag{B.11}$$

where we assume that N_1 and N_2 are even numbers. This gives a total of $N_1 \cdot N_2 = N$ wave vectors in the unit cell.

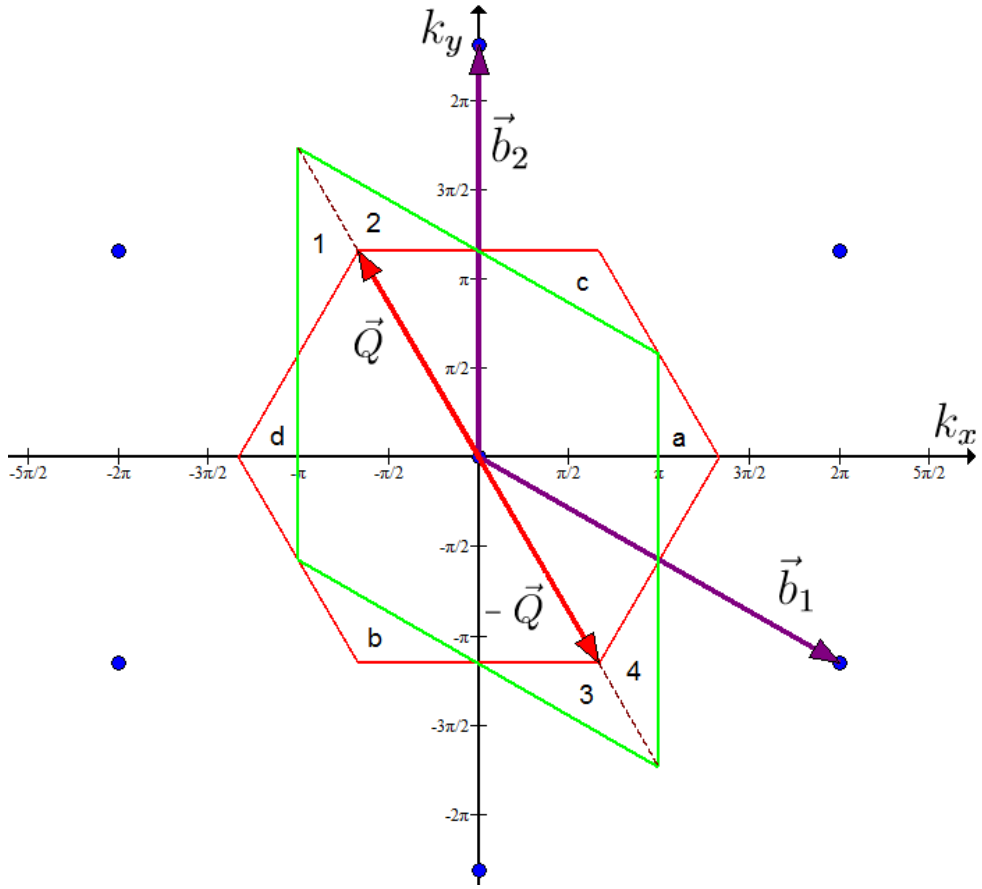

Figure B.3: Illustration of the first Brillouin zone (hexagonal) for the triangular lattice. An equivalent and geometrically simpler unit call is also shown (rhombic). The wave vectors $\pm\boldsymbol{Q}$ that make the structure factor diverge, see chapter 3, are also depicted.

B.2.2 Antiperiodic Boundary Conditions

We are also interested in the triangular grid with antiperiodic boundary conditions in one direction and regular periodic boundaries in the other direction. This is only relevant for the calculations in section 4.4. For simplicity, let us place the antiperiodic boundary in the $\boldsymbol{a}_1$ direction and keep the periodic boundary in the other direction. This means that $\hat{b}_{i\sigma} = -\hat{b}_{i+N_1\boldsymbol{a}_1\sigma}$ and $\hat{b}_{i\sigma} = \hat{b}_{i+N_2\boldsymbol{a}_2\sigma}$, changing the condition in eq. (B.10) to

$$e^{i\boldsymbol{k}\cdot(\boldsymbol{R}+N_2\boldsymbol{a}_2)} = e^{i\boldsymbol{k}\cdot\boldsymbol{R}} \tag{B.12}$$

$$e^{i\boldsymbol{k}\cdot(\boldsymbol{R}+N_1\boldsymbol{a}_1)} = -e^{i\boldsymbol{k}\cdot\boldsymbol{R}} = e^{i(\boldsymbol{k}\cdot\boldsymbol{R}+\pi)}. \tag{B.13}$$

By the same argument as in the previous section, we require that $m_1 = \frac{n_1+1/2}{N_1}$ and $m_2 = \frac{n_2}{N_2}$ to satisfy the boundary conditions. We may still confine ourselves to the first Brillouin zone and choose the same values for n_i as we found in the previous section, giving us

$$\begin{aligned} \boldsymbol{k} =& \frac{n_1 + 1/2}{N_1}\boldsymbol{b}_1 + \frac{n_2}{N_2}\boldsymbol{b}_2 \\ n_1 \in& \left\{-\frac{N_1}{2}, -\frac{N_1}{2}+1, ..., \frac{N_1}{2}-1\right\} \\ n_2 \in& \left\{-\frac{N_2}{2}, -\frac{N_2}{2}+1, ..., \frac{N_2}{2}-1\right\}, \end{aligned} \tag{B.14}$$

The derivation is of course identical for an antiperiodic boundary in the $\boldsymbol{a}_2$ direction, and doubly antiperiodic boundary conditions gives the extra term of $1/2$ for both m_1 and m_2. In respect to our equations, the only noticeable effect of the antiperiodic boundary is the shifting of the wave vectors by $\frac{1}{2N_i}\boldsymbol{b}_i$. This effect decreases rapidly as the size of our system increases, as is expected from a perturbation of the boundary, and it luckily does not alter the form or shape of any equation we have derived.

B.3 A Useful Relation

Finally, we would like to show the relation

$$\sum_{\boldsymbol{R}} e^{i(\boldsymbol{k}-\boldsymbol{k}')\cdot\boldsymbol{R}} = N\delta_{\boldsymbol{k},\boldsymbol{k}'}, \tag{B.15}$$

which is used frequently throughout this report. We first rewrite the dot product using eq. (B.11):

$$(\boldsymbol{k}-\boldsymbol{k}')\cdot\boldsymbol{R} = \Big(\frac{n_1-n_1'}{N_1}\boldsymbol{b}_1 + \frac{n_2-n_2'}{N_2}\boldsymbol{b}_2\Big)\cdot\Big(p_1\boldsymbol{a}_1 + p_2\boldsymbol{a}_2\Big) = 2\pi\Big(p_1\frac{n_1-n_1'}{N_1} + p_2\frac{n_2-n_2'}{N_2}\Big). \tag{B.16}$$

Clearly, this also holds for antiperiodic boundaries as the extra term of $1/2$ in eq. (B.14) will cancel out. If $\boldsymbol{k} = \boldsymbol{k}' \Leftrightarrow n_i = n_i'$, we get

$$\sum_{\boldsymbol{R}} e^{i(\boldsymbol{k}-\boldsymbol{k}')\cdot\boldsymbol{R}} = \sum_{\boldsymbol{R}} e^0 = N. \tag{B.17}$$

In the case where $\boldsymbol{k} \neq \boldsymbol{k}'$, we define $x_j \equiv e^{2\pi i\frac{n_j-n_j'}{N_j}}$ and rewrite the left hand side of eq. (B.15) as

$$\sum_{\boldsymbol{R}} e^{i(\boldsymbol{k}-\boldsymbol{k}')\cdot\boldsymbol{R}} = \sum_{p_1,p_2} x_1^{p_1}x_2^{p_2} = \Big(\sum_{p_1=0}^{N_1-1} x_1^{p_1}\Big)\Big(\sum_{p_2=0}^{N_2-1} x_2^{p_2}\Big) = \frac{1-x_1^{N_1}}{1-x_1}\frac{1-x_2^{N_2}}{1-x_2} = 0. \tag{B.18}$$

This time, $x_j \neq 1$, but $x_j^{N_j} = 1$. Therefore, the sum of the geometric series is zero, giving rise to the original relation eq. (B.15). The dual relation

$$\sum_{\boldsymbol{k}} e^{i(\boldsymbol{R}-\boldsymbol{R}')\cdot\boldsymbol{k}} = N\delta_{\boldsymbol{R},\boldsymbol{R}'} \tag{B.19}$$

can be shown in the same way, and also holds true in the case of antiperiodic boundaries.

Bibliography

[1] J.-C. Toléadano and P. Toléadano. *The Landau Theory of Phase Transitions*. 1st ed. World Scientific Publishing, 1987. isbn: 9971500256.

[2] X.-G. Wen. "Topological order: from long-range entangled quantum matter to an unification of light and electrons". In: *ISRN Condensed Matter Physics* 2013.198710 (2013). url: http://arxiv.org/abs/1210.1281.

[3] B. Normand. "Frontiers in frustrated magnetism". In: *Contemporary Physics* 50.4 (2009). url: http://www.tandfonline.com/doi/abs/10.1080/00107510902850361#preview.

[4] L. Balents. "Spin liquids in frustrated magnets". In: *Nature* 464.199-208 (2010). url: http://www.nature.com/nature/journal/v464/n7286/abs/nature08917.html.

[5] G. H. Wannier. "Antiferromagnetism. The Triangular Ising Net". In: *Physical Review* 79.2 (1950). url: http://journals.aps.org/pr/abstract/10.1103/PhysRev.79.357.

[6] D. Yoshioka and J. Miyazaki. "Boson Mean Field Theory of the Triangular Lattice Heisenberg Model". In: *Journal of the Physical Society of Japan* 60.2 (1991). url: http://www.emis.ams.org/proceedings/Varna/vol2/2geom19.pdf.

[7] P. W. Anderson. "Resonating valence bonds: A new kind of insulator?" In: *Materials Research Bulletin* 8.2 (1973). url: http://www.sciencedirect.com/science/article/pii/0025540873901670.

[8] F. L. Pratt, P. J. Baker, S. J. Blundell, T. Lancaster, S. Ohira-Kawamura, C. Baines, Y. Shimizu, K. Kanoda, I. Watanabe, and G. Saito. "Magnetic and non-magnetic phases of a quantum spin liquid". In: *Nature* 471.612–616 (2011). url: http://www.nature.com/nature/journal/v471/n7340/full/nature09910.html.

[9] F. Wang and A. Vishwanath. "Spin Liquid States on the Triangular and Kagome Lattices: A Projective Symmetry Group Analysis of Schwinger Boson States". In: *Physical Review B* 74.174423 (2006). url: http://journals.aps.org/prb/abstract/10.1103/PhysRevB.74.174423.

[10] A. Mezio, L. O. Manuel, R. R. P. Singh, and A. E. Trumper. "Low temperature properties of the triangular-lattice antiferromagnet: a bosonic spinon theory". In: *New Journal of Physics* 14.123033 (2012). url: http://arxiv.org/abs/1203.3794.

[11] S.-J. Gu. "Fidelity approach to quantum phase transitions". In: *International Journal of Modern Physics B* 24.4371 (2008). url: http://arxiv.org/abs/0811.3127.

[12] M. Thesberg and E. S. Sørensen. “A quantum fidelity study of the anisotropic next-nearest-neighbour triangular lattice Heisenberg model”. In: *Journal of Physics: Condensed Matter* 26.42 (2014). URL: http://iopscience.iop.org/0953-8984/26/42/425602/.

[13] J. O. Fjærestad. “Second quantization (the occupation-number representation)”. Lecture notes from the course TFY4210 "Quantum theory of many-particle systems" at NTNU. 2014.

[14] D. A. Trifonov. “Diagonalization of Hamiltonians, Uncertainty Matrixes and Robertson Inequality”. In: (2001). URL: http://www.emis.ams.org/proceedings/Varna/vol2/2geom19.pdf.

[15] N. Goldenfeld. *Lectures on Phase Transitions and the Renormalization Group*. Addison-Wesley Publishing Company, 1992. ISBN: 0201554087.

[16] A. W. Sandvik. “Finite-size scaling of the ground-state parameters of the two-dimensional Heisenberg model”. In: *Physical Review B* 56.11678 (1997). URL: http://arxiv.org/abs/cond-mat/9707123.

[17] J. Merino, M. Holt, and B. J. Powell. “Spin liquid phase in a spatially anisotropic frustrated antiferromagnet”. In: *Physical Review B* 89.245112 (2014). URL: http://arxiv.org/abs/1402.3463.

[18] A. Y. Kitaev. “Fault-tolerant quantum computation by anyons”. In: *Annals of Physics* 303 (2003). URL: http://arxiv.org/abs/quant-ph/9707021.

[19] J. K. Pachos. *Introduction to Topological Quantum Computation*. Cambridge University Press, 2012. ISBN: 9780511792908.

[20] W. Commons. *Toric Code Torus*. File: ToricCodeTorus.png. 2010. URL: https://commons.wikimedia.org/wiki/File:ToricCodeTorus.png.

[21] X. G. Wen and Q. Niu. “Ground-state degeneracy of the fractional quantum Hall states in the presence of a random potential and on high-genus Riemann surfaces”. In: *Physical Review B* 14.9377 (1990). URL: http://journals.aps.org/prb/abstract/10.1103/PhysRevB.41.9377.

[22] A. Mezio, C. N. Sposetti, L. O. Manuel, and A. E. Trumper. “A test of the bosonic spinon theory for the triangular antiferromagnet spectrum”. In: *Europhysics Letters* 94.47001 (2011). URL: http://arxiv.org/abs/1011.0874.

[23] J. O. Fjærestad. “Transformations and symmetries in quantum mechanics”. Lecture notes from the course TFY4210 "Quantum theory of many-particle systems" at NTNU. 2014.

[24] N. W. Ashcroft and N. D. Mermin. *Solid State Physics*. 1st ed. HRW, 1976. ISBN: 0030839939.